NUMERICAL SOLUTION AND SPECTRUM OF BOUNDARY-DOMAIN INTEGRAL EQUATIONS

A thesis submitted for the degree of Doctor of Philosophy

by

NURUL AKMAL BINTI MOHAMED

School of Information Systems, Computing and Mathematics

Brunel University

June 2013

Abstract

A numerical implementation of the direct Boundary-Domain Integral Equation (BDIE)/ Boundary-Domain Integro-Differential Equations (BDIDEs) and Localized Boundary-Domain Integral Equation (LBDIE)/Localized Boundary-Domain Integro-Differential Equations (LBDIDEs) related to the Neumann and Dirichlet boundary value problem for a scalar elliptic PDE with variable coefficient is discussed in this thesis. The BDIE and LBDIE related to Neumann problem are reduced to a uniquely solvable one by adding an appropriate perturbation operator. The mesh-based discretisation of the BDIE/BDIDEs and LBDIE/LBDIDEs with quadrilateral domain elements leads to systems of linear algebraic equations (discretised BDIE/BDIDEs/LBDIE/BDIDEs). Then the systems obtained from BDIE/BDIDE (discretised BDIE/BDIDE) are solved by the LU decomposition method and Neumann iterations. Convergence of the iterative method is analyzed in relation with the eigen-values of the corresponding discrete BDIE/BDIDE operators obtained numerically. The systems obtained from LBDIE/LBDIDE (discretised LBDIE/LBDIDE) are solved by the LU decomposition method as the Neumann iteration method diverges.

Contents

List of Figures

List of Tables

Nomenclature

Γ, $\partial\Omega$	Boundary of Ω
Ω	Connected domain
$\overline{\Omega}$	$\Omega \cup \partial\Omega$
Ω^+	Interior domain
Ω^-	Exterior domain
ν^+	Outward normal to Ω^+
ν^-	Inward normal w.r.t. Ω^+
∇	Gradient
∇^2	Laplace operator
χ	Cut-off function
$\omega(y)$	Localized domain with respect to collocation point y
λ	Eigen-value
$\mathbb{R}$	Set of real numbers
$\mathbb{C}$	Set of complex numbers
Re	Real

Im	Imaginary
C^0	Class of all continuous functions
C^1	Class of all differentiable functions whose derivative is in C_0
C^2	Class of all differentiable functions whose derivative is in C^1

Acronyms

BEM Boundary Element Method

BDIDE Boundary-Domain Integro-Differential Equation

BDIE Boundary-Domain Integral Equation

BIEM Boundary Integral Element Method

BVP Boundary Value Problem

EFGM Element Free Galerkin Method

FEM Finite Element Method

GEM Green Element Method

GFEM Galerkin Finite Element Method

GMRES Generalized Minimal Residual

LBDIDE Localized Boundary-Domain Integro-Differential Equation

LBDIE Localized Boundary-Domain Integral Equation

LBDIEM Localized Boundary-Domain Integral Equation Method

LBDIO Localized Boundary-Domain Integral Operator

LUWF Local Unsymmetric weak Form

ILBIE Improved Localized Boundary Integral Equation

IMLS Improved Moving Least Square

MFS Method of Fundamental Solution

MLBIE Meshless Local Boundary Integral Equation

MLPG Meshless Local Petrov-Galerkin

MLS Moving Least Square

PDE Partial Differential Equation

RBF Radial Basis Function

Acknowledgments

First and foremost, I would like to thank Allah Almighty for His guidance and help in giving me the strength to complete this thesis. A special thanks to my supervisor, Professor Dr. Sergey Mikhailov, for his constructive advice throughout the period of this research project. I owe Dr. Matthias Winter and Dr. Oleksandr Menshykov a debt of gratitude for devoting their time generously reading my thesis. I am also acknowledge my debt to Ministry of Higher Education Malaysia and Sultan Idris Education University for sponsorship throughout my Ph.D studies.

I am also indebted to my beloved parents, Mohamed bin Yahya and Normadiah binti Awang, who are my source of inspiration, for their continuous encouragement and affection. The writing of this thesis would been impossible without the moral support and unconditional love from my siblings, abe, kak, Epi, Farry and Alia, and also my nephew and nieces, Hazeeq, Sofia and Miriam. I am also acknowledge my other family members who always care for my parents when i was not around. My gratefulness is also to abang Din for constant toleration and many sacrifices. To them, I extend my sincere thanks.

I would also like to thank the staffs of Department of Information Systems, Computing and Mathematics for providing me a comfortable environment for completing this thesis.

Thanks are also due to my friends, Timmy, Aliza, Eliza, Rima, Alex, Samirah, kak Waidah, Fadhilah, Lisa, Pijah who watched me fumble my way to this thesis. I also would like to thank my landlady, Mina and family with whom i stayed for the last 2 years.

Finally, I would like to express my sincere appreciation to all who has helped me in one way or another, but whose names are not mentioned.

To my parents,

Thanks for an unfailing love and the continuous prayers.

Publications arising from this thesis

S.E. Mikhailov, N. A. Mohamed (2011) Iterative solution of boundary-domain integral equation for BVP with variable coefficient, in: *Proceedings of the 8th UK Conference on Boundary Integral Methods* (edited by D. Lesnic), Leeds University Press, Leeds, UK, ISBN 978 0 85316 2957, 127–134.

S.E. Mikhailov, N. A. Mohamed (2012) Numerical solution and spectrum of boundary-domain integral equation for the Neumann BVP with a variable coefficient. *International Journal of Computer Mathematics, DOI: 10.1080/00207160.2012.679733*, 1-17.

Chapter 1

Research Introduction and Overview

1.1 Introduction

It is well-known that a Boundary Value Problem (BVP) for Partial Differential Equation (PDE) with a constant coefficient can be reduced to a Boundary Integral Equation (BIE). The discussion on the BIEs can be found in e.g. Brebbia et al. (1984), Aliabadi (2002), Wrobel (2002). There are two approaches to derive BIEs of BVPs for PDE with constant coefficients. The first integral formulation is often named as a direct method and the integral equations are derived through the application of the second Green's identity. The second integral formulation known as an indirect method is founded on single or double layer potentials. It is from the assumption that the solution can be expressed in terms of a source density function defined on the problem's boundary. However, the density function obtained from the indirect method, in general, has no physical meaning. The method of boundary integral equations has always had two important applications in the theory of boundary value problems for partial differential equations: as a theoretical tool for proving the existence of solutions and as a practical tool for the construction of solutions (Costabel (1988b)). The discussions on the BVPs had been started long time ago. The background of the BIE by examining its

mathematical foundation from potential theory, boundary value problems, Green's functions, Green's identities, to Fredholm integral equations was explored in e.g. (Cheng and Cheng (2005), McLean (2000), M. Costabel (2007)).

It was in the early 19th century when a German mathematician, Gauss introduced the first kind of integral equations of the single layer potential as a tool in numerical computation, see in (Gauss (1877)). At that time, he produced all the numerical calculations by hand since computers were yet to be invented in the 1940s. Later, another German mathematician, Carl Neumann studied the double layer potential, see in (Neumann (1877)). The Neumann iteration and Neumann boundary condition for Ordinary Differential Equations (ODEs) and PDEs were named after him.

He showed in (Neumann (1887)) that for convex domain, the operator $(\frac{1}{2}I + K)$ is contracting such that $||\frac{1}{2}I + K|| < 1$, where K is the double layer potential. In (Plemelj (1911)) it was shown that the spectral radius of $(\frac{1}{2}I + K)$ on $C^0(\Gamma)$ is less than 1 which implies the convergence of the Neumann iteration. The discussions for the spectral properties of $(\frac{1}{2}I + K)$ in three dimensions with Lyapunov boundary were given in e.g. (Mikhlin (1957), Goursat (1964)). In 2001, (Steinbach and Wendland (2001)) showed that $(\frac{1}{2}I + K)$ is a contraction in $H^{1/2}(\Gamma)$. The results were obtained by using the coerciveness properties of the single layer and hypersingular boundary integral operators obtained by (Costabel (1988a)). The application of Neumann series on direct BIEs was also discussed. The result for the Laplace equation in an open set $\Omega \subset R^m$ was proved by different methods in (Medková (2007)) and the result for the Poisson equation in a Lipschitz domain was then proved in (Medková (2009)).

Before that, in 1828, a British mathematician, George Green wrote a book entitled "An Essay on the Application of Mathematical Analysis to the Theories of Electricity and Magnetism"(Green (1828)) that first used the term potential function. Herein we find his remarkable theorem, Green's identities that are studied largely from the point of view of fundamental solutions and the core of integrals formulation for direct method. Although a fundamental solution of PDE is usually highly non-local, numerical implementation of BIEs pose a great advantage since the problem dimensionality is reduced by one which

requires only a line mesh around the boundary of the domain in 2-D and a surface mesh for 3-D geometries. This implies huge reduction of computation time and computer memory requirements since we obtained smaller linear systems and less mesh generation efforts. This effect is most pronounced when we have unbounded domain. It would be a problematic to truncate and approximate an unbounded domain for mesh based method, whereas the BIEs, on the other hand, automatically models the behavior at infinity (e.g. in Cheng and Cheng (2005)). However, the matrix obtained from BIEs is a fully populated matrix.

Even though Green's formula is prominent for potential theory, the idea of Green was then studied to solve other physical problems, e.g. elasticity, Helmholtz and Maxwell BVPs. In 1860, a German physician, Hermann von Helmholtz in (Helmholtz (1860)) formulated the fundamental formula for Helmholtz equation that often arises in the study of physical problems involving PDEs in both space and time. In (Somigliana (1885)), an Italian mathematician, Carlo Somigliana made important contributions in elasticity when he formulated the Somigliana integral equation for elasticity which is counterpart of Greens formula for potential theory.

There are several numerical computational methods of solving linear partial differential equations which have been formulated as integral equations, e.g. boundary element method (BEM) and method of fundamental solutions (MFS). The discussions about BEM can be found, in e.g. (Beer (2001), Paris and Cañas (1997), Katsikadelis (2002)). The MFS was introduced in (Kupradze and Aleksidze (1964)) and then developed as a numerical technique in (Mathon and Johnston (1977)). The advantage of MFS is, it avoids the numerical integration of singular fundamental solution whereas BEM needs special integration method to handle the singular fundamental solution.

However, the fundamental solution is generally not available in an explicit and/or cheaply computable form if the coefficients of the auxiliary PDE depend on the space variables. Therefore, reduction of BVPs with variable coefficients to BIEs is generally not effective for numerical implementations. An Italian mathematician, Levi introduced method of the parametrix which is a way to construct fundamental solutions for elliptic PDE with variable coefficients, see in (Levi (1909)). The existence of a parametrix has been proved for

hypo-elliptic pseudo-differential operators, see in (Hörmander (1965)). An explicit construction of a parametrix for second order partial differential operators based on power series developments was discovered by Hadamard, see in (Hörmander (1985), Hadamard (1932)).

Using a parametrix (Levi function) as a substitute of a fundamental solution, it is possible to reduce a BVP not to BIEs but to Boundary-Domain Integral Equations (BDIEs) (see, e.g. Hilbert (1912), Miranda (1970) and Pomp (1998)). Book written by Miranda (1970) offered a great discussion of Boundary value problems for partial differential equations and can serve as a classic reference on PDEs of elliptic type. The classical works in (Hilbert (1912), Levi (1909), Miranda (1970), Pomp (1998)) deal only with the indirect BDIEs for Dirichlet and Neumann BVPs.

The BDIEs are called segregated BDIEs when the unknown boundary functions are considered as formally unrelated to the unknown functions inside the domain whereas for the united BDIEs, the unknown boundary functions are related to the unknown functions inside the domain. The analysis of direct united BDIEs was discussed in (S.E. Mikhailov (2006)) whereas the analysis of direct segregated BDIEs was presented in (Chkadua et al. (2009b), Chkadua et al. (2010b)). In (Chkadua et al. (2009b)), the discussions of existence, uniqueness and operator invertibility in Sobolev space were provided while in (Chkadua et al. (2010b)), the regularity and asymptotic behaviour of BDIE solutions were discussed. The analysis of segregated BDIEs for mixed variable-coefficient BVPs in exterior domains can be found in (Chkadua et al. (2011b), Chkadua et al. (2013 (to appear))). For the analysis on the direct segregated BDIEs with cracks, see (Chkadua et al. (2009a)) that established the BDIE equivalence to the original BVPs and invertibility of the BDIE operators in the corresponding Sobolev spaces.

However, BDIEs do not enjoy the privilege of having problem dimensionality reduced by one like held for BIEs since they do not only consist of the boundary integral but also the domain integrals. For numerical solving the BDIEs, one should discretize not only the domain boundary but also the domain itself. Moreover, a parametrix is usually highly non-local like a fundamental solution. This leads the discretized BDIEs to systems of equations of the same size as obtained from Finite Element Method (FEM) but unlike FEM, the

systems of equations are fully populated matrices. In addition to that, a parametrix like fundamental solution is singular that implies more expensive computationally in comparison with the FEM. Therefore, Finite Element Method (FEM) is seen to be surpassing the numerical implementation of BDIEs. Mikhailov in 2005 published an article entitled "Will the boundary (-domain) integral equation method survive? Preface to the special issue on non-traditional boundary (-domain) integral equation methods" in (Mikhailov (2005b)). The articles presented the drawbacks of BIEs/BDIEs and discussed some ideas that might make BIEs/BDIEs comparable to FEM.

There are several methods for transforming the domain integrals into equivalent boundary integrals. One of them is boundary node method, which combines BEM with moving least square (MLS) technique, see in e.g. (Mukherjee and Mukherjee (2005)). The MLS technique is a meshfree approximation that will not require any meshing for the interior domain. The discussions on the MLS approximations can be found in e.g. (Levin (1998), Wendland (2001)). Another technique which is commonly used for treating the volume integral without discretising the volume is the dual-reciprocity method, see e.g. (Partridge et al. (1992)). The technique approximates part of the integrand using radial basis functions (RBF) to approximate the unknown variables which enable the transformation of the domain integrals that includes unknown variables to the boundary. For the discussions of RBF, see in e.g. (Buhmann (2000), Buhmann (2003), Gao (2002)).

Since a parametrix is usually highly non-local and to make the BDIEs method competitive with the FEM, the Localized Boundary-Domain Integral Equation Method (LBDIEM) has been recently developed. Several researchers addressed this deficiency by employing specially constructed localised parametrices to reduce linear and non-linear BVPs with variable coefficients to Localized Boundary-Domain Integral Equations (LBDIEs)/Localized Boundary-Domain Integro-Differential Equations (LBDIDEs), see e.g. (Zhu et al. (1998), Mikhailov (2002)). After a locally-supported mesh-based or mesh-less discretisation of LBDIEM, LBDIEs/ LBDIDEs ends up in sparse systems of algebraic equations. The discretized LBDIEs/ LBDIDEs can be solved by well known efficient and economical methods developed for sparsely populated system solution.

In addition to having less computer memory requirements for solving sparse systems of algebraic equations, computer time and memory requirements are also reduced since less domain and integrations need to be carried out. This is since we will only calculate the boundary and domain integrals when the interpolation nodes are within the localisation domain $\omega(y)$ that depend on the location of the collocation points y. Moreover, there are several mesh-less discretisation methods of LBDIEs/ LBDIDEs in LBDIEM to handle boundary integrals so that the problem dimensionality can be diminished by one e.g. MLS technique and dual-reciprocity method as discussed in the previous page.

A method called Green Element Method (GEM) was proposed in (Taigbenu (1995)) which was derived from the BEM over the meshes of the FEM. This approach leads to large sparse matrices like in FEM while still retains the use of fundamental solution. The domain integrations in original GEM is more easily carried out as compared to BDIEs. This is due to the fact that the collocation points always belong to element nodes. In that case, the domain integrations over any polygonal elements can be handled analytically for most Green's functions. The detailed discussions of the idea of GEM can be found in e.g. (Taigbenu (1999)). In (Archer and Horne (1998), Archer et al. (1999)), the GEM and Dual Reciprocity Boundary Element Method (DRBEM) have been applied to reservoir engineering problems. Some other applications using GEM can be found in e.g. (Archer and Horne (2000), Archer and Horne (2002), Taigbenu and Elvin (2006), Taigbenu (2010)). Onyejekwe (2006) studied the GEM for Poisson's equation in polar coordinates and some applications of radial coordinate GEM for the computation of transient fluid flow in a straight rigid pipe is in e.g. Onyejekwe (2005).

Some localized parametrixes were constructed in (Zhu et al. (1998)) to reduce BVPs for PDE with variable coefficients to Localized BIEs (LBIEs). The LBIEs that have been derived combine the advantageous features of the three methods: Galerkin Finite Element Method (GFEM), BEM and Element Free Galerkin method (EFGM). The GFEM leads to bounded, sparse and symmetric matrices. The BEM implicates with the full and unsymmetrical matrices, whereas EFGM still involve domain integrals. The LBIEs that were constructed are meshless, have only boundary integration and lead to banded and sparse system matrices.

Green functions for an auxiliary problem on local spherical domains were used as the local parametrices in (Zhu et al. (1998), Zhu et al. (1999), Sladek et al. (2004a)) to reduce some linear and nonlinear scalar problems with variable coefficients.

In the studies, (Zhu et al. (1998)) use the MLS approximations and a mesh free method that does not need an element mesh for purposes of interpolation of the solution variables. The numerical experiments in the paper were applied to linear potential problems, such as the Laplace and Poisson's equations. In (Zhu et al. (1999)), they extend the work to non-linear boundary value problems. The numerical implementation that had been carried out in the paper was for a cubic solution with mixed boundary conditions. Atluri and Zhu (2000) discussed two kinds of meshless methods. One is Meshless Local Boundary Integral Equation (MLBIE) that is based on a local unsymmetric form and another one is Meshless Local Petrov-Galerkin (MLPG) based on local symmetric weak form.

A LBIE for solving problems in linear elasticity was developed in (Atluri et al. (2000)). As in (Zhu et al. (1998), Zhu et al. (1999)), they solved the LBIE based on the local unsymmetric weak form (LUWF) and the MLS approximation but for linear elasticity problems. Sladek et al. (2000b) proposed a method that use direct limit approach to handle the strong and weak singularities for LBIEs when using MLS approximation. The numerical experiments were done for linear elasticity. In (Sladek et al. (2000a)), an approach based on local parametrices to reduce a linear elasticity problem for a body with a special inhomogeneity, to a LBIE was introduced. The applications of LBIEs on e.g. heat conduction in nonhomogeneous solids, transient heat conduction, anisotropic and functionally graded materials, are discussed in (Sladek et al. (2004a), Sladek et al. (2004b), Sladek et al. (2005)). In (Sladek et al. (2003)), the Green function of the plane Laplace equation was used as a parametrix for the axially symmetric problem of heat transfer with variable coefficients.

Dai and Cheng (2010) applied an Improved Moving Least-Squares (IMLS) approximation on LBIE to obtain an Improved LBIE (ILBIE). Unlike LBIE method, the ILBIE method is a direct meshless boundary integral equation method with the basic unknown quantity is the real solution of the nodal variables, and the boundary conditions can be implemented directly and easily as in the finite element method (Dai and Cheng (2010)). The potential

problems considered in this paper were two-dimensional. Based on the numerical examples, the ILBIE method has greater computational efficiency and precision as compared with the LBIE with original MLS.

Mikhailov in (Mikhailov (2002)) introduced a localized parametrix as the product of a parametrix and cut-off function. This is based on the fact that the parametrix is not unique and has the same singularity at $x = y$ as the fundamental solution but can differ at other points.

In (Mikhailov (2004), Mikhailov (2005a)), the approach of (Mikhailov (2002)) had been extended to the mixed BVP for a second order scalar nonlinear (quasi-linear) elliptic PDE with a variable coefficient that depends on the unknown solution. In (Mikhailov (2003), Mikhailov (2005a)), the mixed BVP for a second order scalar nonlinear (quasi-linear) elliptic PDE with a variable coefficient that depends on the unknown solution and the BVP solution gradient were discussed. The approach in (Mikhailov (2002), Mikhailov (2003), Mikhailov (2004), Mikhailov (2005a)) was then extended in (Mikhailov (2005c)) to the mixed BVP for the system of quasi-linear PDEs of physically nonlinear elasticity for continuously inhomogeneous body.

By using some incomplete information about eigen-solutions of an original and/or adjoint generalized Fredholm operator equation (with zero index), (Mikhailov (1999)) constructed some finite-dimensional perturbation operators. Adding the perturbation operator to the original one can reduce the eigen-space dimension and yield an unconditionally and uniquely solvable perturbed equation. The Neumann problem is not unconditionally solvable, and when it is solvable, its solution can only be unique up to an additive constant. Using results of (Mikhailov (1999)), (Mikhailov and Nakhova (2005)) presented the numerical implementation for the mesh-based discretization of a uniquely solvable perturbed Neumann LBDIE with a variable coefficient. For the approximations, the paper used the linear interpolations for boundary and domain integrations.

Later, a deeper analytical insight into the properties of the corresponding integral operators such as the solvability of LBDIE, uniqueness of a solution, equivalence to the original BVPs and the invertibility of LBDIEs were developed. Chkadua et al. (2010a) described

the equivalence of the LBDIEs to the original mixed type BVPs and the invertibility of the corresponding localized boundary-domain integral operators (LBDIOs) in the appropriately chosen function spaces. The invertibility of the LBDIOs related to Dirichlet problem for PDEs with matrix variable coefficients was discussed in (Chkadua et al. (2011d)). In (Chkadua et al. (2011c)), the discussions on the LBDIEs method for an interface crack problem was discussed. In the paper, the Fredholm properties of the LBDIO and their invertibility in appropriate function spaces were also investigated.

Some numerical implementations for BDIE related with the Neumann problem for PDE with variable coefficient can be seen in e.g. (Mikhailov and Mohamed (2011), Mikhailov and Mohamed (2012)). Even though no analysis is made of the spectral properties for the BDIEs' operator, some conclusions can be attained in (Mikhailov and Mohamed (2012)).

1.2 Research Objectives

The objectives of this research are:

1. To solve the systems obtained from BDIE/BDIDEs and LBDIE/LBDIDEs related to the Neumann and Dirichlet BVPs for a scalar elliptic PDE with variable coefficient by using direct method and iterative method (if the solution converges).

2. To analyze the behavior of eigen-values of the corresponding discrete BDIEs and LBDIEs operators for a scalar elliptic PDE with several different variable coefficients by taking the effect of the maximal eigen-values of the discrete BDIEs and LBDIEs.

1.3 Research Rationale

The project results will benefit the software developers and numerous users in mechanical, structural, civil, marine, and aerospace engineering, who develop and implement computer codes for solving problems of heat transfer and stress analysis of structure elements made of "functionally graded" materials, variable-curvature inhomogeneous elastic shells, filtration through inhomogeneous rocks etc.

1.4 Scope of the Study

In this thesis, we focus on the numerical implementation of the Boundary-Domain Integral Equation (BDIE)/Boundary-Domain Integro-Differential Equations (BDIDEs) and Localized Boundary-Domain Integral Equation (LBDIE)/Localized Boundary-Domain Integro-Differential Equations (LBDIDEs) of BVPs for PDE with variable coefficients. Some simple regions e.g. a square, a circular domain and a parallelogram are used as our test domains.

We use linear and bilinear interpolations for boundary and domain integrations, respectively. These linear and bilinear interpolation methods are chosen since they are amongst the easiest ways of approximation. For evaluating the boundary/domain integrals, we mainly use the the standard Gauss method which is also known as Gauss-Legendre method. However, for integrands that involve singularities, we use special methods in evaluating the integrals i.e. Gauss-Laguerre method for boundary integral with logarithmic singularity and Duffy transformation for domain integrals. In our work, we will also discuss a semi-analytic method to cancel out the influence of the singularity.

In all of the numerical implementations, we use Fortran (Intel Visual Fortran Compiler Professional Edition 11.1) with double accuracy as our main programming software in writing the numerical codes. We also use MATLAB for drawing graphs and computing the eigenvalues of matrix operators. In addition, we also use Mathematica 5.1 to obtain exact solution of some numerical integrations for our semi-analytic method. For solving the systems of linear algebraic equations of discretized BDIE/BDIDEs and discretized LBDIE/LBDIDEs, we use the direct method (LU decomposition method) and iterative method (Neumann iterative method) if the iterations converge. We calculate the eigen-values of the discretized BDIE/BDIDEs and LBDIE/LBDIDEs operators and compute the maximal eigen-values which indicates the spectral radius of the discretized BDIE/BDIDEs and LBDIE/LBDIDEs operators. The behavior of eigen-values of the corresponding discrete BDIE/BDIDEs and LBDIE/LBDIDEs operators for a scalar elliptic PDE with several different variable coefficients are then analyzed.

1.5 Outline of Thesis

The thesis is organized into six chapters. The first chapter details some discussions on the background and rationale of research, objectives of research, scope of the study and chapter organization.

An overview of Boundary Element Method (BEM) related to the Neumann and Dirichlet problems for Laplace equation is given in Chapter 2. The formulations of Boundary Integral Equation (BIE) obtained from the direct and indirect methods are also discussed. Moreover, the uniqueness and solubility of solutions for the boundary value problems for Laplace equation are explored. Several Fredholm's theorems and Fredholm's alternative theorem which are related to the solvability of Fredholm's integral equation are presented. A discussion on the convergence of the Neumann iteration corresponds to spectral properties of an operator K is also given. Furthermore, a method by Mikhlin in investigating the spectral properties of the integral equation related to the Dirichlets and Neumanns problems obtained from the indirect method in three dimensions is introduced. The discussion of the spectral properties for BIE that obtained from the direct method is then extended based on the spectral properties for the BIE obtained from the indirect method,

In Chapter 3, Boundary-Domain Integral Equation (BDIE)/Boundary-Domain Integro-Differential Equations (BDIDEs) which are used to solve boundary value problems (BVPs) for PDE with variable coefficient is introduced. The BDIE related to Neumann problem is reduced to a uniquely solvable one by adding an appropriate perturbation operator. An overview on the discretization for the boundary $\partial\Omega$ of our test domains by using continuous linear elements and for the domain Ω by using quadrilateral domain elements is also given. Then, assembling of the element contributions obtained from the integration of each segment/element to a global matrix is explained. The geometry of three test domains i.e. square, circular domain, and parallelogram that are used in all the numerical experiments in Chapters 3, 4 and 5 is also introduced. Furthermore, the system obtained from perturbed BDIE (discretised perturbed BDIE) related to Neumann problem is solved by LU decomposition method and Neumann iterations. In addition, the spectral properties obtained numerically

from the discrete BDIE operator is also presented. The details on the convergence of the iterative method is also discussed in relation with the maximal eigen-values of the corresponding discrete BDIE operator obtained numerically.

In Chapter 4, the results of numerical implementations on the BDIDEs related to the Dirichlet problem for PDE with a variable coefficient are shown. Two BDIDEs which are associated with the Dirichlet problem are considered. One leads to the discretised BDIDE with the collocation points x^i for $x^i \in \overline{\Omega}$ at all J nodes. The second BDIDE leads to the discretised BDIDE with the collocation points x^i only for $x^i \in \Omega$ at $J - J_D$ nodes where J_D is the number of nodes on the boundary $\partial\Omega$. Similar to the perturbed BDIE (discretised perturbed BDIE) related to Neumann problem as in Chapter 3, the system obtained from BDIDE (discretised BDIDE) related to Dirichlet problem with $x^i \in \overline{\Omega}$ at all J nodes is solved by LU decomposition method and Neumann iterations. To analyze convergence of the iterative method, the maximal eigen-values of the corresponding discrete BDIDE operator were obtained numerically. For the second BDIDE, the system which obtained is solved by LU decomposition method since the Neumann iterations diverge.

In Chapter 5, the discussions on how the BVPs for PDE with variable coefficient can be reduced to the Localized Boundary-Domain Integral Equation (LBDIE)/Localized Boundary-Domain Integro-Differential Equations (LBDIDEs) for Neumann and Dirichlet problems, respectively are discussed.

The discretization of the LBDIE/LBDIDEs which leads to systems of linear equations is explained for the numerical purposes. The algebraic systems of linear equations are then solved by LU decomposition method. The maximal eigen-values for the LBDIE's/LBDIDEs' operators for both Neumann and Dirichlet problems which are related with the convergence of Neumann iteration method is also investigated and analyzed..

In Chapter 6, some conclusions of this study and some suggestions for further study are given.

Chapter 2

Introduction to Boundary Integral Equations

2.1 Introduction

Many equations of physics are second-order PDEs e.g. wave equation, diffusion (heat) equation, Helmholtz equation, equation of fluid-dynamics, Maxwell equations, Schrödinger equation. These PDEs can describe a wide variety of phenomena such as sound, heat, electrostatics, electrodynamics, fluid flow and elasticity.

There are various methods for solving BVPs for PDE analytically e.g. methods of separation of variables, Fourier and Laplace transforms, integral transforms and variation of parameters. However, many problems encountered in applications cannot be solved using analytical methods. Therefore, it is necessary to resort to approximate solution methods.

Many methods have been developed for the numerical solution of partial differential equations and amongst the commonly used are volume-discretisation methods e.g. finite difference method, finite volume method and finite element method.

Another numerical method that can give a comparable efficiency to volume-discretisation methods is the Boundary Element Method (BEM). In order to use the BEM, we need to have representation formulas. Such representation formulas are well known for the classical

boundary value problems of mathematical physics, e.g. Green's third identity for potential theory, Betti's formula for elasticity theory, and the Stratton-Chu formula for electrodynamics (Costabel (1988b)).

In this chapter, we will take a look at Green's third identity. By using explicit knowledge of a fundamental solution of the differential equation, BVPs can be reduced to Boundary Integral Equations (BIEs). However, the fundamental solution is only available for linear PDEs with constant or some specific variable coefficients.

On the other hand, a parametrix is often available for linear PDEs with variable coefficients. Later, in the next chapters, we will see that by using a parametrix, BVPs for PDEs with variable coefficients can be reduced not to BIEs but to Boundary Domain Integral Equation (BDIE)/Boundary Domain Integro-Differential Equations (BDIDEs) instead. The BVPs that will be considered are Dirichlet and Neumann problems.

2.2 Boundary Integral Equation

Boundary integral equations are a classical tool for boundary value problems for partial differential equations. Many boundary value problems of mathematical physics and engineering can be reduced to integral equations over the boundary of the domain of interest. Particularly, boundary integral equations are often used to solve numerically the Dirichlet and Neumann problems and also the mixed boundary value problem (Dirichlet-Neumann).

One of the methods for the approximate numerical solution of these boundary integral equations is called "boundary element method" (BEM). The approximate solution of the boundary value problem obtained by using BEM has the distinguishing feature that it is an exact solution of the differential equation in the domain and is parametrized by a finite set of parameters living on the boundary. Thus, the problem dimensionality is reduced by one which requires only a line mesh around the boundary of the domain in 2-D and a surface mesh for 3-D geometries. This implies huge reduction in mesh generation efforts.

However, the BEM has also some disadvantages, see e.g. (Costabel (1988b)):

Disadvantages of BEM

- Boundary element method requires the explicit knowledge of a fundamental solution of the differential equation. However, a fundamental solution is often not available in an explicit form. That case happens when the coefficient is not constant but a variable.
- From a computational point of view, most of the computer codes for BEM are in an experimental state, and there might exist problems of reliability compared to FEM. This is maybe since more money is being spent on FEM in the building up of the computer codes for numerical purposes.

In discussing the application of BEM, the first thing that we should look at is the boundary value problem for partial differential equation. In this subsection, we only focus on the potential theory which models a broad class of physical phenomena, e. g., heat conduction, potential flow, seepage, magnetic potential and many others. Further discussion on elasticity theory as well as the numerical computations can be found, e.g. in (Kupradze (1968), Ameen (2005)).

Let us consider a scalar function u, defined on a region Ω bounded by a surface $\Gamma := \partial\Omega$, with an outward normal ν. The function u is assumed to satisfy the following partial differential equation:

$$Lu(x) := -\nabla^2 u(x) = f(x), \qquad x \in \Omega. \tag{2.1}$$

Equation (2.1) is usually known as Poisson equation if $f(x) \neq 0$ and as Laplace equation when $f(x) = 0$.

Some of the possible boundary conditions are given below:
Dirichlet boundary condition

$$u(x_0) = \overline{u}(x_0), \qquad x_0 \in \partial\Omega. \tag{2.2}$$

Neumann boundary condition

$$Tu(x_0) = a(x_0)\frac{\partial u(x_0)}{\partial \nu} = \overline{t}(x_0), \qquad x_0 \in \partial\Omega. \tag{2.3}$$

Mixed boundary condition

$$\begin{aligned} u(x_0) &= \overline{u}(x_0), \qquad x_0 \in \partial\Omega_D, \\ Tu(x_0) &= \bar{t}(x_0), \qquad x_0 \in \partial\Omega_N. \end{aligned} \tag{2.4}$$

where $\partial\Omega_D \cap \partial\Omega_N = \emptyset$ and $\overline{\partial\Omega_D} \cup \overline{\partial\Omega_N} = \partial\Omega$.

As discussed above, one of the drawbacks of BEM is the necessity to know explicitly a fundamental solution of the differential equation. Suppose $F(x, y)$ is a fundamental solution for the operator L in (2.1), that is a solution of the following equation:

$$L_x F(x, y) = \delta(x - y),$$

where $\delta(x - y)$ is the Dirac delta function which satisfies

$$\delta(x - y) = \begin{cases} +\infty, & y = x, \\ 0, & \text{elsewhere.} \end{cases}$$

The Dirac delta function also has a special property such that for any continuous function $f(x)$, the following equation holds:

$$\int_\Omega f(x)\delta(x - y)\mathrm{d}\Omega(x) = f(y).$$

It is well known that fundamental solutions are explicitly known for many equations with constant coefficients $a(x)$, where they can be computed by Fourier transformation, and for some elliptic equations with analytic coefficients, e.g. the Laplace-Beltrami equation on the sphere, e.g. in (Costabel (1988b)).

As an example, it is well-known that the fundamental solutions for Laplace equation

$$Lu = -\nabla^2 u = 0, \qquad x \in \Omega^+ \subset \mathbb{R}^n, \tag{2.5}$$

for $n = 2$ and $n = 3$ are given respectively, as

$$F_\triangle(x, y) = -\frac{1}{2\pi} \ln|x - y| \quad \text{for} \quad x, y \in \mathbb{R}^2, \tag{2.6}$$

$$F_\triangle(x, y) = +\frac{1}{4\pi|x - y|} \quad \text{for} \quad x, y \in \mathbb{R}^3. \tag{2.7}$$

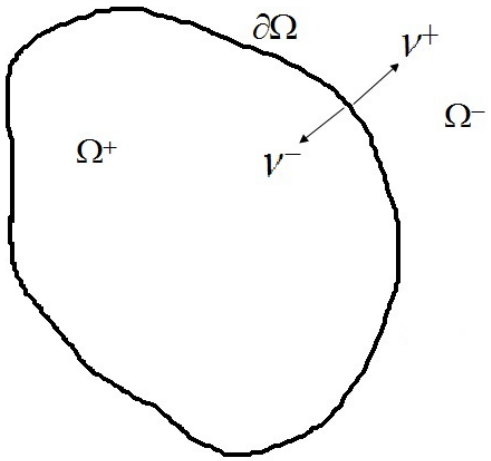

Figure 2.1: Schematic picture of the domain Ω, boundary $\partial\Omega$ and normal ν.

We state here several theorems regarding the uniqueness of solutions for the Dirichlet and Neumann problems for the Laplace equation (2.5) which can also be found in (Lung-An (2006)). The functions for the interior and exterior problems are chosen as $u \in C^2(\Omega^+) \cap C^1(\overline{\Omega^+})$ and $u \in C^2(\Omega^-) \cap C^1(\overline{\Omega^-})$, respectively. We also consider that $\overline{u}(x_0) \in C^1(\partial\Omega)$ and $\overline{t}(x_0) \in C(\partial\Omega)$.

We are interested in well-posed problems. Then some boundary conditions at infinity are required for the exterior problem as follow (see e.g. Lung-An (2006)):

$$\begin{cases} u \text{ is a bounded function on } \Omega, & \Omega \in \mathbb{R}^2, \\ \lim\limits_{|x|\to\infty} u = 0, & \Omega \in \mathbb{R}^3. \end{cases} \tag{2.8}$$

The term well-posed problem was first defined by Jacques Hadamard in (Hadamard (1902)) that have the following properties:

- A solution exists.
- The solution is unique.
- The solution's behavior hardly changes when there's a slight change in the initial condition.

The following theorems will be useful in the next sections, see e.g. (Kupradze (1968)).

Theorem 2.2.1 *(Uniqueness of solutions for the Dirichlet problems for Poisson equation)*

The interior Dirichlet problems for $n \geq 2$ and the exterior Dirichlet problems for $n \geq 3$ have at most one solution.

Theorem 2.2.2 *(Uniqueness of solutions for the Neumann problems for Poisson equation)*

- *Any constant is a solution of the homogeneous interior Neumann problem. Two solution of the interior Neumann problem (with arbitrary f) can differ by at most a constant.*
- *Solution for 2-D exterior Neumann problem is unique up to a constant and the 3-D exterior Neumann problem has at most one solution.*

Next we represent the solution of the partial differential equation (2.5) in the domain by means of boundary potentials. Such representation formulas are well known for the classical boundary value problems of mathematical physics, e. g. Green third identity for potential theory, Betti's formula for elasticity theory, and the Stratton-Chu formula for electrodynamics (Costabel (1988b)).

Let u and v be scalar functions defined on some region Ω in $\mathbb{R}^n$. The first Green identity is given as follows:

$$\int_{\Omega} \left[vLu + \Delta v \cdot \Delta u \right] \, \mathrm{d}\Omega = \int_{\partial\Omega} v \frac{\partial u}{\partial \nu} \, \mathrm{d}\Gamma. \tag{2.9}$$

In particular, we can take $v = 1$ in (2.9), which implies

$$\int_{\Omega} Lu \, \mathrm{d}\Omega = \int_{\partial\Omega} \frac{\partial u}{\partial \nu} \, \mathrm{d}\Gamma. \tag{2.10}$$

Applying (2.10) to the solution of the Neumann problem in (2.1) and (2.3), we obtain

$$\int_{\Omega} f(x) \, \mathrm{d}\Omega(x) = \int_{\partial\Omega} \bar{t}(x_0) \, \mathrm{d}\Gamma(x). \tag{2.11}$$

Equation (2.11) is a compatibility condition that must be satisfied for the existence of the solution for the Neumann problem.

The second Green identity is

$$\int_{\Omega} [uLv - vLu]\,\mathrm{d}\Omega = \int_{\partial\Omega} [uTv - vTu]\ \mathrm{d}\Gamma. \tag{2.12}$$

Taking u as the unknown solution of L in (2.1) and v as the fundamental solution $F_{\triangle}(x,y)$ for Laplace equation defined in (2.6) and (2.7) depending on the type of the dimension of the domain of the problem, we arrive at the third Green identity

$$\begin{aligned} c(y)u(y) \quad &+ \quad \int_{\partial\Omega} [u(x)T_x F_{\triangle}(x,y) - F_{\triangle}(x,y)Tu(x)]\mathrm{d}\Gamma(x) \\ &= \quad \int_{\Omega} F_{\triangle}(x,y)f(x)\mathrm{d}\Omega(x),\ x,y \in \mathbb{R}^n, \end{aligned} \tag{2.13}$$

where

$$c(y) = \begin{cases} 1 & \text{if } y \in \Omega^+, \\ 0 & \text{if } y \in \Omega^-, \\ \alpha(y)/2\pi & \text{if } y \in \partial\Omega \text{ and } \Omega \subseteq \mathbb{R}^2, \\ \alpha(y)/4\pi & \text{if } y \in \partial\Omega \text{ and } \Omega \subseteq \mathbb{R}^3, \end{cases} \tag{2.14}$$

where $\alpha(y)$ is an interior space angle at a corner point y of the boundary $\partial\Omega$. If $\partial\Omega$ is a smooth boundary, then we have $c(y) = 1/2$, see e.g. (Paris and Cañas (1997)).

We can refer to (Paris and Cañas (1997)) for the derivation of all four cases in (2.14). The fixed point $y \in \partial\Omega$ in equation (2.13) is usually called the source point in Potential Theory and the collocation point in BEM while the point x is called the field point or observation point. A pair of boundary functions of the solution u of (2.1), i.e., $u|_{\Gamma}$ and $\partial u/\partial\nu|_{\Gamma}$ are known as Cauchy data.

If u is the solution that satisfies the Laplace equation as in (2.1) with $f = 0$, then the third Green formula in (2.13) becomes

$$c(y)u(y) = -\int_{\partial\Omega} \{u(x)T_x F_{\triangle}(x,y) - F_{\triangle}(x,y)Tu(x)\}\,\mathrm{d}\Gamma(x). \tag{2.15}$$

The representation formula (2.15) consists of two boundary potentials, the single layer potential

$$V\phi(y) := \int_{\partial\Omega} F_{\triangle}(x,y)\phi(x)\ \mathrm{d}\Gamma(x), \quad y \notin \partial\Omega, \tag{2.16}$$

and the double layer potential

$$W\psi(y) := \int_{\partial\Omega} [T_x F(x,y)_{\triangle}]\, \psi(x)\, \mathrm{d}\Gamma(x), \quad y \notin \partial\Omega. \tag{2.17}$$

The corresponding boundary integral (pseudodifferential) operators of the direct values of the single layer potential $\mathcal{V}$ and the double layer potential $\mathcal{W}$, the adjoint double layer potential $\mathcal{W}^*$ and the double layer potential $\mathcal{L}^{\pm}$ are

$$\begin{aligned}
\mathcal{V}\phi(y_0) &:= \int_{\partial\Omega} F_{\triangle}(x,y_0)\phi(x)\, \mathrm{d}\Gamma(x), \\
\mathcal{W}\psi(y_0) &:= \int_{\partial\Omega} [T_x F_{\triangle}(x,y_0)]\, \psi(x)\, \mathrm{d}\Gamma(x), \\
\mathcal{W}^*\phi(y_0) &:= \int_{\partial\Omega} [T_y F_{\triangle}(x,y_0)]\, \phi(x)\, \mathrm{d}\Gamma(x), \\
\mathcal{L}^{\pm}\psi(y_0) &:= -\left[T_y W\psi(y_0)\right]^{\pm},
\end{aligned}$$

where $y_0 \in \partial\Omega$.

Therefore, for $y \notin \partial\Omega$, (2.15) can written in terms of V and W, i.e.,

$$c(y)u(y) = -Wu(y) + VTu(y). \tag{2.18}$$

For $y \in \partial\Omega$, (2.15) can be written in terms of $\mathcal{V}$ and $\mathcal{W}$, i.e.,

$$c(y)u(y) = -\mathcal{W}u(y) + \mathcal{V}Tu(y). \tag{2.19}$$

Here $c(y)$ is defined as in (2.14).

Any boundary value problem can be reduced to Boundary Integral Equation by using several different approaches. The main classifications would fall into two broad categories: direct method and indirect method. The direct method is based on Green formula while the indirect method is based on the single or double layer potentials. However, the density function obtained from the indirect method, in general, has no physical meaning.

We will further in next section assume for simplicity that the boundary $\partial\Omega$ is smooth.

2.2.1 Formulation of Direct boundary integral equations

The following well-known jump relations might be useful for further discussions, see in e.g. (Hsiao and Wendland (2008)):

Theorem 2.2.3 (Jump Relations) *a) Let $\phi \in C(\partial\Omega)$ and $y_0 \in \partial\Omega$. Then*

$$[\mathcal{V}\phi](y_0) = [V\phi]^+(y_0) = [V\phi]^-(y_0), \tag{2.20}$$

$$\partial_\nu^+[V\phi](y_0) = \mathcal{W}^*\phi(y_0) + \frac{1}{2}\phi(y_0), \tag{2.21}$$

$$\partial_\nu^-[V\phi](y_0) = \mathcal{W}^*\phi(y_0) - \frac{1}{2}\phi(y_0). \tag{2.22}$$

b) Let $\phi \in C(\partial\Omega)$ and $y_0 \in \partial\Omega$. Then

$$[W\psi]^+(y_0) = \mathcal{W}\psi(y_0) - \frac{1}{2}\psi(y_0), \tag{2.23}$$

$$[W\psi]^-(y_0) = \mathcal{W}\psi(y_0) + \frac{1}{2}\psi(y_0), \tag{2.24}$$

$$-\mathcal{L}\psi(y_0) := \partial_\nu^+[W\psi](y_0) = \partial_\nu^- W\psi(y_0), \tag{2.25}$$

where $^+$ and $^-$ are the the limiting boundary values on $\partial\Omega$ from Ω^+ and Ω^-, respectively.

We will discuss the formulation of the boundary integral equation by using Green formula (2.15) which is known as "direct method". The Green formula (2.15) admits two ways of approaching the boundary based on the traces $|^\pm$ and on the normal derivative $\partial_\nu^\pm$.

The first way is by considering traces. For the interior Dirichlet and Neumann problem, $c(y) = 1$. Therefore equation (2.15) gives

$$u = -W_{\nu^+}u^+ + V(\partial_{\nu^+}^+ u) \quad \text{on } \Omega^+. \tag{2.26}$$

The notation ν^+ in (2.26) denotes that the direction of ν is outward to Ω^+.

Substituting (2.20) and (2.23) into the trace of (2.26), we obtain

$$u^+ = \frac{1}{2}u^+ - \mathcal{W}_{\nu^+}u^+ + \mathcal{V}(\partial_{\nu^+}^+ u) \quad \text{on } \partial\Omega. \tag{2.27}$$

Now we consider the exterior Dirichlet and Neumann problems which consist of finding u which satisfies the Laplace equation (2.5) in $y \in \Omega^-$ with Dirichlet boundary condition (2.2) and Neumann boundary condition (2.3), respectively.

For the exterior region Ω^-, equation (2.15) gives

$$u = -W_{\nu^-}u^- + V(\partial_{\nu^-}^- u) \quad \text{on } \Omega^-. \tag{2.28}$$

Here the notation ν^- indicates that the direction of ν is inward with respect to Ω^+. Equation (2.28) is true if u satisfies the additional condition at infinity as in (2.8).

Since $\nu^- = -\nu^+$, we can write (2.28) as follows:

$$u = W_{\nu^+} u^- - V(\partial^-_{\nu^+} u) \quad \text{on } \Omega^-. \tag{2.29}$$

Substituting (2.20) and (2.24) into the trace of (2.29), we obtain

$$u^- = \frac{1}{2} u^- + \mathcal{W}_{\nu^+} u^- - \mathcal{V}(\partial^-_{\nu^+} u) \quad \text{on } \partial\Omega. \tag{2.30}$$

Next, one can use the second way of the Green formula (2.15) approaching the boundary, i.e. based on the normal derivative $\partial^\pm_\nu$.

For the interior problem, taking normal derivative (2.26) from Ω^+, we obtain

$$\partial^+_{\nu^+} u = -\partial^+_{\nu^+}[W_{\nu^+} u^+] + \partial^+_{\nu^+}[V(\partial^+_{\nu^+} u)] \quad \text{on } \partial\Omega. \tag{2.31}$$

Therefore, taking into account the jump relations in (2.21) and (2.25) and substituting them into (2.31), we obtain

$$\partial_{\nu^+} u(y_0) = \mathcal{L} u^+(y_0) + \mathcal{W}^*_{\nu^+}(\partial^+_{\nu^+} u(y_0)) + \frac{1}{2}\partial^+_{\nu^+} u(y_0), \quad y_0 \in \partial\Omega. \tag{2.32}$$

For the exterior Dirichlet and Neumann problem, taking the normal derivative of (2.29) from Ω^-, we arrive at the following equation:

$$\partial^-_{\nu^+} u = \partial^-_{\nu^+}[W_{\nu^+}(u^-)] - \partial^-_{\nu^+}[V(\partial^-_{\nu^+} u)] \quad \text{on } \partial\Omega. \tag{2.33}$$

Substitution (2.22) and (2.25) into (2.33), gives

$$\partial^-_{\nu^+} u(y_0) = -\mathcal{L} u^-(y_0) - \mathcal{W}^*(\partial^-_{\nu^+} u(y_0)) + \frac{1}{2}\partial^-_{\nu^+} u(y_0), \quad y_0 \in \partial\Omega. \tag{2.34}$$

Interior Dirichlet Problem

We will look for the solution u which satisfies the Laplace equation (2.5) in $y \in \Omega^+$ with Dirichlet boundary condition (2.2). Equation (2.27) can be written as

$$\left(\frac{1}{2} + \mathcal{W}_{\nu^+}\right) u^+ = \mathcal{V}(\partial^+_{\nu^+} u) \quad \text{on } \partial\Omega. \tag{2.35}$$

Substituting the boundary condition (2.2) into (2.35), we obtain an integral equation of the first kind w.r.t. $\partial^+_{\nu^+}u$:

$$\mathcal{V}(\partial^+_{\nu^+}u(y_0)) = \left(\frac{1}{2} + \mathcal{W}_{\nu^+}\right)\overline{u}(y_0), \qquad y_0 \in \partial\Omega. \tag{2.36}$$

Besides, we can also reduce the interior Dirichlet problem to another integral equation by using (2.32). Substituting the boundary condition (2.2), equation (2.32) can also be written as the following integral equation of the second kind w.r.t. $\partial^+_{\nu^+}u$:

$$\left(\frac{1}{2} - \mathcal{W}^*_{\nu^+}\right)(\partial^+_{\nu^+}u(y_0)) = \mathcal{L}\overline{u}(y_0), \qquad y_0 \in \partial\Omega. \tag{2.37}$$

Exterior Dirichlet Problem

Now we consider the exterior Dirichlet problem which consisits of finding u which satisfies the Laplace equation (2.5) in $y \in \Omega^-$ with Dirichlet boundary condition (2.2) and condition at infinity as in (2.8).

Rearranging, equation (2.30) can be written as

$$\left(\frac{1}{2} - \mathcal{W}_{\nu^+}\right)u^- = -\mathcal{V}(\partial^-_{\nu^+}u) \quad \text{on } \partial\Omega. \tag{2.38}$$

Substituting the boundary condition (2.2) into (2.38), we obtain the following integral equation of first kind w.r.t. $\partial^-_{\nu^+}u$:

$$-\mathcal{V}(\partial^-_{\nu^+}u(y_0)) = \left(\frac{1}{2} - \mathcal{W}_{\nu^+}\right)\overline{u}(y_0), \quad y_0 \in \partial\Omega. \tag{2.39}$$

As in interior Dirichlet case, we can also reduce the exterior Dirichlet problem to another integral equation by taking normal derivative ∂^-_{ν}. Substituting the boundary condition (2.2) into equation (2.34) yields the following integral equation of the second kind w.r.t. $\partial^-_{\nu^+}u$:

$$\left(\frac{1}{2} + \mathcal{W}^*_{\nu^+}\right)(\partial^-_{\nu^+}u(y_0)) = -\mathcal{L}\overline{u}(y_0), \quad y_0 \in \partial\Omega. \tag{2.40}$$

In the later work, we will compare the spectral properties of BIE obtained from indirect method with the BIE from the direct method. We consider the following homogeneous equation with variable parameter ζ:

$$\phi_0(y_0) + 2\zeta\mathcal{W}^*\phi_0(y_0) = 0. \tag{2.41}$$

Note that if $\zeta = -1$, then (2.41) is the homogeneous equation (2.37) with density $\phi_0 = \partial^+_{\nu^+}$, and if $\zeta = 1$, equation (2.41) is the homogeneous equation of (2.40) with the density $\phi_0 = \partial^-_{\nu^+}$. The discussion on the spectral properties of BIE from the direct method will be detailed in subsection 2.3.2.

Interior Neumann Problem

Next, we will look for the solution u which satisfies the Laplace equation (2.5) in $y \in \Omega^+$ with Neumann boundary condition (2.3). Substituting the boundary condition (2.3) into (2.35), we obtain an integral equation of the second kind w.r.t. u^+:

$$\left(\frac{1}{2} + \mathcal{W}_{\nu^+}\right) u^+(y_0) = \mathcal{V}(\bar{t}(y_0)), \qquad y_0 \in \partial\Omega. \tag{2.42}$$

Besides, we can also reduce the interior Neumann problem to another integral equation by using (2.32). Substituting the boundary condition (2.3), equation (2.32) can be written as the following integral equation of the first kind w.r.t. u^+:

$$\mathcal{L}_{\nu^+} u^+(y_0) = \left(\frac{1}{2} - \mathcal{W}^*_{\nu^+}\right) (\bar{t}(y_0)), \qquad y_0 \in \partial\Omega. \tag{2.43}$$

Exterior Neumann Problem

Now we consider the exterior Neumann problem which consists of finding u which satisfies the Laplace equation (2.5) in $y \in \Omega^-$ with Neumann boundary condition (2.3).

Substituting the boundary condition (2.3) into (2.38), we obtain the Fredholm integral equation of the second kind w.r.t. u^-:

$$\left(\frac{1}{2} - \mathcal{W}_{\nu^+}\right) u^-(y_0) = -\mathcal{V}(\bar{t}(y_0)), \qquad y_0 \in \partial\Omega. \tag{2.44}$$

We can also reduce the exterior Neumann problem to another integral equation by taking into account ∂^-_{ν}. Substituting the boundary condition (2.3) into equation (2.34) yields the following integral equation of the first kind w.r.t. u^-:

$$-\mathcal{L} u^-(y_0) = \left(\frac{1}{2} + \mathcal{W}^*_{\nu^+}\right) (\bar{t}(y_0)), \qquad y_0 \in \partial\Omega. \tag{2.45}$$

In order to compare the spectral properties of BIE obtained from indirect method with the BIE from the direct method, we consider the conjugate equation of (2.41), i.e.,

$$\psi_0(y_0) + 2\bar{\zeta}\mathcal{W}\psi_0(y_0) = 0. \tag{2.46}$$

Observe that if $\overline{\zeta} = 1$, then (2.46) is the homogeneous equation of (2.42) with the density $\psi_0 = u^+$, and if $\overline{\zeta} = -1$, equation (2.46) is the homogeneous equation of (2.44) with the density $\psi_0 = u^-$. The discussion on the spectral properties of BIE obtained from the direct method will be continued in subsection 2.3.2.

2.2.2 Fredholm's theorems

Generally, we have to use approximate methods in solving integral equations. The solubility of the integral equation must be established before we can apply the approximate method.

The analysis of the integral equation prior to its solution given by Fredholm consists of four theorems.

These four theorems are applied for the Fredholm integral equations of the second kind with a kernel $k(x, y)$. We define the Fredholm operator K as follows (see e.g. Hunter and Nachtergaele (2001)):

$$K\rho = \int_a^b k(x, y)\rho(x)\, \mathrm{d}\Gamma(x),$$

where limits a and b are finite constants.

We can write the general Fredholm integral equations of the second kind with scalar parameter λ as follows:

$$\rho(y) - \lambda \int_a^b k(x, y)\rho(x)\, \mathrm{d}\Gamma(x) = g(y). \tag{2.47}$$

The parameter λ and the functions $\rho(y)$, $k(x, y)$ and $g(y)$ can be taken as real or complex.

By setting $\lambda = 1/\mu$, we can also write $I - \lambda K$ as $\mu I - K$ such that (2.47) becomes

$$\mu\rho(y) - \int_a^b k(x, y)\rho(x)\, \mathrm{d}\Gamma(x) = \mu g(y).$$

The point λ for which the resolvent

$$R_\mu = (\mu I - K)^{-1} \qquad \text{or} \qquad R_\lambda = (I - \lambda K)^{-1}$$

exists is called regular point of K.

It is well-known that if λ is regular, then the following homogeneous Fredholm's integral equation:

$$\rho(y) - \lambda \int_a^b k(x, y)\rho(x)\mathrm{d}\Gamma(x) = 0, \tag{2.48}$$

has only the trivial solution, see e.g. (Mikhlin (1957)).

The resolvent set $\sigma'(K)$ is the collection of all $\mu \in \mathbb{C}$ for which λ are regular points of K. The spectrum of K is defined as the complement of the resolvent set, $\sigma(K) = \mathbb{C}\backslash\sigma'(K)$. Recall that the spectrum of an operator on a finite-dimensional vector space is precisely the set of eigenvalues, see e.g. Hunter and Nachtergaele (2001). However an operator on an infinite-dimensional space may have additional elements in its spectrum, and may have no eigenvalues.

For $\mu I - K$ bounded implies $(\mu I - K)^{-1}$ is a bounded linear map by the following theorem (see, e.g. (Hunter and Nachtergaele (2001))):

Theorem 2.2.4 *(Open mapping theorem) Suppose that $T : X \to Y$ is a one-to-one, onto and bounded linear map between Banach spaces X and Y. Then $T^{-1} : Y \to X$ is bounded.*

Therefore both $\mu I - K$ and $(\mu I - K)^{-1}$ are one-to-one, onto and bounded linear operators.

The spectrum of a bounded linear operator K on an infinite-dimensional space is divided into three cases:

- The *point spectrum* of K consists of all $\mu \in \sigma(K)$ such that $\mu I - K$ is not one-to-one. The *point spectrum* of K is known as the *eigenvalue set* of K.
- The *continuous spectrum* of K consists of all $\mu \in \sigma(K)$ such that $\mu I - K$ is one-to-one but not onto, and has dense range.
- The *residual spectrum* of K consists of all $\mu \in \sigma(K)$ such that $\mu I - K$ is one-to-one but not onto, and does not have dense range.

Next, we state four Fredholm's theorem which can be found, e.g. in (Mikhlin (1957), Atkinson (1997)). Let the kernel $k(x, y) : [a, b] \times [a, b] \to \mathbb{C}$ be a continuous function. Let also the solutions $\rho(y)$ and $g(y)$ belong to the space $C^0[a, b]$ of continuous functions defined in a closed interval $a \leq x \leq b$ with norm $||\rho|| = \max_{x \in J} |\rho(x)|$ where $J = [a, b]$. Then, the following holds:

Theorem 2.2.5 *(Fredholm's first theorem)*

In any finite portion of the complex λ-plane there exists not more than a finite number of characteristic values λ of Fredholm's integral equation:

$$\rho(y) - \lambda \int_a^b k(x,y)\rho(x)\,\mathrm{d}x = g(y).$$

Theorem 2.2.6 *(Fredholm's second theorem)*

To each characteristic value there corresponds at least one eigenfunction. The number of linearly independent eigenfunctions

$$\rho_1(y),\ \rho_2(y), ...,\ \rho_n(y),$$

corresponding to a given characteristic value, is finite.

Theorem 2.2.7 *(Fredholm's third theorem)*

If λ_0 is characteristic value of the kernel $k(x,y)$, then $\overline{\lambda_0}$ is an characteristic value of the conjugate kernel $\overline{k(y,x)}$ and the number of linearly independent eigenfunctions of the equations

$$\rho(y) - \lambda_0 \int_a^b k(x,y)\rho(x)\,\mathrm{d}x = 0,$$

and of the conjugate equation

$$\varsigma(y) - \overline{\lambda_0} \int_a^b \overline{k(y,x)}\varsigma(x)\,\mathrm{d}x = 0$$

is the same.

Let us introduce the scalar product (ρ, ς) of two functions $\rho(x)$ and $\varsigma(x)$,

$$(\rho, \varsigma) = \int_a^b \rho(x)\overline{\varsigma(x)}\,\mathrm{d}x.$$

It is true that

$$(K\rho, \varsigma) = (\rho, K^*\varsigma).$$

The operator $K^*\varsigma$ is the operator conjugate to $K\rho$ which is defined as follows:

$$K^*\varsigma = \int_a^b \overline{k(y,x)}\varsigma(x)\,\mathrm{d}x.$$

Theorem 2.2.8 *(Fredholm's fourth theorem) Let λ_0 be an characteristic value of the kernel $k(x,y)$. In order that the inhomogeneous equation*

$$\rho(y) - \lambda_0 \int_a^b k(x,y)\rho(x)\,\mathrm{d}x = g(y)$$

has a solution, it is necessary and sufficient that its right-hand side $g(y)$ is orthogonal to all eigenfunctions of the conjugate homogeneous equation

$$\varsigma(y) - \overline{\lambda_0} \int_a^b \overline{k(y,x)}\varsigma(x)\,\mathrm{d}x = 0.$$

Let assume that $k(x,y)$ is a Hilbert-Schmidt kernel i.e. a square integrable function in the square domain $\Pi = \{(x,y) : a \le x \le b,\ a \le y \le b\}$, so that

$$\left\{ \int_a^b \int_a^b |k(x,y)|^2\,\mathrm{d}x\mathrm{d}y \right\} < \infty, \tag{2.49}$$

and $\rho(x),\ g(x) \in L_2[a,b]$, i.e.

$$\int_a^b |\rho(x)|^2\,\mathrm{d}x < \infty, \qquad \int_a^b |g(x)|^2\,\mathrm{d}x < \infty.$$

The operator K with such a kernel is bounded in $L_2[a,b]$. The norm of this operator is estimated as

$$||K||_{L_2} \le \sqrt{\int_a^b \int_a^b |k(x,y)|^2\,\mathrm{d}x\mathrm{d}y}. \tag{2.50}$$

The Fredholm theorems work also in $L_2(a,b)$. From all these four Fredholm's theorems, there follows the very often used theorem in the analysis of operator equations which is called Fredholm's alternative (see in e.g. Porter and Stirling (2004), Atkinson (1997)):

Theorem 2.2.9 *(Fredholm's alternative) Let K be a bounded linear map from L_2 to itself. Then either the inhomogeneous equation $(I - \lambda K)\rho = g(y)$ is soluble whatever its right-hand side maybe, or else the corresponding homogeneous equation $(I - \lambda K)\rho = 0$ has a non-trivial solution $\rho \in L_2$.*

2.2.3 The Neumann series

We have seen from the Fredholm alternative that a Fredholm integral operator with continuous or square integrable kernel is invertible if an associated homogeneous equation has only

trivial solutions. Besides, we can also guarantee that $(I - \lambda K)\rho$ has a bounded inverse if $||\lambda K|| < 1$. We can write $||\lambda K|| < 1$ in terms of μ, i.e., $|\mu| > ||K||$. Therefore, the exterior disc $\{\mu \in \mathbb{C} : \ |\mu| > ||K||\}$ is contained the resolvent set $\sigma'(K)$ and $\sigma'(K)$ is an open subset of $\mathbb{C}$. If $|\mu| > ||K||$, the resolvent operator is given by

$$R_\mu = (\mu I - K)^{-1} = \sum_{n=0}^{\infty} \frac{K^n}{\mu^{n+1}} \quad \text{or} \quad R_\lambda = (I - \lambda K)^{-1} = \sum_{n=0}^{\infty} \lambda^n K^n.$$

We then can write the solution of the integral equation

$$(I - \lambda K)\rho = g \tag{2.51}$$

in the Neumann series expansion i.e. (see e.g. Porter and Stirling (2004)),

$$\rho = (I - \lambda K)^{-1} g = \sum_{n=0}^{\infty} \lambda^n K^n g.$$

Since the spectrum $\sigma(K)$ of K is the complement of the resolvent set $\sigma'(K)$ which is open, it follows that the spectrum $\sigma(K)$ is a closed subset of $\mathbb{C}$ and $\sigma(K) \subset \{\mu \in \mathbb{C} : \ |\mu| \leq ||K||\}$.

It is standard to define the spectral radius of an operator K as the radius of the smallest disk centered at 0 in $\mathbb{C}$ containing the spectrum, i.e. (Hunter and Nachtergaele (2001)),

$$r(K) = |\sigma(K)| = \sup\{|\mu| : \ \mu \in \sigma(K)|\}.$$

In the case of bounded linear operator K on some Banach space, the spectral radius $r(K)$ is defined by the Gelfand formula

$$r(K) = \lim_{n \to \infty} ||K^n||^{\frac{1}{n}}.$$

Note that $r(K)$ lies between 0 and $||K||$, i.e., $0 \leq r(K) \leq ||K||$ and if K is self-adjoint, we will have $r(K) = ||K||$ (see e.g. Hunter and Nachtergaele (2001)).

There are several methods of testing the convergence or divergence of an infinite series $\sum_{n=0}^{\infty} \lambda^n K^n$ such as ratio test, root test, integral test, limit comparison test and Cauchy condensation test. Now, let us consider one of these methods e.g. the root test. Defining $r_1 = \lim_{n \to \infty} \sup ||K^n||^{1/n}$, we have the following three cases (see e.g. Hunter and Nachtergaele (2001)):

- If $r_1 < 1$, the series $\sum_{n=0}^{\infty} K^n$ converges.
- If $r_1 > 1$, the series $\sum_{n=0}^{\infty} K^n$ diverges.
- If $r_1 = 1$, the series $\sum_{n=0}^{\infty} K^n$ may converge or diverge.

The ordinary limit $\lim_{n\to\infty} ||K^n||^{1/n}$ is the common value of $\lim_{n\to\infty} \sup ||K^n||^{1/n}$ and $\lim_{n\to\infty} \inf ||K^n||^{1/n}$. Therefore, whenever the original limit exists we will have $r_1 = r(K) = \lim_{n\to\infty} ||K^n||^{1/n}$. We first consider the first case. Letting $r(K) < 1$ implies there is an R such that $r(K) < R < 1$ and an N such that $||K^n|| \leq R^n$ for all $n \geq N$. Then, it follows that for $r(K) < \mu$, the sum $\sum_{n=0}^{\infty} \lambda^n K^n$ converges and $(\mu I - K)^{-1}$ exists.

For $r(K) > 1$, there is an R such that $1 < R < r(K)$ and an N such that $||K^n|| \geq R^n$ for all $n \geq N$. Recall that the spectrum of K is contained inside the disc $\{\mu \in \mathbb{C} : \ |\mu| \leq r(K)\}$, i.e., $\sigma(K) \subset \{\mu \in \mathbb{C} : \ |\mu| \leq r(K)\}$ and that the Neumann series must diverge, so $\mu I - K$ is not invertible, for some $\mu \in \mathbb{C}$ with $|\mu| = r(K)$.

2.2.4 Compact linear operator and its spectrum

In this subsection, we will state a special theorem for a compact operator. The proof of the theorem can be found in (Kreyszig (1978)).

Previously, we said that the spectrum for a bounded linear operator on the infinite-dimensional Hilbert space L_2 may not only consist of point spectrum but also may include continuous spectrum and residual spectrum.

However, a compact operator has special properties such that the spectrum consists entirely of eigenvalues. One needs a condition for the kernel k which is sufficient for the operator K to be compact.

For the space $C^0[a, b]$ with

$$||K|| = \max_{0\leq y\leq 1} \left\{ \int_a^b k(x, y) \mathrm{d}\Gamma(x) \right\},$$

the continuity of the kernel $k : [a, b] \times [a, b] \to \mathbb{C}$ will imply compactness of the operator K. This compactness follows from Ascoli Theorem (Kreyszig (1978), Atkinson (1997)).

For space $L_2[a,b]$, the norm of this operator is estimated as in (2.50). The kernel $k : [a,b] \times [a,b] \to \mathbb{C}$ needs to be a Hilbert-Schmidt kernel such that equation (2.49) is satisfied for the operator K to be a compact operator (Conway (1990)).

The spectral theory of compact linear operators is a relatively simple generalization of the eigenvalue theory of finite matrices and resembles the finite dimensional case in many respects which can be be seen in the following theorem (Kreyszig (1978)):

Theorem 2.2.10 *A compact linear operator $K : X \to Y$ where X and Y are Banach spaces has the following properties:*

- *The set of the eigenvalues of K is countable (perhaps finite or even empty).*
- *$\mu = 0$ is the only possible accumulation point of the set of eigenvalues (limit point of the set of eigenvalues).*
- *If K is infinite dimensional, then the spectrum of K contains 0, i.e., $0 \in \sigma(K)$.*
- *Every spectral value $\mu \neq 0$ is an eigenvalue.*

In the next Section, we state the spectral properties of indirect BIEs that have been discussed in e.g. (Goursat (1964), Mikhlin (1957)) and will extend them to the discussions of direct BIEs.

2.3 Spectral properties of BIEs

Let us consider the method in investigating the spectral properties of the indirect BIEs related to the Dirichlet and Neumann problems that have been discussed in (Goursat (1964), Mikhlin (1957)). In their discussions, they studied the spectral properties of the indirect BIEs for the BVPs in 3-dimensional domains. The results also hold true for several cases of the BVPs in 2-dimensional domains (Goursat (1964)).

2.3.1 Spectral properties of indirect BIEs

We can obtain the indirect Dirichlet BIEs by seeking the solution of the Dirichlet problems in the form of the double layer potential and by taking into account the jump relations as in Theorem 2.2.3. The Dirichlet BIEs for the region Ω^+ lying inside $\partial\Omega$ and Ω^- exterior of $\partial\Omega$ are as in equations (2.52) and (2.53), respectively.

$$\psi(y_0) - 2\mathcal{W}\psi(y_0) = -2\overline{u}(y_0), \qquad \text{for region } \Omega^+,\ y_0 \in \partial\Omega, \tag{2.52}$$

$$\psi(y_0) + 2\mathcal{W}\psi(y_0) = 2\overline{u}(y_0), \qquad \text{for region } \Omega^-,\ y_0 \in \partial\Omega. \tag{2.53}$$

For the Neumann problem, we want to look for the solution in the form of single layer potential V. The Neumann BIEs for interior and exterior regions are given in (2.54) and (2.55), respectively.

$$\phi(y_0) + 2\mathcal{W}^*\phi(y_0) = 2\bar{t}(y_0) \quad \text{for region } \Omega^+,\ y_0 \in \partial\Omega, \tag{2.54}$$

$$\phi(y_0) - 2\mathcal{W}^*\phi(y_0) = -2\bar{t}(y_0) \quad \text{for region } \Omega^-,\ y_0 \in \partial\Omega. \tag{2.55}$$

We consider the following homogeneous equation:

$$\phi(y_0) + 2\zeta\mathcal{W}^*\phi(y_0) = 0. \tag{2.56}$$

Note that equation (2.56) is the homogeneous form of equations (2.55) and (2.54) when $\zeta = -1$ and $\zeta = 1$, respectively.

Goursat (1964), Mikhlin (1957) showed that $\zeta = -1$ is the regular value, and the characteristic values of (2.56) are distributed on the rays $\zeta \geq 1$ and $\zeta < -1$.

For the discussion in finding the set of characteristic values for the interior and exterior Dirichlet problems, let us consider the following equations:

$$\psi(y_0) + 2\overline{\zeta}\mathcal{W}\psi(y_0) = 0, \tag{2.57}$$

where $\overline{\zeta}$ is the conjugate of ζ. Observe that equation (2.57) is the homogeneous equation of equations (2.52) and (2.53) when $\overline{\zeta} = -1$ and $\overline{\zeta} = 1$, respectively.

We can show that ζ is real valued such that $\zeta = \overline{\zeta}$.

Therefore as in the Neumann BIEs, we have $\overline{\zeta} = -1$ as the regular value and the characteristic values are distributed on the rays $\overline{\zeta} \geq 1$ and $\overline{\zeta} < -1$.

Recall Theorem 2.2.10 that states the spectral points $\mu \neq 0$ are eigenvalues. Therefore, we conclude that the spectra of $\mathcal{W}$ and $\mathcal{W}^*$ do not include residual spectrum sets.

2.3.2 Spectral properties of direct BIEs

After obtaining the spectral properties for the indirect BIEs, we can also obtain the spectral properties for BIEs of the direct method. We have seen before that the set of the characteristic values of (2.56) lies on the rays $\zeta \geq 1$ and $\zeta < 1$ and has regular value at $\zeta = -1$. Observe that equation (2.56) is the same as equation (2.41). Therefore the set of the characteristic values of the integral equation for the Dirichlet problem obtained from the direct method also lies on the rays lies on the rays $\zeta \geq 1$ and $\zeta < -1$ with the regular value at $\zeta = -1$.

Note that the homogeneous equation (2.57) is the same as equation (2.46) i.e. the homogeneous equation for the Neumann problem obtained from the direct method. Therefore, we can conclude that $\overline{\zeta} = -1$ is the regular value of equation (2.46) and the characteristic values are distributed on the rays $\overline{\zeta} \geq 1$ and $\overline{\zeta} < -1$.

2.4 Conclusion

In this chapter, we have given brief discussion on BVPs for PDE and stated various methods in solving BVSs for PDE analytically and numerically. We focused on one of the numerical method in solving BVPs, i.e., Boundary Element Method (BEM). We discussed the formulations of Boundary Integral Equation (BIE) related with Neumann and Dirichlet problems

for the Laplace equation obtained from the direct and indirect method. The direct method is based on Green formula while the indirect method is based on the single or double layer potentials. The uniqueness and solubility of solutions for the boundary value problems for Laplace equation was also discussed. We presented four Fredholm's theorems and Fredholm's alternative theorem which are related to the solvability of Fredholm's integral equation. However, without investigating whether the homogeneous equation has only trivial solution as stated in Fredholm's alternative theorem, we can guarantee the uniqueness of the linear map $(I - \lambda K)\rho$, where λ is the characteristic value, K is the Fredholm operator and ρ is the solution, if $||\lambda K|| < 1$. If the uniqueness of the linear map is established, the Neumann iteration method for the solution of the linear map will converges. Some review on the convergence of the Neumann iteration corresponding to spectral properties of operator K is also given. We also gave the spectral properties of the integral equations related to the Dirichlet's and Neumann's problems obtained from the indirect method in three dimensions as studied in e.g. (Goursat (1964), Mikhlin (1957)). We employed the spectral properties for the BIEs obtained from the indirect method for the discussion on the spectral properties of the direct BIEs.

Chapter 3

The Boundary-Domain Integral Equation for Neumann Problem

3.1 Introduction

In Chapter 2, it has been discussed that we can reduce a boundary-value problem (BVP) for a partial differential equation (PDE) to a boundary-integral equation (BIE) useful for numerical implementation. However, in order for the reduction to be enabled, it is necessary to ensure the availability of the fundamental solution for the PDE. It is well-known that the fundamental solutions are explicitly known for many equations with constant coefficients a, where they can be computed, e.g. by Fourier transformation. Unfortunately, such a fundamental solution is not available in the general case of partial differential operators with coefficients varying throughout the domain.

In handling such case, we can use a parametrix (Levi function), which is wider available, instead of the fundamental solution, see in e.g. (Mikhailov (2002), Hilbert (1912), Miranda (1970), Pomp (1998) and references therein). This option allows reduction of the PDEs with variable coefficients not to boundary integral equation (BIE) but to boundary-domain integral equation (BDIE) or boundary-domain integro-differential equation (BDIDE).

In the beginning of this chapter, we will give an introduction to the derivation of BDIE

related to Neumann's and Dirichlet's problems for PDE with variable coefficient.

We also give an overview on how we approximate the BDIEs on two-dimensional domains. We will discretize the boundary $\partial\Omega$ of our test domains by using the boundary linear elements and the domain Ω is meshed into quadrilateral domain elements. We also describe how element contributions obtained from the integration of each segment/element will be assembled to a global matrix based on the relation between local nodes and global nodes.

For the numerical experiments, we present results of numerical implementations on the perturbed BDIE related to the Neumann problem for PDE with variable coefficient. Then the system obtained from BDIE (discretised BDIE) related to Neumann problem is solved by the Neumann iterations and LU decomposition method. The spectral properties obtained numerically from the discrete BDIE operator will be presented. The details on the convergence of the iterative method is discussed in relation with the maximal eigen-values of the corresponding discrete BDIE operator obtained numerically.

The numerical results for BDIDE related to the Dirichlet problem for PDE with variable coefficient will be discussed in the next chapter.

3.2 The Boundary-Domain Integral Equation

Let us consider the following linear second-order elliptic PDE:

$$Lu(x) = \sum_{i=1}^{n} \frac{\partial}{\partial x_i} a(x) \frac{\partial}{\partial x_i} u(x) = f(x), \tag{3.1}$$

where $u(x)$ is the unknown function, while $f(x)$, and $a(x) > const > 0$ are prescribed functions.

Suppose $P(x, y)$ is a parametrix for the operator L in (3.1), that is, it satisfies the following equation:

$$L_x P(x, y) = \delta(x - y) + R(x, y), \tag{3.2}$$

where $\delta(x - y)$ is the Dirac delta function and the remainder $R(x, y)$ may have a weak singularity at most, at $x = y$.

A parametrix for PDE with variable coefficient as in (3.1) is given by the fundamental solution for the same equation but with 'frozen coefficients' $a(x) = a(y)$ i.e.

$$P(x,y) = \frac{\ln|x-y|}{2\pi a(y)}, \quad x,y \in \mathbb{R}^2, \tag{3.3}$$

$$P(x,y) = -\frac{1}{4\pi a(y)\,|x-y|}, \quad x,y \in \mathbb{R}^3, \tag{3.4}$$

where $|x-y| = \sqrt{(x_i-y_i)(x_i-y_i)}$.

The remainder $R(x,y)$ can be calculated using equations (3.2), (3.3) and (3.4) which are as in the following:

$$R(x,y) = \frac{x_i-y_i}{2\pi a(y)\,|y-x|^2}\frac{\partial a(x)}{\partial x_i}, \quad x,y \in \mathbb{R}^2, \tag{3.5}$$

$$R(x,y) = \frac{x_i-y_i}{4\pi a(y)\,|y-x|^3}\frac{\partial a(x)}{\partial x_i}, \quad x,y \in \mathbb{R}^3. \tag{3.6}$$

Let $v(x) = P(x,y)$ and take $u(x)$ as a solution of equation (3.1), we can then write the Green's formula (2.12) as follows:

$$\begin{aligned} c(y)u(y) &- \int_{\partial\Omega} [u(x)T_x P(x,y) - P(x,y)Tu(x)]\,\mathrm{d}\Gamma(x) \\ &+ \int_\Omega R(x,y)u(x)\,\mathrm{d}\Omega(x) = \int_\Omega P(x,y)f(x)\,\mathrm{d}\Omega(x), \end{aligned} \tag{3.7}$$

where $c(y)$ is the same as in (2.14).

As described in (Mikhailov (2002)), substituting boundary condition (2.3) in the integrals in (3.7) and taking (3.7) at $y \in \Omega \cup \partial\Omega$ will give the linear direct boundary-domain integral equation, BDIE.

For the pure Neumann problem, the BDIE is as given below.

$$\begin{aligned} c(y)u(y) &- \int_{\partial\Omega} u(x)T_x P(x,y)\,\mathrm{d}\Gamma(x) + \int_\Omega R(x,y)u(x)\,\mathrm{d}\Omega(x) \\ &= -\int_{\partial_N\Omega} P(x,y)\bar{t}(x)\,\mathrm{d}\Gamma(x) + \int_\Omega P(x,y)f(x)\,\mathrm{d}\Omega(x), \quad y \in \Omega\cup\partial\Omega. \end{aligned} \tag{3.8}$$

The Neumann problem is not unconditionally solvable, and when it is solvable, its solution can only be unique up to an additive constant. These properties are inherited by the BDIE, cf. (Chkadua et al. (2011a)).

As in (Mikhailov and Nakhova (2005)), one can add the perturbation operator

$$[Qu] := \frac{1}{|\partial\Omega|}\int_{\partial\Omega} u(x)\,\mathrm{d}\Gamma(x). \tag{3.9}$$

to equation (3.8) where $|\partial\Omega| = \int_{\partial\Omega}\mathrm{d}\Gamma(x)$ i.e. denotes the length of the boundary $\partial\Omega$.

Therefore, we obtain the perturbed Neumann BDIE as follows:

$$\begin{aligned} c(y)u(y) \;&-\; \int_{\partial\Omega} u(x)T_xP(x,y)\,\mathrm{d}\Gamma(x) + \frac{1}{|\partial\Omega|}\int_{\partial\Omega} u(x)\,\mathrm{d}\Gamma(x) \\ &+\; \int_{\Omega} R(x,y)u(x)\,\mathrm{d}\Omega(x) = -\int_{\partial\Omega} P(x,y)\bar{t}(x)\,\mathrm{d}\Gamma(x) \\ &+\; \int_{\Omega} P(x,y)f(x)\,\mathrm{d}\Omega(x), \qquad y\in\Omega\cup\partial\Omega. \end{aligned} \tag{3.10}$$

Using results of (Mikhailov (1999)), one can prove that equation (3.10) is uniquely solvable for any right-hand side and moreover, when the solvability condition for equation (3.8) is satisfied, one of its solutions, such that

$$\int_{\partial\Omega} u(x)\,\mathrm{d}\Gamma(x) = 0,$$

is delivered by the solution of its perturbed counterpart (3.10).

In the next subsection, we will discuss the discretization of the BDIE for the pure Neumann problem as in equation (3.10).

The Discretization of the BDIE with Linear Element

In order to evaluate the boundary integral involved in the boundary-domain integral equation (3.8), the boundary is represented as an L-sides polygon i.e. $\partial\Omega \simeq \partial\Omega_1\cup\partial\Omega_2\cup\cdots\cup\partial\Omega_L$. In the linear element technique, the nodes are allocated at the edges of elements and boundary values are linearly interpolated in between.

For the integral over domain Ω, we discretized the domain into M quadrilateral elements $\Omega_m \subset \Omega,\ 1 \le m \le M$. The domain is represented as $\Omega \simeq \Omega_1\cup\Omega_2\cup\cdots\cup\Omega_M$.

Similar to the finite element approximation, the unknown function $u(x)$ at any point $x\in\overline{\Omega}$ is interpolated over its values $u(x^j)$ at the global nodes x^j as,

$$u(x) = \sum_{j=1}^{J}\phi_j(x)u(x^j), \qquad x, x^j \in \Omega\cup\partial\Omega,$$

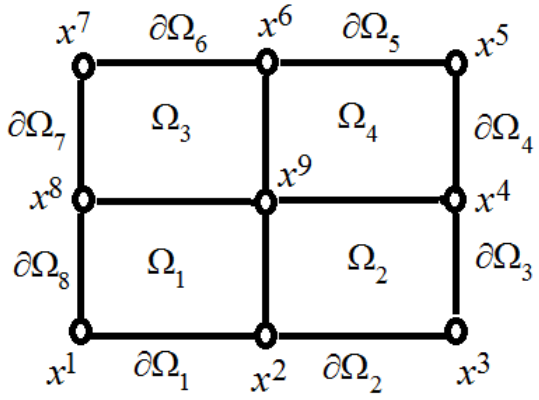

Figure 3.1: Figure shows $\partial\Omega_l$ and Ω_m on a rectangle domain with 9 nodes.

where $\phi_j(x)$ is the global shape function and J is the number of nodes.

By applying the interpolation to equation (3.10) and placing the collocation point x^i at all J nodes of the mesh, we get the system of J linear algebraic equations for J unknowns $u(x^j)$, as follows

$$c(x^i)u(x^i) + \sum_{x^j \in \overline{\Omega}} K_{ij} u(x^j) + \sum_{x^j \in \Gamma} \overset{\circ}{K}_{ij} u(x^j) = \sum_{x^j \in \partial\Omega} Q_{ij} \bar{t}(x^j) + D_i, \quad x^i \in \overline{\Omega}, \tag{3.11}$$

where K_{ij}, $\overset{\circ}{K}_{ij}$, Q_{ij} and D_{ij} are defined as in the following:

$$K_{ij} = -\int_{\partial\Omega} \phi_j(x) T_x P(x^i, x)\, \mathrm{d}\Gamma(x) + \int_{\Omega} \phi_j(x) R(x^i, x)\, \mathrm{d}\Omega(x), \tag{3.12}$$

$$\overset{\circ}{K}_{ij} = \frac{1}{|\partial\Omega|} \int_{\partial\Omega} \phi_j(x)\, \mathrm{d}\Gamma(x), \tag{3.13}$$

$$Q_{ij} = -\int_{\partial\Omega} \phi_j(x) P(x^i, x)\, \mathrm{d}\Gamma(x), \tag{3.14}$$

$$D_i = \int_{\Omega} P(x^i, x) f(x)\, \mathrm{d}\Omega(x). \tag{3.15}$$

The boundary $\partial\Omega$ and the domain Ω in (3.12)-(3.15) are then approximated by $\partial\Omega = \bigcup_l \partial\Omega_l$ and $\Omega = \bigcup_m \Omega_m$ respectively.

Therefore, we obtain

$$K_{ij} = -\sum_{l=1}^{L} \int_{\partial\Omega_l} \phi_j(x) T_x P(x^i, x)\, \mathrm{d}\Gamma(x) + \sum_{m=1}^{M} \int_{\Omega_m} \phi_j(x) R(x^i, x)\, \mathrm{d}\Omega(x),$$

$$\begin{aligned}
\overset{\circ}{K}_{ij} &= \frac{1}{|\partial\Omega|}\sum_{l=1}^{L}\int_{\partial\Omega_l}\phi_j(x)\,\mathrm{d}\Gamma(x),\\
Q_{ij} &= -\sum_{l=1}^{L}\int_{\partial\Omega_l}\phi_j(x)P(x^i,x)\,\mathrm{d}\Gamma(x),\\
D_i &= \sum_{m=1}^{M}\int_{\Omega_m}P(x^i,x)f(x)\,\mathrm{d}\Omega(x),
\end{aligned}$$

which can be written as follows:

$$K_{ij} = -\sum_{\partial\Omega_l\ni x^j}\int_{\partial\Omega_l}\phi_j(x)T_xP(x^i,x)\,\mathrm{d}\Gamma(x)+\sum_{\Omega_m\ni x^j}\int_{\Omega_m}\phi_j(x)R(x^i,x)\,\mathrm{d}\Omega(x), \quad (3.16)$$

$$\overset{\circ}{K}_{ij} = \frac{1}{|\partial\Omega|}\sum_{\partial\Omega_l\ni x^j}\int_{\partial\Omega_l}\phi_j(x)\,\mathrm{d}\Gamma(x), \quad (3.17)$$

$$Q_{ij} = -\sum_{\partial\Omega_l\ni x^j}\int_{\partial\Omega_l}\phi_j(x)P(x^i,x)\,\mathrm{d}\Gamma(x), \quad (3.18)$$

$$D_i = \sum_{m=1}^{M}\int_{\Omega_m}P(x^i,x)f(x)\,\mathrm{d}\Omega(x). \quad (3.19)$$

Instead of writing (3.16)-(3.19) in global node numbering, it is useful for numerical purposes to write them in terms of local nodes numbering.

The relations between the local node (x_n^l or x_N^m) and the global node x^j are as follows:

$$x^j = x^{j(l,n)}=x_n^l,\ \text{for } x_n^l\in\partial\Omega_l,\quad 1\le l\le L,\ n=1,2, \quad (3.20)$$

$$x^j = x^{j(m,N)}=x_N^m,\ \text{for } x_N^m\in\Omega_m,\quad 1\le m\le M,\ N=1,\cdots,4. \quad (3.21)$$

This implies

$$u(x^j) = u(x_n^l),\ \text{for } x_n^l\in\partial\Omega_l,\quad 1\le l\le L,\ n=1,2, \quad (3.22)$$

$$u(x^j) = u(x_N^m),\ \text{for } x_N^m\in\Omega_m,\quad 1\le m\le M,\ N=1,\cdots,4. \quad (3.23)$$

We can express the coordinates of a point placed somewhere in the one-dimensional element using an intrinsic coordinate η. The Cartesian coordinates of a point on boundary element $\partial\Omega_l\subset\partial\Omega$ with the intrinsic coordinate η are given by

$$\begin{Bmatrix} x_1(\eta)\\ x_2(\eta)\end{Bmatrix}=\sum_{n=1}^{2}\Psi_n(\eta)\begin{Bmatrix} x_{1n}^l\\ x_{2n}^l\end{Bmatrix},\quad -1\le\eta\le 1, \quad (3.24)$$

where $\Psi_n(\eta)$ are element shape functions.

There are two nodes for each element $\partial\Omega_l$ and the shape functions are given as in the following (see e.g. Beer (2001)):

$$\Psi_1(\eta) = \frac{1}{2}(1-\eta), \tag{3.25}$$

$$\Psi_2(\eta) = \frac{1}{2}(1+\eta), \qquad -1 \le \eta \le 1. \tag{3.26}$$

For the the discretization of integrals over domain Ω, the derivation is analogous to the boundary integral case except that now there are two intrinsic coordinates $\xi = (\xi_1, \xi_2)$ instead of only one intrinsic coordinate η. In our work, we discretized the domain into several quadrilateral elements where each element consists of four straight edges defined by four vertices.

The Cartesian coordinates of a point on a domain element $\Omega_m \subset \Omega$ with the intrinsic coordinate $\xi = (\xi_1, \xi_2)$ are given as follows

$$\left\{ \begin{array}{c} x_1(\xi) \\ x_2(\xi) \end{array} \right\} = \sum_{N=1}^{4} \Phi_N(\xi) \left\{ \begin{array}{c} x_{1N}^m \\ x_{2N}^m \end{array} \right\}, \qquad -1 \le \xi_1 \le 1,\ -1 \le \xi_2 \le 1,$$

where $\Phi_N(\eta)$ are local shape functions.

For the linear isoparametric two-dimensional elements, there are four nodes for each element Ω_m, and the shape functions are given as in the following:

$$\begin{aligned} \Phi_1(\xi) &= \frac{1}{4}(1-\xi_1)(1-\xi_2), \\ \Phi_2(\xi) &= \frac{1}{4}(1+\xi_1)(1-\xi_2), \\ \Phi_3(\xi) &= \frac{1}{4}(1+\xi_1)(1+\xi_2), \\ \Phi_4(\xi) &= \frac{1}{4}(1-\xi_1)(1+\xi_2). \end{aligned}$$

For the boundary element, equation (3.24) implies that the tangent vector in the η direction can be written as in the following:

$$\frac{\partial \mathbf{x}}{\partial \eta} = \frac{\partial}{\partial \eta} \left\{ \begin{array}{c} x_1(\eta) \\ x_2(\eta) \end{array} \right\} = \sum_{n=1}^{2} \frac{\partial \Psi_n(\eta)}{\partial \eta} \left\{ \begin{array}{c} x_{1n}^l \\ x_{2n}^l \end{array} \right\}, \quad x \in \partial\Omega_l. \tag{3.27}$$

It can be established that the Jacobian $J_{l1} = |\partial\Omega_l|/2$ where $|\partial\Omega_l|$ represents the length of each boundary element $\partial\Omega_l$ i.e.

$$|\mathrm{d}\Gamma| = \sqrt{\left(\frac{\mathrm{d}x_1}{\mathrm{d}\eta}\right)^2 + \left(\frac{\mathrm{d}x_2}{\mathrm{d}\eta}\right)^2}\,\mathrm{d}\eta = J_{l1}(\eta)\,\mathrm{d}\eta, \quad 1 \le l \le L.$$

The Jacobian matrix of the mapping from the x_1x_2 to the $\xi_1\xi_2$ plane is defined as

$$V_2 = \begin{pmatrix} \partial x_1/\partial\xi_1 & \partial x_2/\partial\xi_1 \\ \partial x_1/\partial\xi_2 & \partial x_2/\partial\xi_2 \end{pmatrix}.$$

The determinant of the Jacobian matrix is the surface metric coefficient,

$$J_{m2}(\xi) = \mathrm{Det}\mathrm{V}_2 = \frac{\partial x_1}{\partial\xi_1}\frac{\partial x_2}{\partial\xi_2} - \frac{\partial x_1}{\partial\xi_2}\frac{\partial x_2}{\partial\xi_1}, \quad 1 \le m \le M.$$

The elements $\partial\Omega_l$ and Ω_m are mapped to the reference elements i.e. $\partial\Omega_l$ is mapped to the segment $-1 \le \eta \le 1$ and Ω_m is mapped to the square such that $-1 \le \xi_1 \le 1$ and $-1 \le \xi_2 \le 1$.

Therefore, we can write equations (3.16)-(3.19) as follows:

$$\begin{aligned}
K_{ij} &= -\sum_{\Gamma_l \ni x^j} A^l_{n(j,l),i} + \sum_{\Omega_m \ni x^j} G^m_{N(j,m),i}, \\
\overset{\circ}{K}_{ij} &= \frac{1}{|\partial\Omega|}\sum_{\Gamma_l \ni x^j} B^l_{n(j,l),i}, \\
Q_{ij} &= -\sum_{\Gamma_l \ni x^j} F^l_{n(j,l),i}, \\
D_i &= \sum_{m=1}^{M} H^m_i,
\end{aligned}$$

where $n(j,l)$ is the local number of the node x^j on the boundary element Γ_l, $N(j,m)$ is the local number of the node x^j on the domain element Ω_m.

The integrals that we have to evaluate are denoted as

$$A^l_{ni} = \int_{-1}^{1} \Psi_n(\eta) T_x P(x^i, x(\eta)) J_{l1}(\eta)\,\mathrm{d}\eta, \tag{3.28}$$

$$B^l_{ni} = \int_{-1}^{1} \Psi_n(\eta) J_{l1}(\eta)\,\mathrm{d}\eta, \tag{3.29}$$

$$F_{ni}^{l} = \int_{-1}^{1} \Psi_n(\eta) P(x^i, x(\eta)) J_{l1}(\eta)\, \mathrm{d}\eta, \tag{3.30}$$

$$G_{Ni}^{m} = \int_{-1}^{1}\int_{-1}^{1} \Phi_N(\xi) R(x^i, x(\xi)) J_{m2}(\xi)\, \mathrm{d}\xi_1 \mathrm{d}\xi_2, \tag{3.31}$$

$$H_{i}^{m} = \int_{-1}^{1}\int_{-1}^{1} P(x^i, x(\xi)) f(x(\xi)) J_{m2}(\xi)\, \mathrm{d}\xi_1 \mathrm{d}\xi_2. \tag{3.32}$$

The integrals in (3.28)-(3.32) are evaluated by Gauss-Legendre integration formulas. The Gauss-Legendre integration formulas in one-dimensional and two-dimensional cases, respectively are (see e.g. Beer (2001)):

$$\int_{-1}^{1} f(\eta)\, \mathrm{d}\eta = \sum_{i=1}^{\imath} W_i f(\eta_i),$$

$$\int_{-1}^{1}\int_{-1}^{1} f(\xi)\, \mathrm{d}\xi_1 \mathrm{d}\xi_2 = \sum_{j=1}^{\jmath}\sum_{i=1}^{\imath} W_i W_j f(\xi_{1i}, \xi_{2j}),$$

where $\imath$ and $\jmath$ are the number of quadrature points used to evaluate the integrals, and ξ_{1i} and ξ_{2j} are quadrature point abscissas. The weights associated to point i and j are denoted as W_i and W_j, respectively.

However, special treatment has to be taken when the collocation point x^i is an element node or is close to the integration element since the kernels of the integrals (3.28), (3.29),(3.31) and (3.32) are singular at the collocation points. This will prevent us from using the normal Gauss-Legendre integral formula.

For calculating the first integral (3.28) when the collocation point x^i belongs to the integration element i.e when $x^i = s_1$ or $x^i = s_2$ (refer Figure 3.2), $\overrightarrow{r} = \overrightarrow{(x^i, x(\eta))}$ and ν are perpendicular to each other along the interval of integration. Therefore, $T_x P(x, y)$ becomes

$$T_x P(x, x^i) = \frac{\cos 90^\circ}{2\pi\ r} = 0.$$

From relation in (3.20), we have $A_{ni}^{l} = A_{j(l,n),i}$. Therefore, when $x^i = x^j$,

$$A_{j(l,n),i} = A_{ii} = \lim_{\varepsilon \to 0} \int_{-1+\varepsilon}^{1} \frac{\Phi(\eta) \cos 90^\circ}{2\pi r} J_{l1}(\eta)\, \mathrm{d}\eta = 0.$$

We will use linear semi-analytic method to handle the influence of the singularity $1/r$ when the collocation point x^i is near to the integration element. As the beginning of the

discussion in this semi-analytic method, we introduce the following notations (See Figure 3.2):

$$W_1 = \left|x^i - x(s_{l1})\right|, \tag{3.33}$$

$$W_2 = \left|x(s_{l2}) - x(s_{l1})\right|, \tag{3.34}$$

$$W_3 = \left(x^i - x(s_{l1})\right) \cdot \left(x(s_{l2}) - x(s_{l1})\right), \tag{3.35}$$

$$\widetilde{e} = \left(\widehat{W}_1 \cdot \widehat{W}_2\right)^2 = \left(\frac{\overrightarrow{W}_1 \cdot \overrightarrow{W}_2}{W_1 W_2}\right)^2 = \left(\frac{W_3}{W_1 W_2}\right)^2, \tag{3.36}$$

$$h = \frac{\left|\overrightarrow{W}_1 \times \overrightarrow{W}_2\right|}{W_2} = \frac{W_1 W_2 \sqrt{1 - \left(\widehat{W}_1 \cdot \widehat{W}_2\right)^2}}{W_2} = W_1\sqrt{1-\widetilde{e}}, \tag{3.37}$$

$$d = W_2 \cos\theta = \overrightarrow{W}_2 \cdot \widehat{W}_1 = \frac{\overrightarrow{W}_1 \cdot \overrightarrow{W}_2}{W_1} = \frac{W_3}{W_1}, \tag{3.38}$$

$$s = \frac{W_2}{2}(\eta + 1). \tag{3.39}$$

Here $\widehat{W}_1$ and $\widehat{W}_2$ are the unit vector.

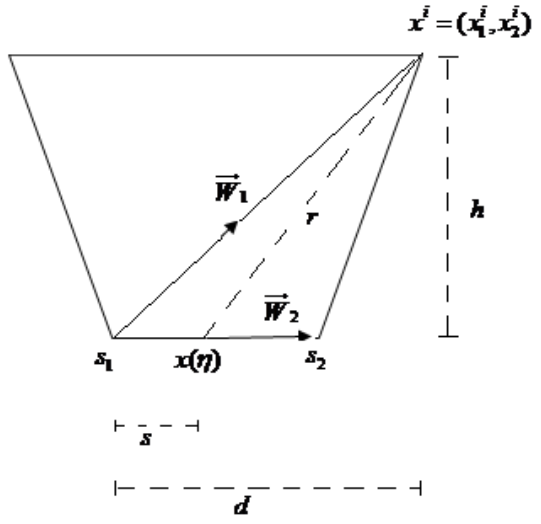

Figure 3.2: Illustration of the notations used in describing this semi-analytic method.

Evidently,

$$T_x P(x, x^i) = \left(\left(\left(x_1 - x_1^i\right)\nu_1(x) + \left(x_2 - x_2^i\right)\nu_2(x)\right)\frac{a(x)}{2\pi r^2 a(x^i)}\right),$$

We also define

$$\begin{aligned} T_x^{(1)} P(x,x^i) &= \left(\left(\left(x_1(s_{l1}) - x_1^i\right) \nu_1(x) + \left(x_2(s_{l1}) - x_2^i\right) \nu_2(x) \right) \frac{a(x(s_{l1}))}{2\pi r^2 a(x^i)} \right), \\ T_x^{(2)} P(x,x^i) &= \left(\left(\left(x_1(s_{l2}) - x_1^i\right) \nu_1(x) + \left(x_2(s_{l2}) - x_2^i\right) \nu_2(x) \right) \frac{a(x(s_{l2}))}{2\pi r^2 a(x^i)} \right), \end{aligned}$$

where $r = |x - x^i|$.

The semi-analytic formula is arranged as follows:

$$\sum_{l=1}^{L} \int_{\partial\Omega_l} T_x P(x,x^i) d\Gamma(x) = G_B + G_A,$$

where

$$\begin{aligned} G_B &= \sum_{l=1}^{L} \int_{\partial\Omega_l} \left(T_x P(x,x^i) - G_a \right) \, \mathrm{d}\Gamma(x), \\ G_a &= \left(\frac{s_{l2} - s}{s_{l2} - s_{l1}} \right) T_x^{(1)} P(x,x^i) \phi_j(x(s_{l1})) + \left(\frac{s - s_{l1}}{s_{l2} - s_{l1}} \right) T_x^{(2)} P(x,x^i) \phi_j(x(s_{l2})), \\ G_A &= \sum_{l=1}^{L} \int_{\partial\Omega_l} \left(\frac{s_{l2} - s}{s_{l2} - s_{l1}} \right) T_x^{(1)} P(x,x^i) \phi_j(x(s_{l1})) \, \mathrm{d}s \\ &+ \sum_{l=1}^{L} \int_{\partial\Omega_l} \left(\frac{s - s_{l1}}{s_{l2} - s_{l1}} \right) T_x^{(2)} P(x,x^i) \phi_j(x(s_{l2})) \, \mathrm{d}s \\ &= \sum_{l=1}^{L} \int_{s_{l1}}^{s_{l2}} \left(\frac{s_{l2} - s}{s_{l2} - s_{l1}} \right) T_x^{(1)} P(x,x^i) \phi_j(x(s_{l1})) \, \mathrm{d}s \\ &+ \sum_{l=1}^{L} \int_{s_{l1}}^{s_{l2}} \left(\frac{s - s_{l1}}{s_{l2} - s_{l1}} \right) T_x^{(2)} P(x,x^i) \phi_j(x(s_{l2})) \, \mathrm{d}s. \end{aligned} \tag{3.40}$$

The idea in this method is to calculate integrals of G_B by using normal Gaussian quadrature and integrals in G_A will be calculated analytically.

Since

$$(s_{l2} - s) = \frac{(s_{l2} - s_{l1})}{2} (1 - \eta), \tag{3.41}$$

$$(s - s_{l1}) = \frac{(s_{l2} - s_{l1})}{2} (1 + \eta), \tag{3.42}$$

we can then write (3.40) as

$$G_A = \sum_{l=1}^{L} \int_{s_{l1}}^{s_{l2}} \phi_j(x(s_{l1})) \left(\frac{1 - \eta}{2} \right) T_x^{(1)} P(x,x^i) \, \mathrm{d}s$$

$$
\begin{aligned}
&+ \sum_{l=1}^{L} \int_{s_{l1}}^{s_{l2}} \phi_j(x(s_{l2})) \left(\frac{1+\eta}{2}\right) T_x^{(2)} P(x, x^i)\, \mathrm{d}s \\
&= \sum_{l=1}^{L} \frac{\phi_j(x(s_{l1}))a(x(s_{l1}))h_{l1}}{4\pi a(x^i)} \int_{-1}^{1} (1-\eta)\, \frac{1}{r^2} \frac{ds}{d\eta}\, \mathrm{d}\eta \\
&+ \sum_{l=1}^{L} \frac{\phi_j(x(s_{l2}))a(x(s_{l2}))h_{l2}}{4\pi a(x^i)} \int_{-1}^{1} (1+\eta)\, \frac{1}{r^2} \frac{ds}{d\eta}\, \mathrm{d}\eta, \qquad (3.43)
\end{aligned}
$$

where

$$
\begin{aligned}
h_{l1} &= \left(\left(x_1(s_{l1}) - x_1^i\right) \nu_1(x) + \left(x_2(s_{l1}) - x_2^i\right) \nu_2(x)\right), \\
h_{l2} &= \left(\left(x_1(s_{l2}) - x_1^i\right) \nu_1(x) + \left(x_2(s_{l2}) - x_2^i\right) \nu_2(x)\right).
\end{aligned}
$$

Defining

$$
g_{A1} = \int_{-1}^{1} (1-\eta)\, \frac{1}{r^2} \frac{ds}{d\eta}\, \mathrm{d}\eta, \qquad (3.44)
$$

$$
g_{A2} = \int_{-1}^{1} (1+\eta)\, \frac{1}{r^2} \frac{ds}{d\eta}\, \mathrm{d}\eta, \qquad (3.45)
$$

equation (3.43) can be written as

$$
G_A = \sum_{l=1}^{L} \frac{\phi_j(x(s_{l1}))a(x(s_{l1}))h_{l1}}{4\pi a(x^i)} g_{A1} + \sum_{l=1}^{L} \frac{\phi_j(x(s_{l2}))a(x(s_{l2}))h_{l2}}{4\pi a(x^i)} g_{A2}.
$$

The integrals (3.44) and (3.45) are calculated analytically.

The radius r can be written as

$$
r = \sqrt{h^2 + (d-s)^2}, \qquad (3.46)
$$

where h, d and s are defined in (3.37)-(3.39).

Therefore we can write (3.44) and (3.45) as

$$
g_{A1} = \int_{-1}^{1} \left(\frac{1-\eta}{h^2 + (d-s)^2}\right) \frac{ds}{d\eta}\, \mathrm{d}\eta, \qquad (3.47)
$$

$$
g_{A2} = \int_{-1}^{1} \left(\frac{1+\eta}{h^2 + (d-s)^2}\right) \frac{ds}{d\eta}\, \mathrm{d}\eta. \qquad (3.48)
$$

The analytic solutions for integrals and in (3.47) and (3.48) are

$$
g_{A1} = \frac{\left(2J_{l1}(\eta)\left(2\left(W_2^2 - W_3\right) f_1 - \sqrt{W_1^2 W_2^2 - W_3^2} f_2\right)\right)}{\left(W_2^2 \sqrt{W_1^2 W_2^2 - W_3^2}\right)}, \qquad (3.49)
$$

$$g_{A2} = \frac{(2J_{l1}(\eta)(2W_3 f_1 + \sqrt{W_1^2W_2^2 - W_3^2}f_2))}{(W_2^2\sqrt{W_1^2W_2^2 - W_3^2})}, \tag{3.50}$$

where

$$\begin{aligned} J_{l1}(\eta) &= \frac{ds}{d\eta} = \frac{W_2}{2}, \\ f_1 &= ArcTan\left[\frac{\sqrt{W_1^2W_2^2 - W_3^2}}{(W_1^2 - W_3)}\right], \qquad (3.51) \\ f_2 &= \ln\left[\frac{(W_1^2 + W_2^2 - 2W_3)}{W_1^2}\right]. \qquad (3.52) \end{aligned}$$

Defining

$$\begin{aligned} \widetilde{c} &= \cos\theta = \frac{W_3}{W_1W_2}, \\ \kappa &= \frac{W_1}{W_2}, \end{aligned}$$

we can then write (3.49) -(3.52) as

$$g_{A1} = \left(-\left(\frac{(2(\widetilde{c}W_1W_2 - W_2^2)f_1)}{(\sqrt{1-\widetilde{c}^2}W_1W_2^2)}\right) - \frac{f_2}{W_2}\right), \tag{3.53}$$

$$g_{A2} = \left(\frac{2\widetilde{c}f_1}{\sqrt{1-\widetilde{c}^2}W_2} + \frac{f_2}{W_2}\right), \tag{3.54}$$

$$f_1 = ArcTan\left[\frac{\sqrt{1-\widetilde{c}^2}}{(\kappa - \widetilde{c})}\right], \tag{3.55}$$

$$f_2 = \ln\left[1 + \frac{1}{\kappa^2} - \frac{2\widetilde{c}}{\kappa}\right]. \tag{3.56}$$

The second integral (3.30) i.e. the integral of F_{ni}^l for $x^i = x^j$ involves the weak singularity. The integration with the kernel involving $\ln(1/r)$ can be be evaluate numerically by using the modified Gauss Quadrature called the Gauss-Laguerre integration i.e.

$$\int_0^1 f(\overline{\eta})\ln\left(\frac{1}{\overline{\eta}}\right)\mathrm{d}\eta \approx \sum_{i=1}^{\imath} W_i f(\overline{\eta}_i),$$

where $\imath$ is the number of integration points, see e.g. Beer (2001). Note that for this integration scheme, we have singularity at $\bar{\eta} = 0$ and the limits are from 0 to 1. Therefore, the change of coordinates has to be made in order that the integral (3.29) can be calculated using the Gauss-Laguerre integration formula. The change in coordinate is given by

$$\eta = 2\overline{\eta} - 1 \qquad \text{when } x^i \text{ is at the first node of the element } \partial\Omega_l,$$

$$\eta = 1 - 2\overline{\eta} \qquad \text{when } x^i \text{ is at the second node of the element } \partial\Omega_l.$$

Note that for the numerical integrals over domain, we have singular integrals G^m_{Ni} and H^m_i whenever the collocation point x^i is a node $x^j = x^m_N$ belongs to the element.

In order to evaluate the integrals when x^i is a node of the integration element, we split the element into triangular subelements as explained in (Beer (2001)).

We divide the element into two triangles and the formulas are as follows

$$G^m_{Ni} = \sum_{s=1}^{2} \int_{-1}^{1}\int_{-1}^{1} \Phi_N(\overline{\xi}) R(x^i, x(\overline{\xi})) J_m(\overline{\xi}) \overline{J}_{m2}(\overline{\xi})\, \mathrm{d}\overline{\xi}_1 \overline{\xi}_2,$$

$$H^m_i = \sum_{s=1}^{2} \int_{-1}^{1}\int_{-1}^{1} P(x^i, x(\overline{\xi})) f(x(\overline{\xi})) J_m(\overline{\xi}) \overline{J}_{m2}(\overline{\xi})\, \mathrm{d}\overline{\xi}_1 \overline{\xi}_2,$$

where $\overline{J}_{m2}(\overline{\xi})$ is the Jacobian from $\overline{\xi}$ to ξ.

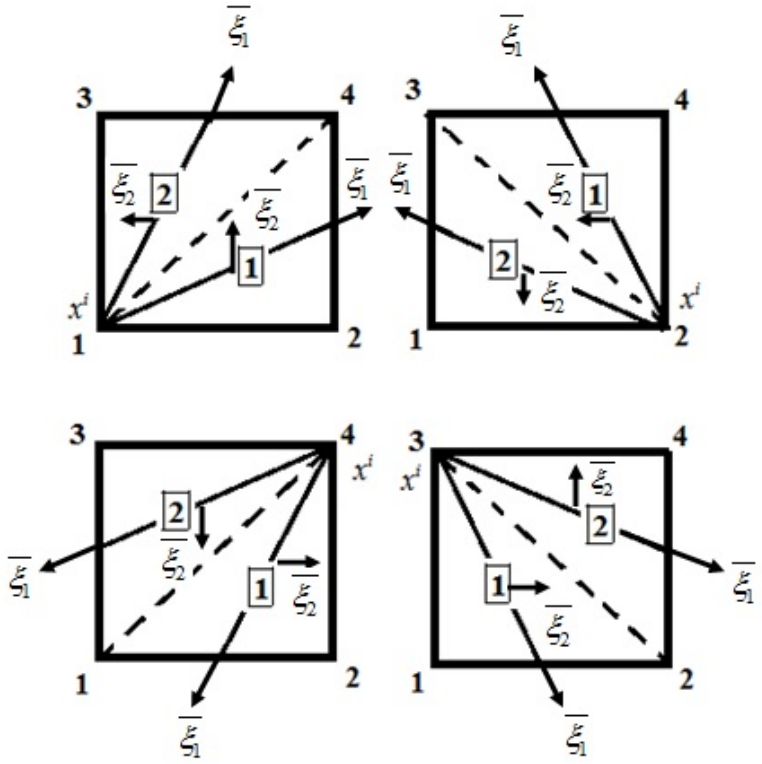

Figure 3.3: Triangular subelements for numerical integration when x^i is a node of an element.

The transformation from local coordinates to sub-element coordinates is given by the following formulas:

$$\xi_1(\overline{\xi}) = \sum_{j \in tri_s} \overline{\Phi}_j(\overline{\xi}) \xi_{1t(j)}, \qquad \xi_2(\overline{\xi}) = \sum_{j \in tri_s} \overline{\Phi}_j(\overline{\xi}) \xi_{2t(j)},$$

where tri_s is triangular element, $\overline{\xi} = \overline{\xi_1}, \overline{\xi_2}$, and $s = 1, 2$.

The local node number of sub-element node $t(j),\ j = 1, \ldots, 3$ are arranged according to the following table:

Table 3.1: The local node number of sub-element node $t(j)$.

x_i at node	Subelement 1			Subelement 2		
	$j=1$	$j=2$	$j=3$	$j=1$	$j=2$	$j=3$
1	2	3	1	3	4	1
2	3	4	2	4	1	2
3	1	2	3	4	1	3
4	1	2	4	2	3	4

The shape functions $\overline{N}_j(\overline{\xi_1}, \overline{\xi_2})$ for each triangle element tri_s are given as in the following:

$$\begin{aligned}
\overline{\Phi}_1(\overline{\xi}) &= \frac{1}{4}(1+\overline{\xi}_1)(1-\overline{\xi}_2), \\
\overline{\Phi}_2(\overline{\xi}) &= \frac{1}{4}(1+\overline{\xi}_1)(1+\overline{\xi}_2), \\
\overline{\Phi}_3(\overline{\xi}) &= \frac{1}{2}(1-\overline{\xi}_1).
\end{aligned}$$

The Jacobian $\overline{J}_{m2}(\overline{\xi})$ is given by

$$\overline{J}_{m2}(\overline{\xi}) = \frac{\partial \xi_1}{\partial \overline{\xi}_1}\frac{\partial \xi_2}{\partial \overline{\xi}_2} - \frac{\partial \xi_2}{\partial \overline{\xi}_1}\frac{\partial \xi_1}{\partial \overline{\xi}_2},$$

where

$$\begin{aligned}
\frac{\partial \xi_1}{\partial \overline{\xi}_1} &= \sum_{j \in tri_s} \frac{\partial \overline{\Phi}_j(\overline{\xi})}{\partial \overline{\xi}_1} \xi_{lj}, \\
\frac{\partial \xi_1}{\partial \overline{\xi}_2} &= \sum_{j \in tri_s} \frac{\partial \overline{\Phi}_j(\overline{\xi})}{\partial \overline{\xi}_2} \xi_{1j},
\end{aligned}$$

$$\frac{\partial \xi_2}{\partial \bar{\xi}_1} = \sum_{j \in tri_s} \frac{\partial \overline{\Phi}_j(\bar{\xi})}{\partial \bar{\xi}_1} \xi_{2j},$$
$$\frac{\partial \xi_2}{\partial \bar{\xi}_2} = \sum_{j \in tri_s} \frac{\partial \overline{\Phi}_j(\bar{\xi})}{\partial \bar{\xi}_2} \xi_{2j}.$$

The next process is assembling the element contributions in (3.28), (3.29), (3.30), (3.31) and (3.32) as matrices' element.

After we calculate the element contributions in (3.28), (3.29), (3.30), (3.31) and (3.32), we need to assembly the element contributions into the global coefficient matrix.

In the global coefficient matrix, rows correspond to the collocation point x^i and columns correspond to the global node number x^j. The global node numbering x^j are assigned such that nodes $x^1, \cdots, x^h$ are the nodes on the boundary and $x^{h+1}, \cdots, x^J$ are nodes in the domain.

In the assembly process, the boundary element contributions from (3.28), (3.29) and (3.30) give the row elements that belong to the columns $1, \cdots, h$ that represent the nodes on the boundary. Therefore, the columns of the matrix that represent the nodes in the domain i.e. with numbers $h+1, \cdots, J$ are set to be 0.

The domain element contributions from (3.31) and (3.32) populate each of the row elements that belongs to the columns $1, \cdots, h, \cdots, J$.

The system of equation (3.11) can now be solved numerically by any numerical method for solving linear algebraic systems, e.g. by LU decomposition method or Neumann series expansion (if the latter converges).

In order to apply the Neumann series expansion, we rewrite (3.11) as

$$\sum_{x^j \in \Omega \cup \partial\Omega} \left(c_{ij} + K_{ij} + \overset{\circ}{K}_{ij} \right) u(x^j) = \sum_{x^j \in \partial\Omega} Q_{ij} \bar{t}(x^j) + D_i, \quad x^j \in \Omega \cup \partial\Omega, \tag{3.57}$$

where $c_{ij} = c_i \delta_{ij}$ is a diagonal matrix.

Denoting

$$\mathcal{F}(x^i) = \sum_{x^j \in \partial\Omega} Q_{ij} \bar{t}(x^j) + D_i,$$

we can write (3.57) as in the following:

$$\sum_{x^j \in \Omega \cup \partial\Omega} \left(c_{ij} + K_{ij} + \overset{\circ}{K}_{ij} \right) u(x^j) = \mathcal{F}(x^i). \tag{3.58}$$

There many possibilities to apply the Neumann series to solve equation (3.58). Let us consider one of them.

It is known that the inverse c_{ij}^{-1} of the diagonal matrix c_{ij} is given by

$$c_{ij}^{-1} = \frac{1}{c_i}\delta_{ij}.$$

Multiplying by the inverse matrix of c_{ij} i.e. c_{ij}^{-1} both sides of equation (3.58) and denoting the matrices

$$\begin{aligned} \hat{K_{ij}} &= K_{ij} + \overset{\circ}{K}_{ij}, \\ c^{-1} &= c_{ij}^{-1}, \\ u &= u(x^j), \\ \mathcal{F} &= \mathcal{F}(x^i), \end{aligned}$$

we get

$$(I + c^{-1}\hat{K})u = c^{-1}\mathcal{F}. \tag{3.59}$$

Denoting $c^{-1}\hat{K} = -K_1$ and $c^{-1}\mathcal{F} = B$, we can write (3.59) as in the following:

$$(I - K_1)u = B.$$

This enable us to try to apply Neumann series expansion as in the following:

$$u = \sum_{n=0}^{N} K_1^n B, \tag{3.60}$$

where N here is the number of iterations.

However, our numerical results show that the Neumann series expansion (3.60) failed to converge to the corresponding results obtained by LU decomposition method. The numerical results that illustrate the divergence will be shown in the next section. Therefore, we deduce that the Neumann series expansion in equation (3.60) might not be the best version of the Neumann series expansion. We derived a new one that will converge to the solutions obtained by LU decomposition method.

For the new version, we write (3.58) as

$$(I - K_2)u = \mathcal{F},$$

where

$$\begin{aligned} I &= \delta_{ij}, \\ u &= u(x^j), \\ \mathcal{F} &= F(x^i), \\ K_{0ij} &= -c_{ij} + \delta_{ij} - K_{ij}, \qquad (3.61) \\ K_{2ij} &= -c_{ij} + \delta_{ij} - K_{ij} - \overset{\circ}{K}_{ij}. \qquad (3.62) \end{aligned}$$

This enables us to apply the Neumann series expansion in the form

$$u = \sum_{n=0}^{N} K_2^n \mathcal{F} \qquad (3.63)$$

that will be used in the later numerical experiments.

Since it is rather expensive for numerical purposes to calculate the power of K_2 in equation (3.63), we will denote

$$\begin{aligned} g_0 &= \mathcal{F}, \\ g_n &= K_2 g_{n-1}, \end{aligned}$$

therefore the Neumann series expansion (3.63) can be written as

$$u = \sum_{n=0}^{N} K_2^n \mathcal{F} = \mathcal{F} + \sum_{n=1}^{N} g_n. \qquad (3.64)$$

3.3 Numerical Examples of BDIE for Neumann Problem

For the numerical experiments, we solve the BDIE for Neumann problem (3.10) on several two-dimensional test domains such as square, circular and parallelogram domains. These test domains will also be used in the next chapters that deals with solving BDIE for Dirichlet problem and Localized-Boundary Domain Integral equation (LBDIEs) for Neumann and Dirichlet problems.

The first test domain that we consider is a square $1 < x_1 < 2$, $1 < x_2 < 2$. The second test domain is a circular domain with centre $(2, 2)$ and unit radius. The final test domain is

a parallelogram domain with vertices $(3,1)$, $(4,1)$, $(6,2)$ and $(5,2)$. Figure 3.4 shows some meshes examples for the three test domains where J is the number of nodes.

In the numerical experiments, we consider several interior Neumann problems with the following parameters:

1. $a(x) = 1,\ \ f(x) = 0$ for $x \in \Omega \cup \partial\Omega$, with $\bar{t}(x) = \nu_1(x),\ x \in \partial\Omega$,
2. $a(x) = x_2^2,\ \ f(x) = 0$ for $x \in \Omega \cup \partial\Omega$, with $\bar{t}(x) = x_2^2\nu_1(x),\ x \in \partial\Omega$,
3. $a(x) = x_2^4,\ \ f(x) = 0$ for $x \in \Omega \cup \partial\Omega$, with $\bar{t}(x) = x_2^4\nu_1(x),\ x \in \partial\Omega$,
4. $a(x) = x_2^6,\ \ f(x) = 0$ for $x \in \Omega \cup \partial\Omega$, with $\bar{t}(x) = x_2^6\nu_1(x),\ x \in \partial\Omega$,
5. $a(x) = x_2^8,\ \ f(x) = 0$ for $x \in \Omega \cup \partial\Omega$, with $\bar{t}(x) = x_2^8\nu_1(x),\ x \in \partial\Omega$,
6. $a(x) = x_2^{10},\ \ f(x) = 0$ for $x \in \Omega \cup \partial\Omega$, with $\bar{t}(x) = x_2^{10}\nu_1(x),\ x \in \partial\Omega$,
7. $a(x) = x_2^2,\ \ f(x) = 2x_2^2$ for $x \in \Omega \cup \partial\Omega$, with $\bar{t}(x) = 2x_1x_2^2\nu_1(x),\ x \in \partial\Omega$,

The exact solutions for Neumann problem in Tests 1-6 and Test 7 are given in (3.65) and (3.66), respectively,

$$u(x) = x_1, \quad x \in \Omega \cup \partial\Omega, \tag{3.65}$$

$$u(x) = x_1^2, \quad x \in \Omega \cup \partial\Omega. \tag{3.66}$$

All numerical computations are done using Fortran package written by the author, with the double precision. We solve the linear system (3.11) by two approaches. The first one is using LU decomposition and the second is using the Neumann series (3.64).

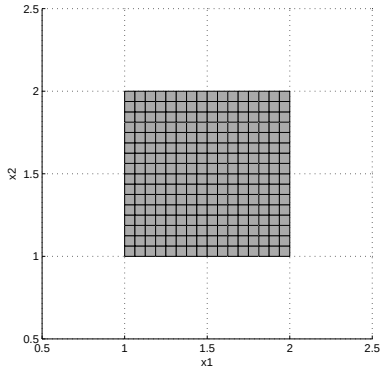

(a) Square domain with $J = 289$.

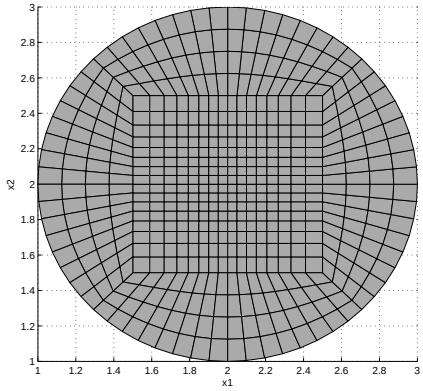

(b) The unit-radius circular domain with $J = 545$.

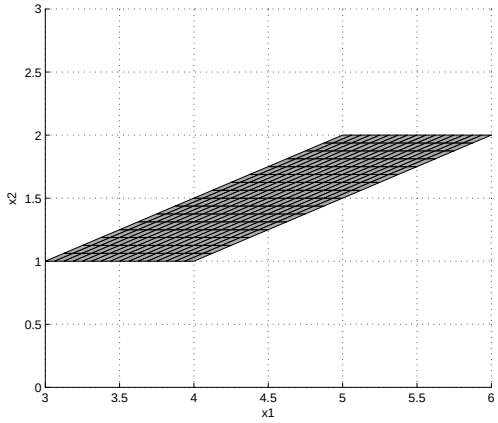

(c) The parallelogram domain with $J = 289$.

Figure 3.4: Test domains.

For each domain, we present a posteriori relative errors for the approximate solution

$$\epsilon(u) = \frac{\max\limits_{1\le j\le J} \left|u_{approx}(x^j) - u_{exact}(x^j)\right|}{\max\limits_{1\le j\le J} |u_{exact}(x^j)|}, \tag{3.67}$$

and for its gradient

$$\epsilon(\nabla u) = \frac{\max\limits_{1\le m\le M} |\nabla u_{approx}(x_c^m) - \nabla u_{exact}(x_c^m)|}{\max\limits_{1\le m\le M} |\nabla u_{exact}(x_c^m)|}, \tag{3.68}$$

where x_c^m are centres of the quadrilateral domain elements e_m.

We determine $\partial u_{approx}/\partial x_1$ and $\partial u_{approx}/\partial x_2$ at the middle of each interior domain element. The numerical results of $\partial u/\partial x_1$ and $\partial u/\partial x_2$ are based on the following interpolation:

$$\frac{\partial u}{\partial x_1} = \sum_j \frac{\partial \phi_j(x)}{\partial x_1} u(x^j), \tag{3.69}$$

$$\frac{\partial u}{\partial x_2} = \sum_j \frac{\partial \phi_j(x)}{\partial x_2} u(x^j), \qquad x,\ x^j \in \Omega \cup \partial\Omega. \tag{3.70}$$

The interpolation formulas in the local coordinates are given as follows:

$$\frac{\partial u}{\partial x_1} = \sum_{N=1}^{4}\sum_{j=1}^{2} \frac{\partial \Phi_N(\xi(x))}{\partial \xi_j}\frac{\partial \xi_j}{\partial x_1} u(x_N^m), \tag{3.71}$$

$$\frac{\partial u}{\partial x_2} = \sum_{N=1}^{4}\sum_{j=1}^{2} \frac{\partial \Phi_N(\xi(x))}{\partial \xi_j}\frac{\partial \xi_j}{\partial x_2} u(x_N^m), \quad x,\ x_N^m \in \Omega \cup \partial\Omega. \tag{3.72}$$

3.3.1 Numerical results related to the Neumann series expansion (3.60)

Figure 3.5 shows the divergence of the solutions correspond to the arrangement of the Neumann series in equation (3.60). The divergence of the solutions is more obvious for the test on circular domain. The numerical experiments illustrated in Figure 3.5 are done for Test 2.

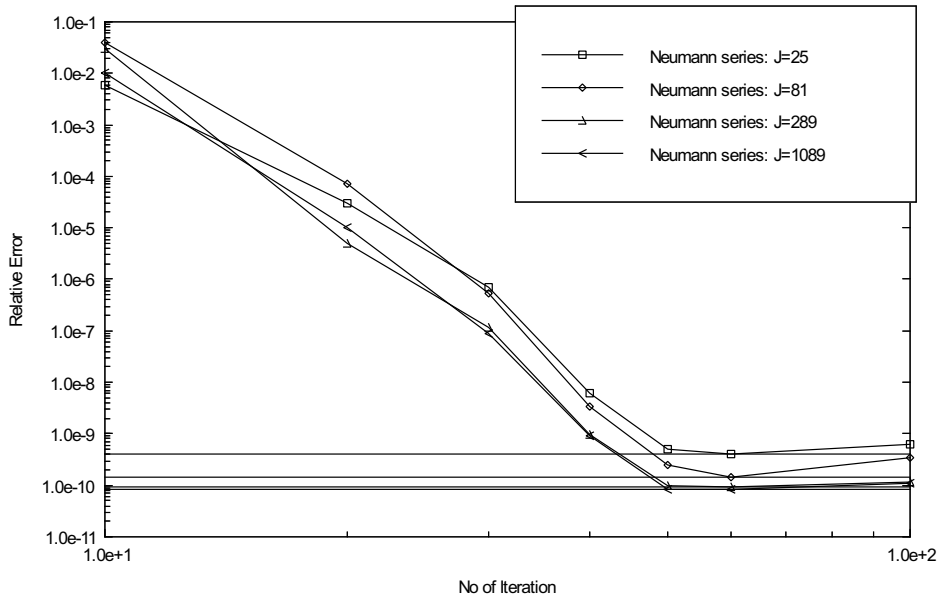

(a) Square

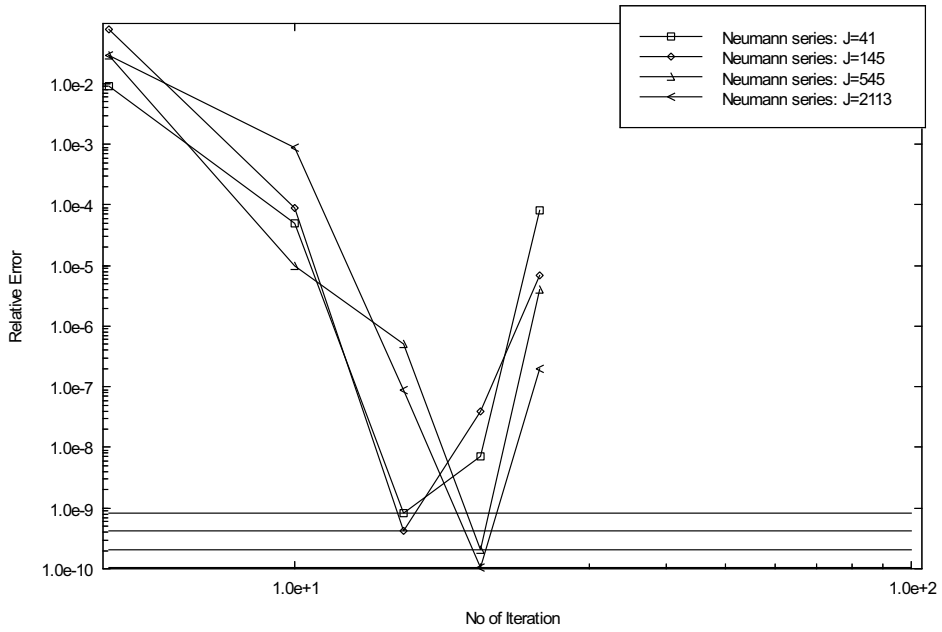

(b) Circular domain.

Figure 3.5: Relative errors of the solutions on the square and circle vs. number of Neumann iterations, compared with the error of the LU decomposition solution (horizontal lines), for different number of mesh nodes J.

3.3.2 Numerical results related to the Neumann series expansion (3.64)

In this subsection, we will present the numerical results obtained from the Neumann series expansion as arranged in (3.64). This new arrangement of the Neumann series expansion converges to the solutions obtained by LU decomposition method.

The comparative results for relative errors of approximate solutions u_{approx} obtained by LU decomposition method and their gradient ∇u_{approx} versus number of nodes J for Test 2 and Test 7 on square domain are shown in Figure 3.6.

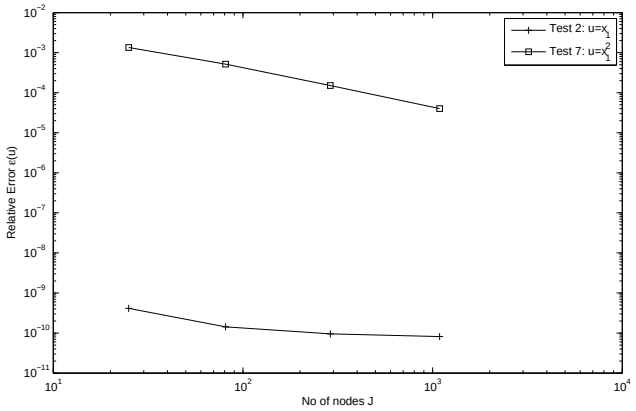

(a)

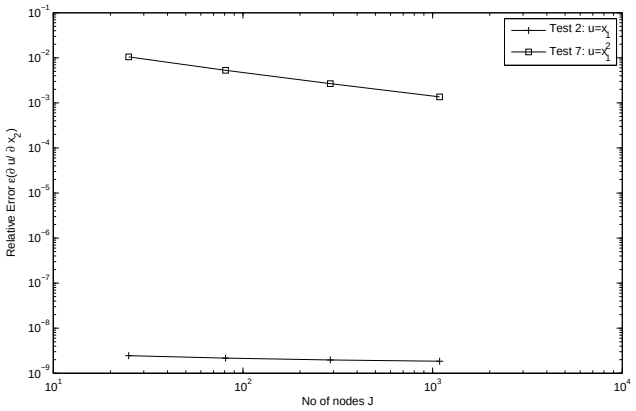

(b)

Figure 3.6: Relative errors of the approximate solutions (a) and their gradients (b), on the square vs. number of nodes J.

The comparative results for relative errors of approximate solutions obtained by Neumann iteration method versus number of nodes J for Test 2 and Test 7 on square domain is shown in Figure 3.7.

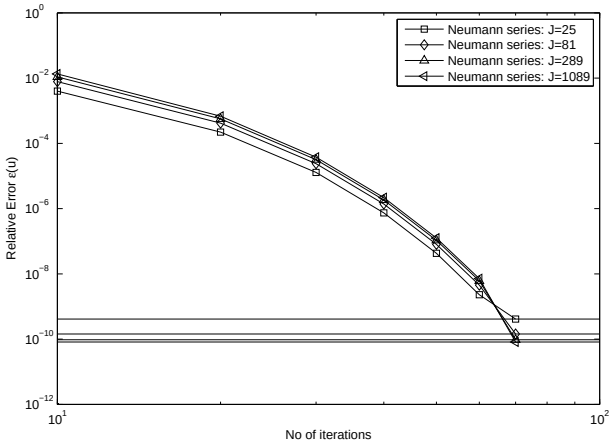

(a) Test 2.

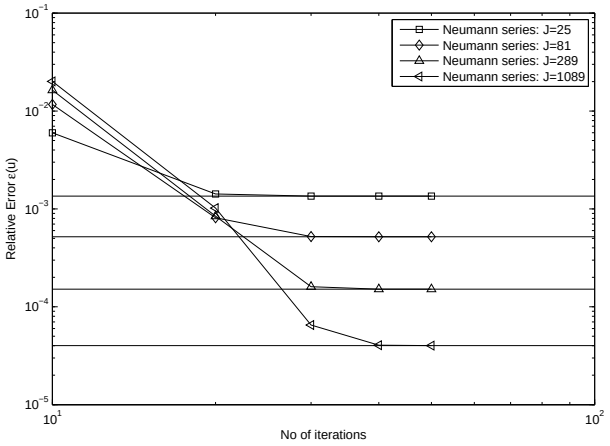

(b) Test 7.

Figure 3.7: Relative errors of the solutions on the square vs. number of Neumann iterations, compared with the error of the LU decomposition solution (horizontal lines), for different number of mesh nodes J.

The comparative results for relative errors of approximate solutions u_{approx} obtained by LU decomposition method versus number of nodes J for Test 2 and Test 7 on circular domain is shown in Figure 3.8.

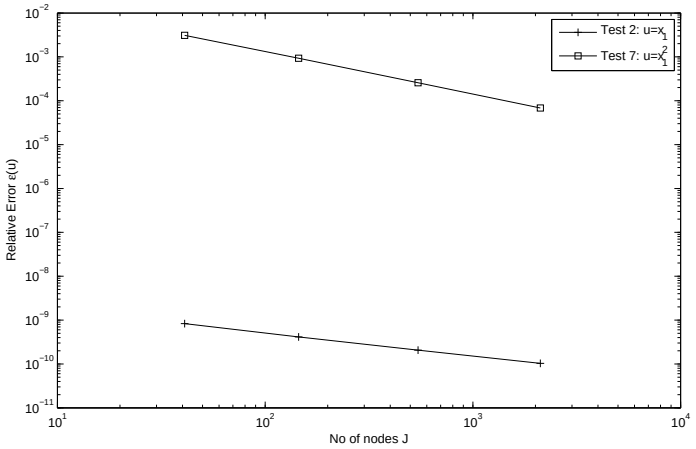

(a)

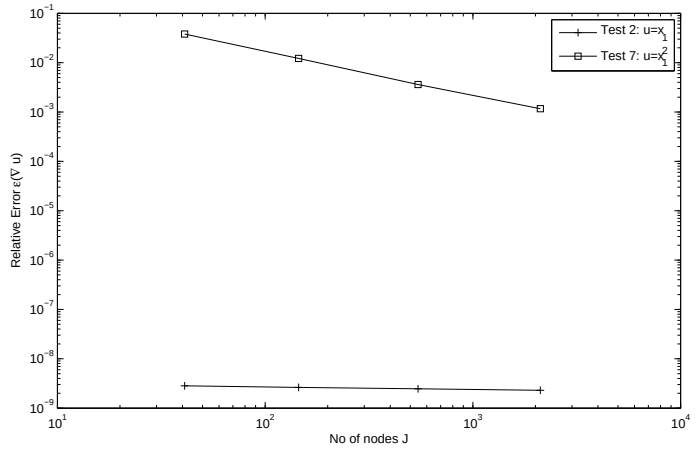

(b)

Figure 3.8: Relative errors of the approximate solutions (a) and their gradients (b), on circular domain vs. number of nodes J.

The comparative results for relative errors of approximate solutions obtained by Neumann iteration method versus number of nodes J for Test 2 and Test 7 is shown in Figure 3.9.

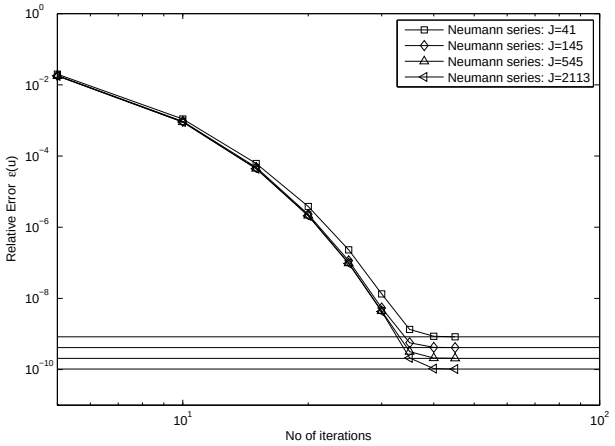

(a) Test 2.

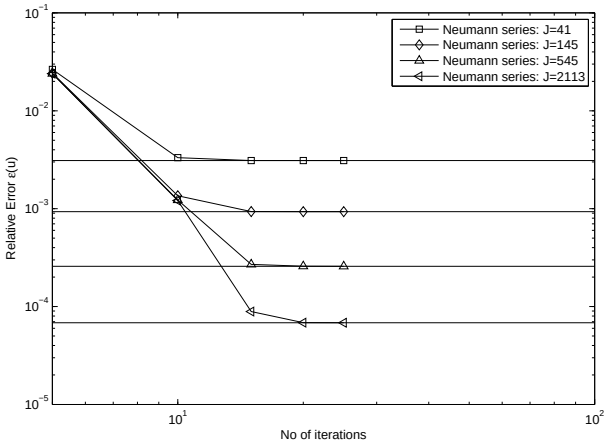

(b) Test 7.

Figure 3.9: Relative errors of the solutions on circular domain vs. number of Neumann iterations, compared with the error of the LU decomposition solution (horizontal lines), for different number of mesh nodes J.

The comparative results for relative errors of approximate solutions u_{approx} obtained by LU decomposition method versus number of nodes J for Test 2 and Test 7 on parallelogram is shown in Figure 3.10.

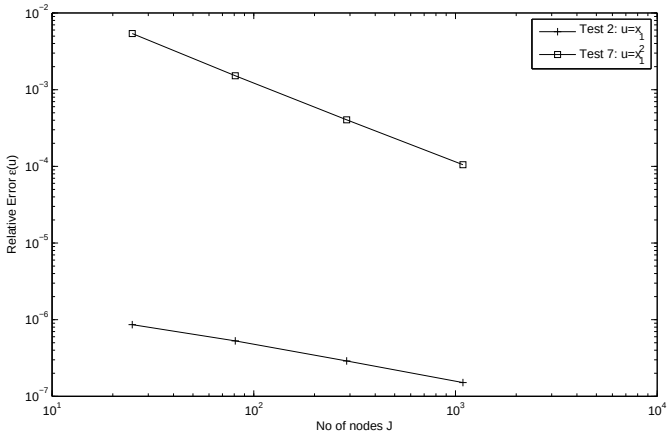

(a)

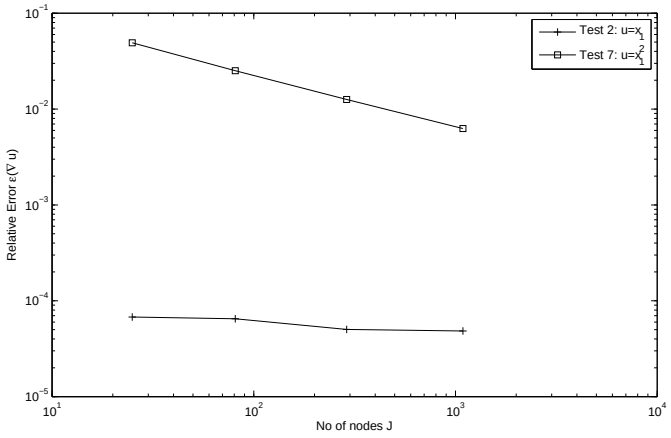

(b)

Figure 3.10: Relative errors of the approximate solutions (a) and their gradients (b), on the parallelogram vs. number of nodes J.

The comparative results for relative errors of approximate solutions obtained by Neumann iteration method versus number of nodes J for Test 2 and Test 7 on parallelogram is shown in Figure 3.11.

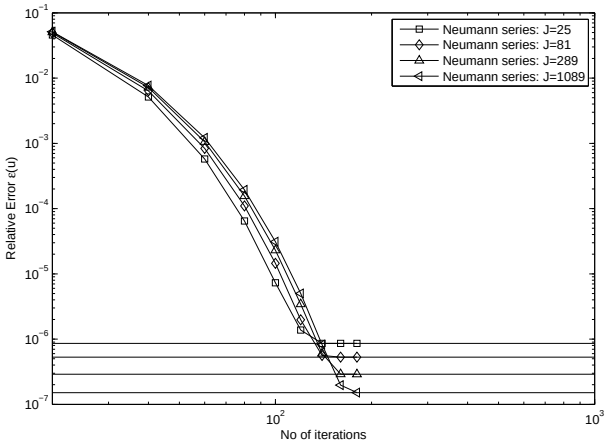

(a) Test 2.

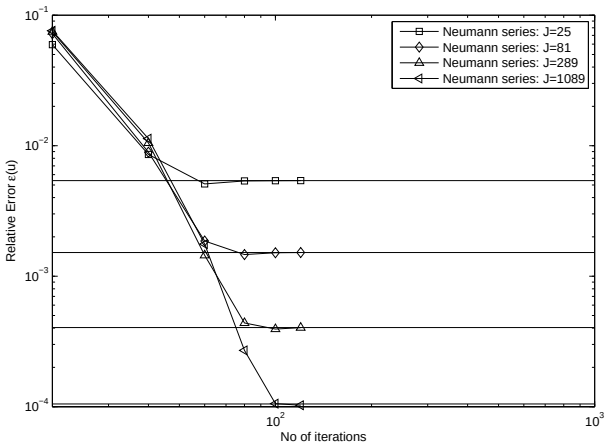

(b) Test 7.

Figure 3.11: Relative errors of the solutions on parallelogram vs. number of Neumann iterations, compared with the error of the LU decomposition solution (horizontal lines), for different number of mesh nodes J.

From figures 3.6, 3.8 and 3.10, we can see the dependence of the solution error on the number of collocation points J for the solution of the algebraic system by the LU decomposition.

The dependence of the error $\epsilon(u)$ on the number of nodes J can be fitted with a power function (i.e. with straight line in the double logarithmic coordinates in the graphs), giving $\epsilon \sim 1/\sqrt{J} \sim h$ for Test 2 and $\epsilon \sim 1/J \sim h^2$ for Test 7 i.e. respectively, linear and quadratic convergence with respect to the average linear size of the elements, h.

For the gradient error we similarly have $\epsilon(\nabla u) \sim J^{-q'/2} \sim h^{q'}$, where $q' = 0.1$ for the square and circular domains and $q' = 0.2$ for the parallelogram domain in Test 2, while $q' = 1$ for the square and parallelogram domains and $q' = 2$ for the circular domain in Test 7.

The accuracy in Test 2 is much higher since the implemented piece-wise bi-linear interpolation is exact on the linear exact solution, and only the integral operator approximation error, related with the accuracy of the numerical integration, is involved. In the Test 7, on the contrary, the piece-wise bi-linear interpolation of the quadratic exact solution gives its contribution in the total error. On the other hand, the higher convergence rate in Test 7 can be attributed to the quadratic convergence rate of the piece-wise linear interpolation of smooth nonlinear function, while the lower convergence rate in Test 2 can be explained by the linear convergence of the approximation of the the integral operator.

As follows from Figures 3.7, 3.9 and 3.11 the Neumann series converges to the LU decomposition solutions, reaching the LU decomposition accuracy after 70 iterations for the square, 40 iterations for the circle and $140 - 160$ iterations for the parallelogram in Test 2 and after $20 - 40$ iterations for the square, $15 - 20$ iterations for the circle and $60 - 100$ iterations for the parallelogram in Test 7. The number of the Neumann iterations necessary to reach the same accuracy as the LU decomposition slightly grows with the the number of collocation points since the accuracy of the LU decomposition numerical solution taken for comparison also grows. The dependence of the iteration number on the test (i.e. on the exact solution behaviour) and on the domain shape is also related with the different accuracy of the LU numerical solution taken for comparison.

3.3.3 Eigen-values

To investigate the convergence of the iterative method and whether it holds for other variable coefficients of the PDE, we consider in this section the eigen-values of the obtained algebraic systems approximating the eigen-values of the BDIEs. It is well known that the Neumann series in the form of equation (3.64) for a matrix operator K_2 converges for any right hand side if and only if all eigen-values of the operator K_2 belong to the open unit disc (cf. Section 2.2.3). Moreover, the number of terms in the Neumann series sufficient for the error to be lower than a prescribed value, can be estimated in terms of the maximum eigen-value modulus. Let $\widetilde{\lambda}_k,\ k = 1, 2, \cdots J$, denote the eigen-values of the matrix K_0 defined by (3.61) i.e. the numbers for which the homogeneous equation

$$(\widetilde{\lambda}_k I - K_0)u = 0$$

has non-trivial solutions. Similarly, let $\widehat{\lambda}_k,\ k = 1,\ 2, \cdots J$, denote the eigen-values of the perturbed matrix K_2.

When the coefficient $a(x)$ is a constant, the remainder R vanishes and boundary-domain integral equation (3.8) can be split on the purely boundary integral equation for the boundary values (traces) of u on $\partial\Omega$, and on the representation formula for u in Ω. The same will hold also for the perturbed equation (3.10) and its discrete counterpart (3.11).

From (Goursat (1964), Mikhlin (1957)) one can deduce that in this case the eigen-values of the non-perturbed boundary integral operator (and thus the whole operator K_0) in the appropriate function spaces are real and belong to the interval $(0, 1]$. Application of (Mikhailov (1999)) gives that the spectrum of the perturbed operator K_2 belongs to the interval $[0,\ 1)$, that is its spectral norm is less than 1 implying convergence of the corresponding Neumann series.

When the coefficient $a(x)$ is not constant, the spectral properties and thus a proof of convergence of the Neumann series for BDIEs is not available but some conclusions about the convergence can be drown from the following graphs presenting the numerically obtained largest-modulus eigen-values of the discrete operators K_0 and K_2 and influence of the coefficient $a(x)$ on them.

Figure 3.12 show the first five eigen-values $\widetilde{\lambda}_k$ of the matrix K_0 in (3.61) with the largest moduli for the examples in Test 2 for square, circular domain and parallelogram, respectively. These five eigen-values appear to be real for the square and parallelogram and have an imaginary part less than 0.006 for the circle. Numerically obtained largest eigen-values $\widehat{\lambda}_k$ of the perturbed matrix K_2 in (3.62) coincide (up to the third digit) with those for the unperturbed matrix K_0 in (3.61), except the eigen-value $\widetilde{\lambda}_1 = 1$, that vanishes for K_2, as predicted by the theory. Indeed, the eigen-values of the discrete operators K_0 and K_2 approximate the spectra of the corresponding integral operators K_0 and K_2. The operators K_0 and K_2 differ only by the perturbation operator (3.9) and, according to (Mikhailov (1999)), their eigen-values coincide except the eigen-value $\widetilde{\lambda} = 1$ that is transferred to the spectrum point $\widehat{\lambda} = 0$, for the operator K_2 , under the assumption that there are no associated functions corresponding to the eigen-value $\widetilde{\lambda} = 1$.

The maximal eigen-values of the matrix K_2 i.e. $\widetilde{\lambda}_2$ on Figure 3.12 gives the spectral radius of the matrix K_2 influencing the convergence rate of the Neumann series. In our examples in Test 2, the spectral radii are less than one, implying convergence of the Neumann series. For the circular domain it converges after 25 iterations, while for the parallelogram only after 100 iterations correlating well with max $|\widehat{\lambda}_k| = 0.5$ for the circular domain and max $|\widehat{\lambda}_k| = 0.9$ for the parallelogram.

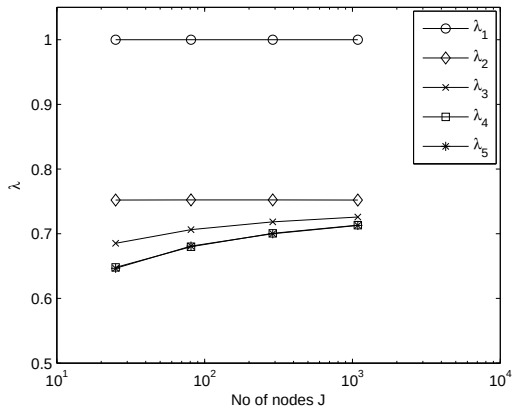

(a) Square domain.

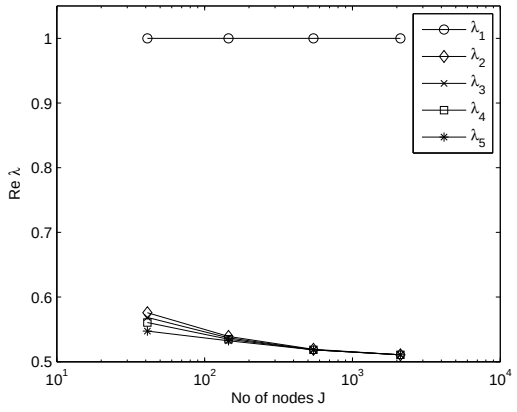

(b) Circular domain.

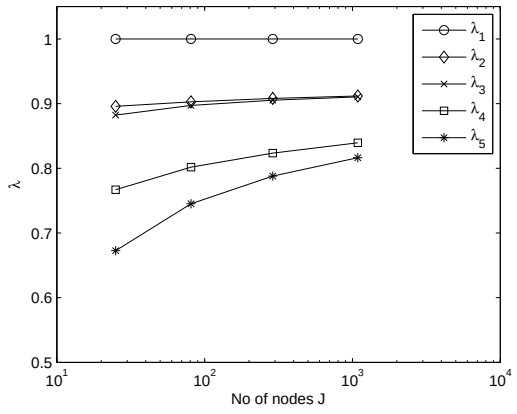

(c) Parallelogram domain.

Figure 3.12: Eigen-values of the matrix K_0 vs. the number of nodes J.

To investigate the influence of the coefficient $a(x)$ on the maximum eigen-values of the perturbed matrix K_2, we calculated them for $a(x) = x_2^k$ with different $0 \leq k \leq 10$ as in Tests 1 – 6. (Note that our previous examples were calculated for $k = 2$ i.e. for Test 2.)

The results of influence of the coefficient $a(x)$ are presented in Figures 3.13 – 3.15 for the finest meshes, $J = 1089$ for the square and parallelogram, and $J = 2113$ for the circular domain. For the overlapping eigen-values seen on the figures our calculation shown that their eigen-functions are linearly independent i.e. the eigen-values are geometrically multiple. The figures show that for sufficiently high k i.e. for sufficiently sharp variation of the coefficient, the eigen-values are generally complex and can lay outside the unit circle, unlike the constant-coefficient case. This means that the standard Neumann series for the BDIE with such variable coefficients can generally diverge. Note however that from these figures one can conclude that $0 \leq \text{Re}\ \widehat{\lambda}_k < 1$ for the all considered examples, similar to the constant coeficient case, while $|\text{Im}\ \widehat{\lambda}_k| < C$ with some constant $C < 1.5$.

Next, we will analyze the eigen-values for discrete BDIE in our test examples. In our example, the coefficient $a(x)$ is as follows

$$a(x) = x_2^k, \qquad 0 \leq k \leq 10.$$

Note that

$$\nabla a = (0, k x_2^{k-1}), \quad \text{and} \quad \frac{|\nabla a|}{a} = \frac{k}{x_2}.$$

Therefore

$$\max \left| \frac{L \nabla a}{a} \right| = \max \left| \frac{Lk}{x_2} \right|, \tag{3.73}$$

where L is denoted as the characteristic size of the domain.

Equation (3.73) then implies

$$\max \left| \frac{L \nabla a}{a} \right| = \max \left| \frac{k}{x_2} \right| = \frac{k}{2} < k, \quad \text{for square,} \tag{3.74}$$

$$\max \left| \frac{L \nabla a}{a} \right| = \max \left| \frac{2k}{x_2} \right| = \frac{2k}{3} < k, \quad \text{for circle,} \tag{3.75}$$

$$\max \left| \frac{L \nabla a}{a} \right| = \max \left| \frac{k}{x_2} \right| = \frac{k}{2} < k, \quad \text{for parallelogram.} \tag{3.76}$$

Hence, by considering equations (3.74)-(3.76) and taking into account the results in Figures 3.13-3.15, we can deduce that

$$\max \left| \frac{L\nabla a}{a} \right| < 5, \tag{3.77}$$

in order to ensure that the Neumann series expansion converges.

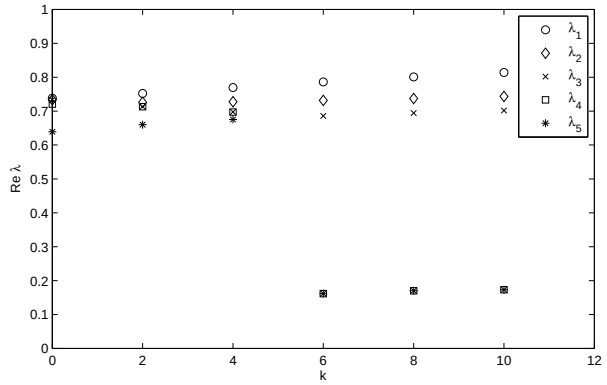

(a) Re λ.

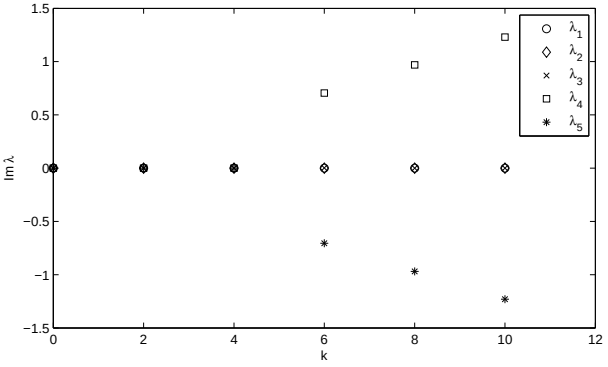

(b) Im λ.

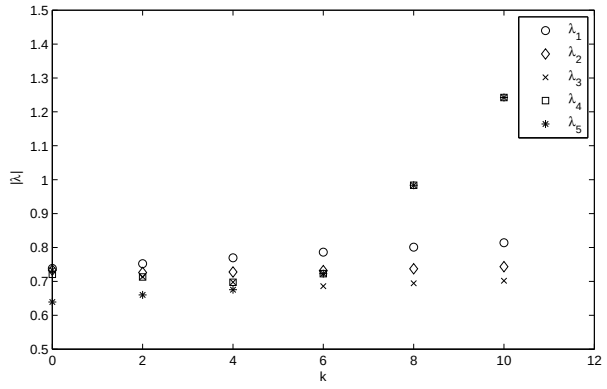

(c) $|\lambda|$.

Figure 3.13: The largest eigen-values of the matrix K_2 for the square vs. k for $a(x) = x_2^k$.

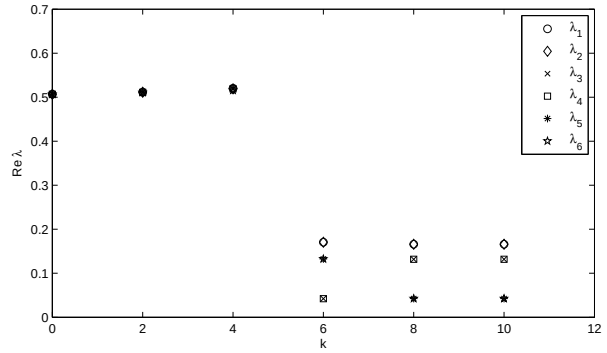

(a) Re λ.

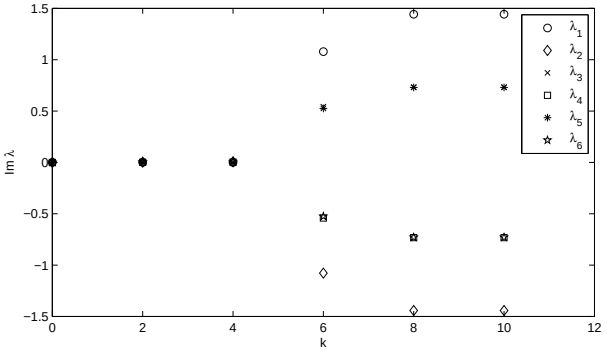

(b) Im λ.

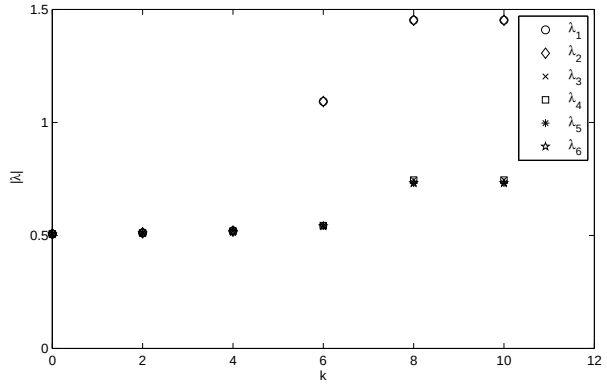

(c) $|\lambda|$.

Figure 3.14: The largest eigen-values of the matrix K_2 for the circular domain vs. k for $a(x) = x_2^k$.

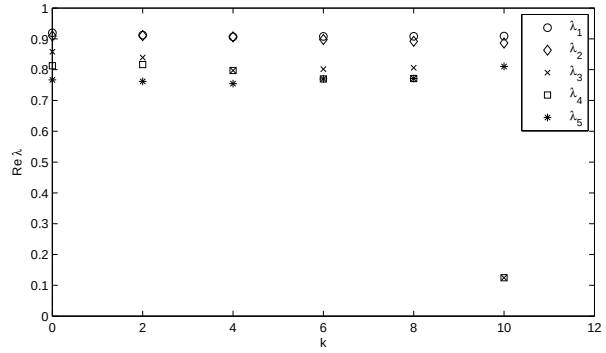

(a) Re λ.

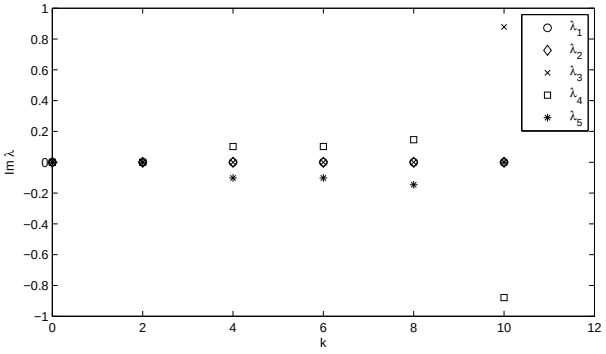

(b) Im λ.

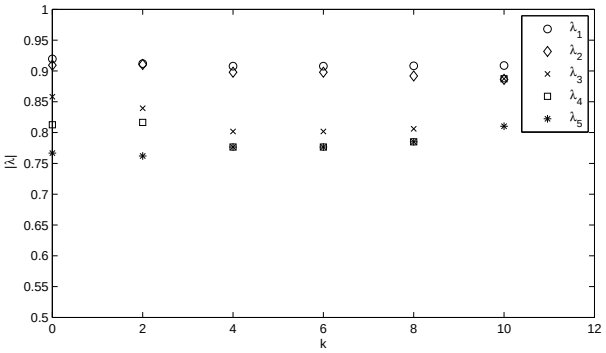

(c) $|\lambda|$.

Figure 3.15: The largest eigen-values of the matrix K_2 for the parallelogram vs. k for $a(x) = x_2^k$.

3.4 Conclusion

The finite-dimensional perturbation allows to reduce the BDIE of the Neumann problem to an unconditionally and uniquely solvable integral equation. The numerical results presented in this chapter show that the mesh-based discretization of the BDIE with a quadrilateral bilinear approximation leads to a system of linear algebraic equations that can be solved e.g. by LU-decomposition with linear convergence with respect to the element size (diameter). For some variable coefficients and shapes of the domains, the discrete BDIE can be also solved by fast converging Neumann iterations, which is related to the beneficial spectral properties of the BDIE. A more detailed analysis of the discrete BDIE eigen-values demonstrated that when the PDE coefficient moderately varies with coordinates i.e. when the coefficient gradient is small or moderate (e.g. $\max\left|\frac{L\nabla a}{a}\right| < 5$ in the considered examples, where L is a characteristic size of the domain) the spectrum is contained in the unit circle, which implies the Neumann series convergence. Then the standard Neumann iteration method is a good alternative to the direct methods, especially when the computer storage and CPU time needs for the latter become prohibitive. However, this spectrum property does not hold generally, and when the coefficient varies sharply enough, some eigen-values appear also outside the unit circle, which can lead to divergence of the standard Neumann series; in these cases the modified Neumann series, other iterative (e.g. GMRES) or direct methods will be more appropriate.

Chapter 4

The Boundary-Domain Integro-Differential Equations for Dirichlet Problem

4.1 Introduction

In Chapter 3, we have discussed that by using a parametrix, the Neumann boundary-value problem for a partial differential equation with variable coefficient can be reduced to a BDIE. We also have shown how Boundary Element Method can be used for the approximation and numerical solution of the BDIE. In this chapter, we extend the work that have been done on the perturbed BDIE of Neumann problem in Chapter 3 to the united BDIDE of Dirichlet problem.

From two versions of the BDIDEs for Dirichlet problem, we can obtain two sets of linear algebraic systems. This can be also interpreted as two different ways in the interpolation process. The first one is by taking the collocation points x^i only for $x^i \in \Omega$ i.e. at $J - J_D$ nodes of the mesh during the interpolation process where J_D is the number of nodes on the boundary $\partial\Omega$. The second one is by taking the collocation points x^i for $x^i \in \overline{\Omega}$ at all J nodes like in BDIE related to Neumann problem. The spectral properties obtained from the

numerical experiment for the discrete BDIDE operator related to Dirichlet problem will also be presented.

4.2 The BDIDEs for Dirichlet Problem

Let us consider the same second-order linear elliptic PDE in a two-dimensional bounded domain, Ω as in Chapter 3,

$$(Lu)(x) := \sum_{i=1}^{2} \frac{\partial}{\partial x_i} \left[a(y) \frac{\partial u(x)}{\partial x_i} \right] = f(x),\ x \in \Omega,$$

with the Dirichlet boundary condition

$$u(x) = \overline{u}(x),\ x \in \partial\Omega.$$

Equation (3.7) can be used for formulating different boundary-domain integro-differential equations (BDIDEs) with respect to u and its derivatives, e.g. by united formulation and partly segregated formulation. The BDIDEs are called segregated BDIDEs when the unknown boundary functions are considered as formally unrelated to the unknown functions inside the domain whereas for the united BDIDEs, the unknown boundary functions are related to the unknown functions inside the domain.

As described in (Mikhailov (2002)), for united formulation, substituting boundary condition (2.2) in the integrals in (3.7) and taking (3.7) at $y \in \Omega \cup \partial\Omega$ will give the following linear direct boundary-domain integro-differential equation, BDIDE:

$$c(y)u(y) + \int_{\partial\Omega} P(x,y) T u(x)\, \mathrm{d}\Gamma(x) + \int_{\Omega} R(x,y) u(x)\, \mathrm{d}\Omega(x) = F(y), \tag{4.1}$$

where

$$F(y) = \int_{\partial\Omega} \overline{u}(x) T_x P(x,y)\, \mathrm{d}\Gamma(x) + \int_{\Omega} P(x,y) f(x)\, \mathrm{d}\Omega(x), \quad y \in \Omega \cup \partial\Omega. \tag{4.2}$$

For the partly segregated formulation, equation (4.1) is applied at $y \in \Omega \cup \partial\Omega$, substitute $\overline{u}(y)$ for $u(y)$ when $y \in \partial\Omega$. This gives rise to another direct boundary domain integro-differential equation, BDIDE, for $t(x)$ at $x \in \partial\Omega$, i.e.,

$$c^0(y)u(y) \quad + \quad \int_{\partial\Omega} P(x,y) t(x)\, \mathrm{d}\Gamma(x) + \int_{\Omega} R(x,y) u(x)\, \mathrm{d}\Omega(x) = F^0(y), \tag{4.3}$$

$$\begin{aligned} F^0(y) &= \left[c^0(y) - c(y)\right]\overline{u}(y) + F(y), \quad y \in \Omega \cup \partial\Omega, \\ c^0(y) &= 0 \quad \text{if} \quad y \in \partial\Omega, \\ c^0(y) &= 1 \quad \text{if} \quad y \in \Omega^+, \quad c^0(y) = 0 \quad \text{if} \quad y \in \Omega^-. \end{aligned} \tag{4.4}$$

Note that both BDIDEs (4.1) and (4.3) do not only contain the usual line integral over the boundary $\partial\Omega$ as in the case when the parametrix is a fundamental solution but also an integral over the entire solution domain Ω. Furthermore, the unknown function u appears in the integrand of the integral over the domain.

Rearranging (4.1), applying the same interpolation as in Chapter 3 to equation (4.1) and placing the collocation point x^i for $x^i \in \overline{\Omega}$ at all J nodes of the mesh, we obtain the system of J linear algebraic equations for J unknowns $u(x^j)$, as follows:

$$c(x^i)u(x^i) + \sum_{x^j \in \overline{\Omega}} K_{ij}^D u(x^j) = Q_i^D + D_i^D, \quad x^i \in \overline{\Omega}, \tag{4.5}$$

where K_{ij}^D, Q_i^D and D_i^D are defined as follows:

$$K_{ij}^D = \sum_{m=1}^{M} \int_{\Omega_m} \phi_j(x) R(x, x^i)\, \mathrm{d}\Omega(x) + \sum_{l=1}^{L} \int_{\partial\Omega_l} P(x, x^i) \left[a(x) \left(\frac{\partial \phi_j(x)}{\partial \nu(x)}\right)\right] \mathrm{d}\Gamma(x), \tag{4.6}$$

$$Q_i^D = \sum_{l=1}^{L} \int_{\partial\Omega_l} \overline{u}(x) T_x P(x, x^i)\, \mathrm{d}\Gamma(x), \tag{4.7}$$

$$D_i^D = \sum_{m=1}^{M} \int_{\Omega_m} P(x, x^i) f(x)\, \mathrm{d}\Omega(x), \tag{4.8}$$

Equation (4.6) can then be written as

$$\begin{aligned} K_{ij}^D &= \sum_{\overline{\Omega}_m \ni x^j} \int_{\Omega_m} \phi_j(x) R(x, x^i)\, \mathrm{d}\Omega(x) \\ &+ \sum_{\partial\Omega_l \subset \left\{\overline{\Omega}_m : \overline{\Omega}_m \ni x^j\right\}} \int_{\partial\Omega_l} P(x, x^i) \left[a(x) \left(\frac{\partial \phi_j(x)}{\partial \nu(x)}\right)\right] \mathrm{d}\Gamma(x). \end{aligned} \tag{4.9}$$

Denoting $G_{N,i}^m$ and H_i^m as in (3.31) and (3.32), and

$$\widetilde{A}_{N,i}^l = \int_{-1}^{1} P(x(\eta), x^i) \left[a(x(\eta)) \left(\sum_{p=1}^{2} \sum_{k=1}^{2} \frac{\partial \Phi_N(\xi)}{\partial \xi_k} \left.\frac{\partial \xi_k}{\partial x_p}\right|_{\xi=\xi(\eta)} \nu_p(x(\eta))\right)\right] J_{l1}(\eta)\, \mathrm{d}\eta,$$

(4.10)

$$\widetilde{F}_i^l = \int_{-1}^{1} \overline{u}(x(\eta))T_x P(x(\eta), x^i) J_{l1}(\eta)\, \mathrm{d}\eta, \tag{4.11}$$

we then can write (4.6)-(4.8) as follows:

$$K_{ij}^D = \sum_{\overline{\Omega}_m \ni x^j} G^m_{N(j,m),i} + \sum_{\partial\Omega_l \subset \left\{\overline{\Omega}_m : \overline{\Omega}_m \ni x^j\right\}} \widetilde{A}^l_{N(j,m),i}, \tag{4.12}$$

$$Q_i^D = \sum_{l=1}^{L} \widetilde{F}_i^l, \tag{4.13}$$

$$D_i^D = \sum_{m=1}^{M} H_i^m. \tag{4.14}$$

where $N(j,m)$ is the local number of the node x^j on the domain element Ω_m.

Partly using the Dirichlet condition in the out-of-integral term, we obtain the following modification of equation (4.1).

$$\begin{aligned} u(y) &+ \int_\Omega R(x,y)u(x)\, \mathrm{d}\Omega(x) + \int_{\partial\Omega} P(x,y)Tu(x)\, \mathrm{d}\Gamma(x) \\ &= (1 - c(y))\overline{u}(y) + \int_{\partial\Omega} \overline{u}(x) T_x P(x,y)\, \mathrm{d}\Gamma(x) \\ &+ \int_\Omega P(x,y) f(x)\, \mathrm{d}\Omega(x), \qquad y \in \overline{\Omega}. \end{aligned} \tag{4.15}$$

4.2.1 The discretized BDIDE with the collocation points $x^i \in \overline{\Omega}$

Applying interpolation to equation (4.15) and placing the collocation point x^i for $x^i \in \overline{\Omega}$ at all J nodes of the mesh, we obtain the system of J linear algebraic equations for J unknowns $u(x^j)$, as follows:

$$u(x^i) + \sum_{x^j \in \overline{\Omega}} K_{ij}^D u(x^j) = (1 - c(x^i))\overline{u}(x^i) + Q_i^D + D_i^D, x^i \in \overline{\Omega}, \tag{4.16}$$

where K_{ij}^D, Q_i^D and D_i^D are defined in (4.6)-(4.8).

Defining

$$F(x^i) = (1 - c(x^i))\overline{u}(x^i) + Q_i^D + D_i^D,$$

we can then write (4.16) as

$$u(x^i) + \sum_{x^j \in \overline{\Omega}} K_{ij}^D u(x^j) = F(x^i), \qquad x^i \in \overline{\Omega}. \tag{4.17}$$

The integral in (4.10) needs a special treatment when a collocation point x^i is a vertex of the integration element since the kernels of these integrals are weakly singular at collocation points.

The integral (4.10) with the kernel involving $\ln(1/r)$ are evaluated numerically by using the following semi-analytic formula:

$$\int_{\partial\Omega_l} P(x,x^i)a(x)\frac{\partial\phi_j(x)}{\partial\nu(x)}\,\mathrm{d}\Gamma(x) = \int_{\partial\Omega_l}\left[P(x,x^i)a(x)\frac{\partial\phi_j(x)}{\partial\nu(x)} - g_{ijl}\right]\,\mathrm{d}\Gamma(x) + G_{ijl},$$

where

$$\begin{aligned} g_{ijl} &= \left(\frac{s_2-s}{s_2-s_1}\right)P(x,x^i)a(x(s_1))\frac{\partial\phi_j(x)}{\partial\nu(x)} \\ &+ \left(\frac{s-s_1}{s_2-s_1}\right)P(x,x^i)a(x(s_2))\frac{\partial\phi_j(x)}{\partial\nu(x)}, \qquad (4.18) \\ G_{ijl} = \int_{\partial\Omega_l} g_{ijl}\,\mathrm{d}s &= \int_{\partial\Omega_l}\left(\frac{s_2-s}{s_2-s_1}\right)P(x,x^i)a(x(s_1))\frac{\partial\phi_j(x(s_1))}{\partial\nu(x)}\,\mathrm{d}s \\ &+ \int_{\partial\Omega_l}\left(\frac{s-s_1}{s_2-s_1}\right)P(x,x^i)a(x(s_2))\frac{\partial\phi_j(x(s_2))}{\partial\nu(x)}\,\mathrm{d}s. \qquad (4.19) \end{aligned}$$

Since

$$\begin{aligned} (s_2-s) &= \frac{(s_2-s_1)}{2}(1-\eta), \\ (s-s_1) &= \frac{(s_2-s_1)}{2}(1+\eta), \end{aligned}$$

one can write (4.18) and (4.19) as

$$\begin{aligned} g_{ijl} &= \frac{(1-\eta)}{2}P(x,x^i)a(x(s_1))\frac{\partial\phi_j(x)}{\partial\nu(x)} \\ &+ \frac{(1+\eta)}{2}P(x,x^i)a(x(s_2))\frac{\partial\phi_j(x)}{\partial\nu(x)}, \qquad (4.20) \\ G_{ijl} &= \int_{s_1}^{s_2}\frac{(1-\eta)}{2}P(x,x^i)a(x(s_1))\frac{\partial\phi_j(x(s_1))}{\partial\nu(x)}\,\mathrm{d}s \\ &+ \int_{s_1}^{s_2}\frac{(1+\eta)}{2}P(x,x^i)a(x(s_2))\frac{\partial\phi_j(x(s_2))}{\partial\nu(x)}\,\mathrm{d}s \\ &= a(x(s_1))\frac{\partial\phi_j(x(s_1))}{\partial\nu(x)}\int_{-1}^{1}\frac{(1-\eta)}{2}P(x,x^i)\frac{ds}{d\eta}\,\mathrm{d}\eta \\ &+ a(x(s_2))\frac{\partial\phi_j(x(s_2))}{\partial\nu(x)}\int_{-1}^{1}\frac{(1+\eta)}{2}P(x,x^i)\frac{ds}{d\eta}\,\mathrm{d}\eta. \qquad (4.21) \end{aligned}$$

Defining

$$g_{A1} = \int_{-1}^{1} \frac{(1-\eta)}{2} P(x, x^i) \frac{ds}{d\eta} \, \mathrm{d}\eta, \tag{4.22}$$

$$g_{A2} = \int_{-1}^{1} \frac{(1+\eta)}{2} P(x, x^i) \frac{ds}{d\eta} \, \mathrm{d}\eta, \tag{4.23}$$

We then can write (4.21) as

$$G_{ijl} = \left(a(x(s_1)) \frac{\partial \phi_j(x(s_1))}{\partial \nu(x)} \right) g_{A1} + \left(a(x(s_2)) \frac{\partial \phi_j(x(s_2))}{\partial \nu(x)} \right) g_{A2}.$$

The integrals g_{A1} and g_{A2} are calculated analytically.

The radius r can be written as

$$r = \sqrt{h^2 + (d-s)^2},$$

where h, d and s are defined as (3.37)-(3.39).

Therefore we can write g_{A1} and g_{A2} in (4.22) and (4.23) as

$$g_{A1} = \int_{-1}^{1} \left(\frac{1-\eta}{2} \right) \left(\frac{1}{2} \right) \left(\frac{\ln[h^2 + (d-s)^2]}{2\pi a(x^i)} \right) \frac{ds}{d\eta} \, \mathrm{d}\eta, \tag{4.24}$$

$$g_{A2} = \int_{-1}^{1} \left(\frac{1+\eta}{2} \right) \left(\frac{1}{2} \right) \left(\frac{\ln[h^2 + (d-s)^2]}{2\pi a(x^i)} \right) \frac{ds}{d\eta} \, \mathrm{d}\eta. \tag{4.25}$$

The analytic solutions for integrals g_{A1} and g_{A2} are calculated by using Mathematica 5.1 as given in equations (4.26) and (4.27) below.

$$g_{A1} = \frac{J_{l1}(\eta) \, (h_1 + h_2 + h_3 + h_4)}{4\pi a(x^i) W_2^4}, \tag{4.26}$$

$$g_{A2} = \frac{J_{l1}(\eta) \, (f_1 + f_2 + f_3 + f_4)}{4\pi a(x^i) W_2^4}, \tag{4.27}$$

where

$$J_{l1}(\eta) = \frac{\mathrm{d}s}{\mathrm{d}\eta},$$

$$h_1 = -3W_2^4 + 2W_2^2 W_3 + 4(W_2^2 - W_3)\sqrt{W_1^2 W_2^2 - W_3^2} \, ArcTan \left[\frac{(W_2^2 - W_3)}{\sqrt{W_1^2 W_2^2 - W_3^2}} \right],$$

$$h_2 = 4(W_2^2 - W_3)\sqrt{W_1^2 W_2^2 - W_3^2} \, ArcTan \left[\frac{W_3}{\sqrt{W_1^2 W_2^2 - W_3^2}} \right],$$

$$
\begin{aligned}
h_3 &= (W_1^2W_2^2 + 2W_2^2W_3 - 2W_3^2)\ln[W_1^2],\\
h_4 &= (-W_1^2W_2^2 + W_2^4 - 2W_2^2W_3 + 2W_3^2)\ln[W_1^2 + W_2^2 - 2W_3],\\
f_1 &= -W_2^4 - 2W_2^2W_3 + 4W_3\sqrt{W_1^2W_2^2 - W_3^2}\,ArcTan\left[\frac{(W_2^2 - W_3)}{\sqrt{W_1^2W_2^2 - W_3^2}}\right],\\
f_2 &= 4W_3\sqrt{W_1^2W_2^2 - W_3^2}\,ArcTan\left[\frac{W_3}{\sqrt{W_1^2W_2^2 - W_3^2}}\right],\\
f_3 &= (-W_1^2W_2^2 + 2W_3^2)\ln[W_1^2],\\
f_4 &= (W_1^2W_2^2 + W_2^4 - 2W_3^2)\ln[W_1^2 + W_2^2 - 2W_3].
\end{aligned}
$$

The notations W_1, W_2 and W_3 are given in (3.33)-(3.35) and illustrated in Figs. 3.2-**??**.

The analytic solutions for integrals g_{A1} and g_{A2} in (4.26) and (4.27) are uncertainty of the type 0/0 when $x^i = s_1$ and $x^i = s_2$.

Therefore, when $x^i = s_1$, by taking the limit as $W_1 \to 0$, we obtain

$$
\begin{aligned}
g_{A1} &= \left(\frac{1}{4\pi a(x^i)}\right) J_{l1}(\eta)(-3 + \ln[W_2^2]),\\
g_{A2} &= \left(\frac{1}{4\pi a(x^i)}\right) J_{l1}(\eta)(-1 + \ln[W_2^2]).
\end{aligned}
$$

When $x^i = s_2$, by taking the limit as $W_1 \to W_2$, we have

$$
\begin{aligned}
g_{A1} &= \left(\frac{1}{4\pi a(x^i)}\right) J_{l1}(\eta)(-1 + \ln[W_2^2]),\\
g_{A2} &= \left(\frac{1}{4\pi a(x^i)}\right) J_{l1}(\eta)(-3 + \ln[W_2^2]).
\end{aligned}
$$

4.2.2 The discretized BDIDE with the collocation points $x^i \in \Omega$

Instead of BDIDE (4.1) employed at $y \in \partial\Omega$, we can employ Dirichlet boundary condition $u = \overline{u}$ on $\partial\Omega$. This means that instead of taking the collocation point x^i for $x^i \in \overline{\Omega}$ at all J nodes of the mesh, we can take the collocation point x^i only for $x^i \in \Omega$ at $J - J_D$ nodes of the mesh during the interpolation process. Here J_D is the number of boundary nodes of the mesh.

Therefore, we split $\sum\limits_{x^j \in \overline{\Omega}} K_{ij}^D u(x^j)$ in (4.5) to two parts such that

$$
\sum_{x^j \in \overline{\Omega}} K_{ij}^D u(x^j) = \sum_{x^j \in \Omega} K_{ij}^D u(x^j) + \sum_{x^j \in \partial\Omega} K_{ij}^D \overline{u}(x^j).
$$

The second part $\sum_{x^j \in \partial\Omega} K_{ij}^D \overline{u}(x^j)$ can be transferred to the right-hand side.

Therefore, from (4.5) we obtain the system of $J - J_D$ linear algebraic equations for $J - J_D$ unknowns $u(x^j)$, as in the following:

$$u(x^i) + \sum_{x^j \in \Omega} K_{ij}^D u(x^j) = - \sum_{x^j \in \partial\Omega} K_{ij}^D \overline{u}(x^j) + Q_i^D + D_i^D, \; x^i \in \Omega, \tag{4.28}$$

where K_{ij}^D, Q_i^D, and D_i^D are given by (4.9) and (4.7)-(4.8).

4.2.3 Numerical Examples for System (4.28)

In the earlier discussion of Section 4.2, we have seen that, in solving the BDIDE for Dirichlet problem as in (4.1), we have two ways of BDIDE implementation.

The first one is by taking into account the collocation points x^i for $x^i \in \overline{\Omega}$ at all J nodes as in equation (4.5).

The second way is by taking the collocation points x^i only for $x^i \in \Omega$ at $J - J_D$ nodes of the mesh during the interpolation process as in equation (4.28).

The second way looks more interesting in terms of computation time since we have less collocation points x^i. In this Section 4.2.3, we present several test examples of solving equation (4.28) by LU decomposition. However, the Neumann series expansion does not converge for the solution of equation (4.28). We will discuss details on the spectrum of BDIDE operator for equation (4.28) in Section 4.2.4.

In Section 4.2.5, we consider the first method i.e. we solve equation (4.5) with the collocation points $x^i \in \overline{\Omega}$ at all J nodes. For equation (4.5), the Neumann series converges to the desired solution.

As in the previous test examples on Neumann problem, we will consider three test domains i.e. a square domain, a circular domain and a parallelogram. The geometry of the three test domains are as in Figure 3.4.

For each domain, we solve the following interior Dirichlet problems:

1. $a(x) = 1$ with $f(x) = 0$ for $x \in \Omega \cup \partial\Omega$ and $\overline{u}(x) = x_1$ for $x \in \partial\Omega$,

2. $a(x) = x_2^2$ with $f(x) = 0$ for $x \in \Omega \cup \partial\Omega$ and $\overline{u}(x) = x_1$ for $x \in \partial\Omega$,

3. $a(x) = x_2^4$ with $f(x) = 0$ for $x \in \Omega \cup \partial\Omega$ and $\overline{u}(x) = x_1$ for $x \in \partial\Omega$,

4. $a(x) = x_2^6$ with $f(x) = 0$ for $x \in \Omega \cup \partial\Omega$ and $\overline{u}(x) = x_1$ for $x \in \partial\Omega$,

5. $a(x) = x_2^8$ with $f(x) = 0$ for $x \in \Omega \cup \partial\Omega$ and $\overline{u}(x) = x_1$ for $x \in \partial\Omega$,

6. $a(x) = x_2^{10}$ with $f(x) = 0$ for $x \in \Omega \cup \partial\Omega$ and $\overline{u}(x) = x_1$ for $x \in \partial\Omega$,

7. $a(x) = x_2^2$ with $f(x) = 2x_2^2$ for $x \in \Omega \cup \partial\Omega$ and $\overline{u}(x) = x_1^2$ for $x \in \partial\Omega$,

Let us define the relative error for the approximate solution $\epsilon(u)$ and and the relative errors for its gradient $\epsilon(\nabla u)$, as in (3.67) and (3.68).

The comparative results for relative error of approximate solutions u_{approx} obtained by LU decomposition method and their gradient ∇u_{approx} versus number of nodes J for Test 2 and Test 7 on square domain, circular domain, and parallelogram are shown in Figures 4.1-4.3.

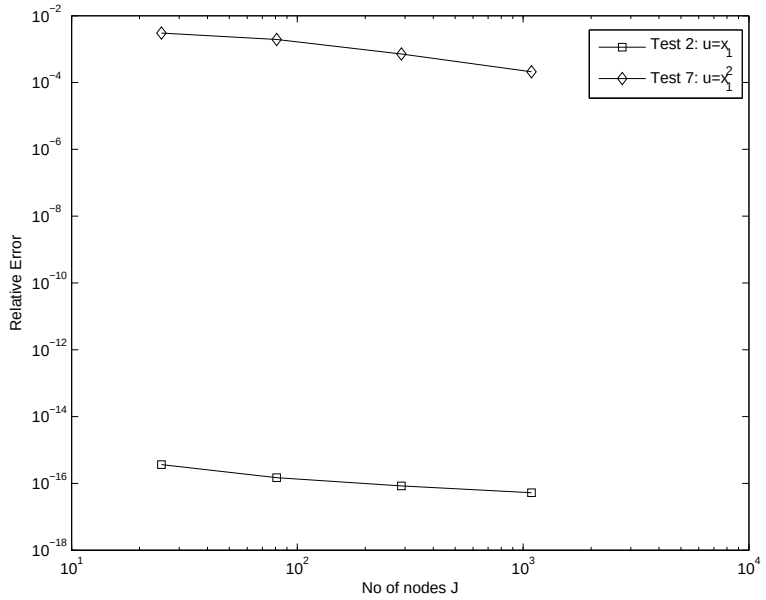

(a)

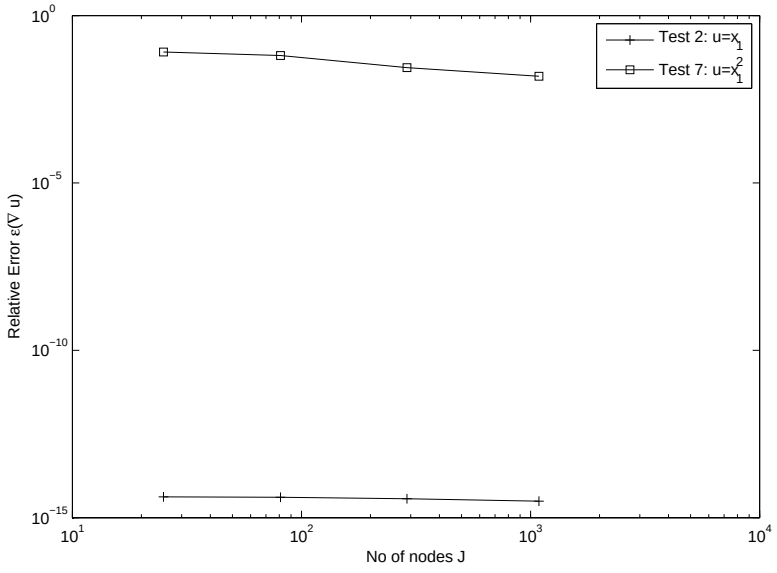

(b)

Figure 4.1: Relative errors of the approximate solutions (a) and their gradients (b), on the square vs. number of nodes J.

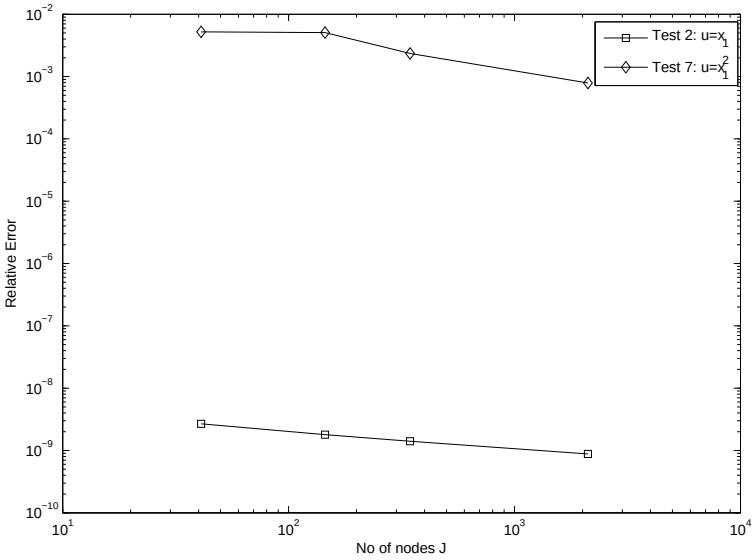

(a)

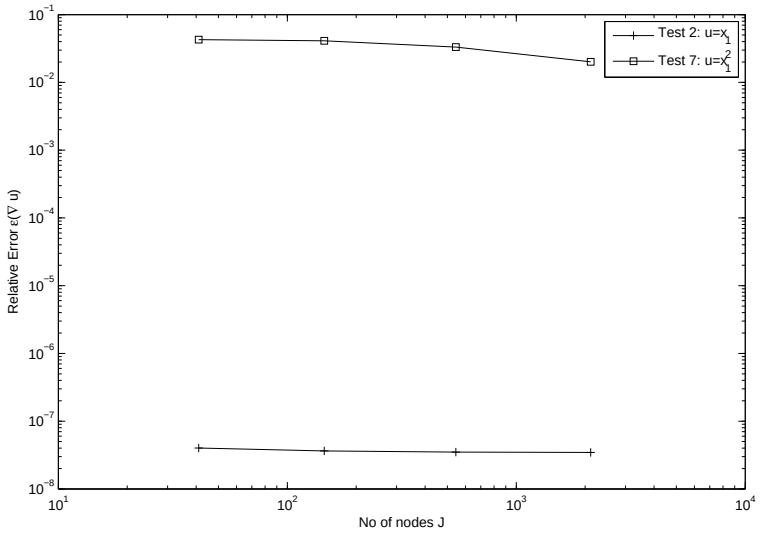

(b)

Figure 4.2: Relative errors of the approximate solutions (a) and their gradients (b), on circular test domain vs. number of nodes J.

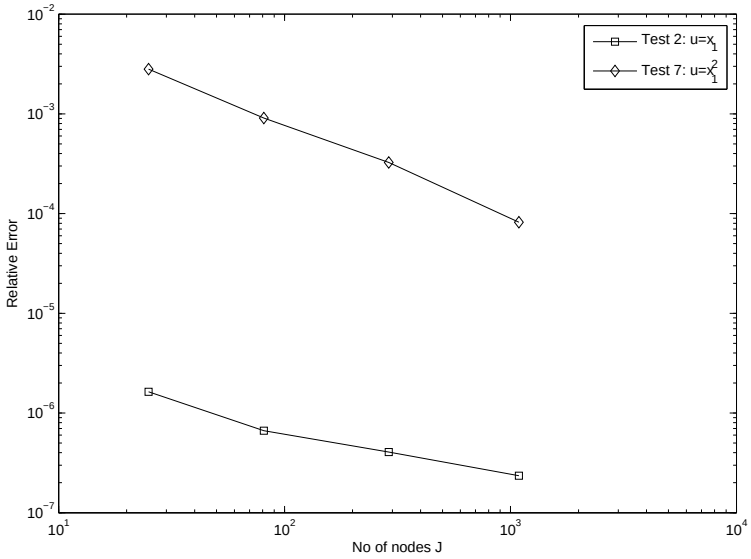

(a)

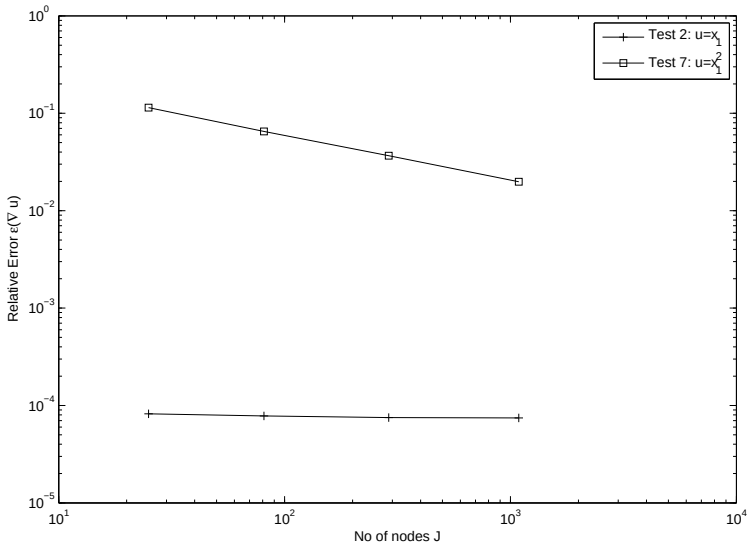

(b)

Figure 4.3: Relative errors of the approximate solutions (a) and their gradients (b), on parallelogram vs. number of nodes J.

As in Section 3.3, the dependence of the error $\epsilon(u)$ on the number of nodes J (an on the average linear size of the elements, h) can be fitted with a power function (i.e. with a straight line in the double logarithmic coordinates in the graphs) so that $\epsilon \approx J^{-q/2} \approx h^q$.

From our numerical results, the convergence rate of BDIDE for Dirichlet problem as in equation (4.28) when J increases is close to the convergence rate of BDIE for Neumann problem as discussed in Section 3.3 i.e. $q \approx 1$ in Test 2 and $q \approx 2$ in Test 7 i.e. respectively, linear and quadratic convergence with respect to the element size h.

The accuracy in Test 2 is much higher as compared to the Test 7 as only the integral operator approximation error, related with the accuracy of the numerical integration, is involved. However, for Test 7, in addition to the integral operator approximation error, the implementation of the piece-wise bi-linear interpolation on the quadratic exact solution gives its contribution in the total error.

4.2.4 Eigen-values for the System (4.28)

In this section, we will discuss the distribution of eigen-values of the corresponding discrete operators calculated numerically in (4.28). This is helpful in investigating the convergence of Neumann series expansion.

Defining

$$F(x^i) = -\sum_{x^i \in \partial\Omega} K_{ij}^D \overline{u}(x^j) + Q_i^D + D_i^D,$$

we can then write (4.28) as

$$c(x^i)u(x^i) + \sum_{x^j \in \Omega} K_{ij}^D u(x^j) = F(x^i), \quad x^i \in \Omega. \tag{4.29}$$

In solving equation (4.29) by using Neumann series expansion, and since $c(x^i) = 1$ for $x^i \in \Omega$, we write (4.29) as

$$(I - K_3)u = \mathcal{F},$$

where

$$I = \delta_{ij},$$

$$\begin{aligned} u &= u(x^j), \\ K_3 &= -K_{ij}, \\ \mathcal{F} &= F(x^i). \end{aligned} \tag{4.30}$$

These notations enable us to present the Neumann series expansion as in the following:

$$u = \sum_{n=0}^{N} K_3^n \mathcal{F}. \tag{4.31}$$

Since it is rather expensive for numerical purposes to calculate the power of K_3 in equation (4.31), we will denote

$$\begin{aligned} g_0 &= \mathcal{F}, \\ g_n &= K_3 g_{n-1}. \end{aligned}$$

Therefore (4.31) can be written as

$$u = \sum_{n=0}^{N} K_3^n \mathcal{F} = \mathcal{F} + \sum_{n=1}^{N} g_n. \tag{4.32}$$

It is well known that the Neumann series in the form (4.32) for a matrix operator K_3 converges for any right hand side if and only if all eigen-values of the operator K_3 belong to the open unit disc.

We have seen in Section 3.3.3, the detailed analysis of the discrete BDIE eigen-values for Neumann problem demonstrated that when the PDE coefficient moderately varies with coordinates, the spectrum is contained in the unite circle, which implies the Neumann series convergence. However, this property does not hold generally, and when the coefficient varies sharp enough, some eigen-values appear also outside the unite circle, which can lead to divergence of the standard Neumann series. Similar behavior will be observed also for the BDIDE of the Dirichlet problem.

In checking the distribution of eigen-values of the corresponding discrete operator K_3 calculated numerically in (4.30), we will consider here the simplest test example i.e. $a = 1$ as in Test 1. Observe that when $a = 1$, the BDIDE will be reduced to a BIE and the maximal eigen-values should lies within a unit circle. However, in contrast to the theory for

the original BIE, in our numerical experiment of discrete BIE for Dirichlet problem, some eigen-values of the operator K_3 (4.30) appears also outside the unite circle even for Test 1 i.e. when $a = 1$.

Let $\tilde{\lambda}_k,\ k = 1, 2, J - J_D$, denote the eigen-values of the matrix $K_3 = K_{ij}$ i.e. the numbers λ_k for which the homogeneous equation

$$(\tilde{\lambda}_k I - K_3)u = 0$$

has non-trivial solutions.

We calculate several eigen-values with the maximum modulus for Test 2 on a square (see Figure 3.4a) in Figure 4.4.

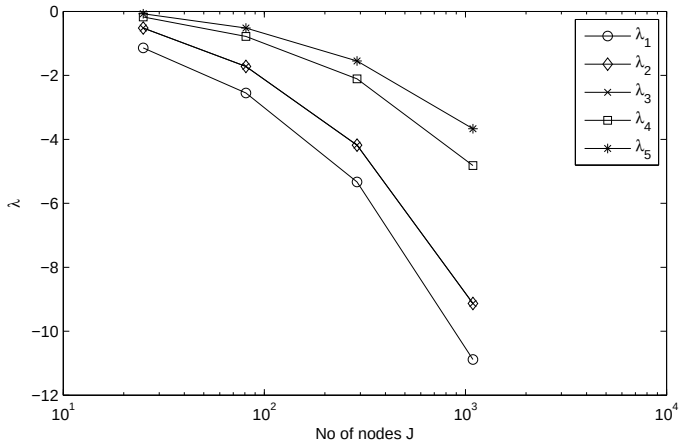

Figure 4.4: Eigen -values of the matrix K_3 for the square vs. the number of nodes $J - J_D$.

The values of J that are taken in the experiments on a square are $25, 81, 289$ and 1089. From the figure, we can see that there is no convergence of the eigen-values as J increases and the spectrum is not contained in the unite circle that leads to divergence of the Neumann iteration. Note also that the five maximal eigen-values are all real.

This can be explained by the fact that the left-hand side operator in (4.29) can be considered as the discrete approximation of the closed unbounded BDIDE operator which domain of definition consists of the function u that are equal 0 on the boundary but the range consists of the functions that may be non-zero on the boundary. But the resolvent

of closed unbounded operator has an essential singularity at infinity, see e.g. (Kato (1980), Theorem 6.13).

Therefore, to obtain the convergence of the Neumann series expansion, we will analyze in the next Subsection, the eigen-values for equation (4.17) i.e. for collocation points $x^i \in \overline{\Omega}$.

4.2.5 Numerical Examples for System (4.17)

In solving equation (4.17) by using Neumann series expansion, we write (4.17) as

$$(I - K_4)u = \mathcal{F},$$

where

$$\begin{aligned} I &= \delta_{ij}, \\ u &= u(x^j), \\ K_4 &= -K_{ij}, \\ \mathcal{F} &= F(x^i). \end{aligned}$$

This arrangement enables us to apply the Neumann series expansion as in the following:

$$u = \sum_{n=0}^{N} K_4^n \mathcal{F}. \tag{4.33}$$

We denote

$$\begin{aligned} g_0 &= \mathcal{F}, \\ g_n &= K_4 g_{n-1}. \end{aligned}$$

Therefore (4.33) can be written as

$$u = \sum_{n=0}^{N} K_4^n \mathcal{F} = \mathcal{F} + \sum_{n=1}^{N} g_n. \tag{4.34}$$

As previously, we give numerical examples for square, circular domain and parallelogram domains presented in Figure 3.4. For all tests, we give numerical results for the relative error for the approximate solution $\epsilon(u)$ and its gradient $\epsilon(\nabla u)$ as given in (3.67) and (3.68), respectively.

The comparative results obtained by LU decomposition method versus number of nodes J for Test 2 and Test 7 on square, circular and parallelogram domains are shown in the Figures 4.5, 4.7 and 4.9, respectively.

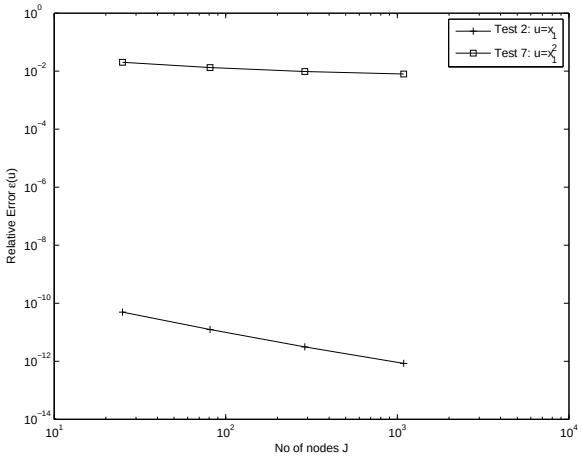

(a)

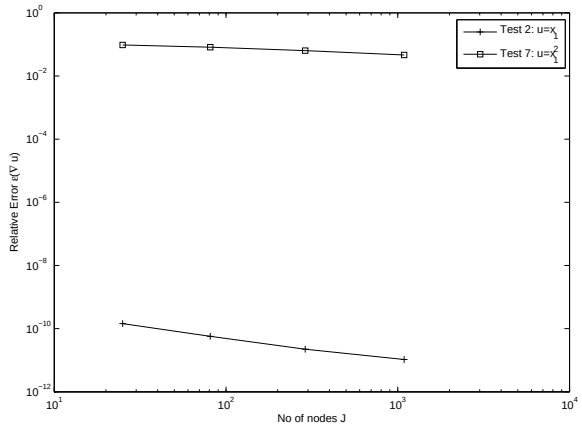

(b)

Figure 4.5: Relative errors of the approximate solutions (a) and their gradients (b), on the square vs. number of nodes J.

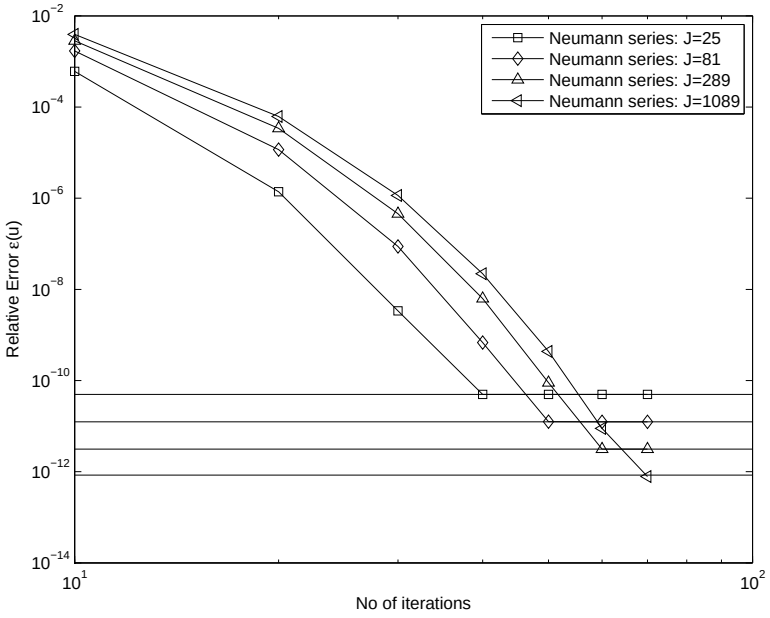

(a) Test 2.

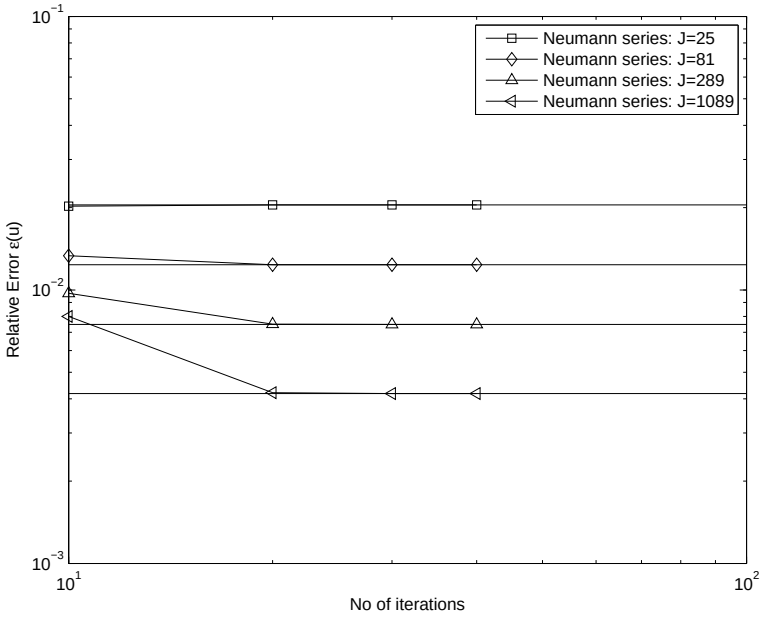

(b) Test 7.

Figure 4.6: Relative error of the solutions on the square vs. number of Neumann iterations, compared with the error of the LU decomposition solution (horizontal lines), for different number of mesh nodes J.

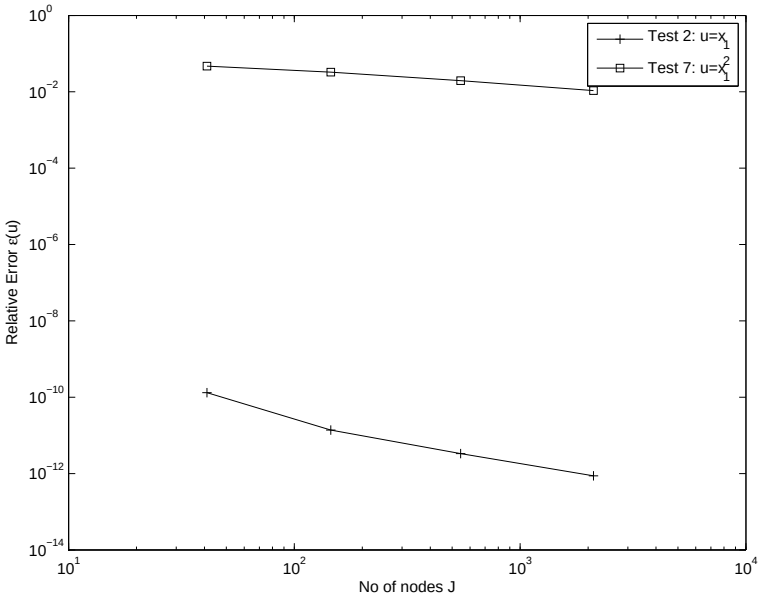

(a)

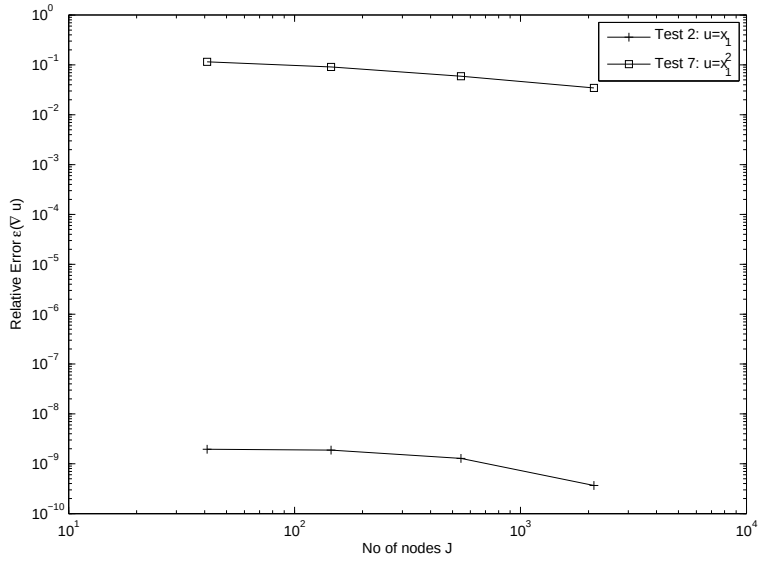

(b)

Figure 4.7: Relative errors of the approximate solutions (a) and their gradients (b), on circular domain vs. number of nodes J.

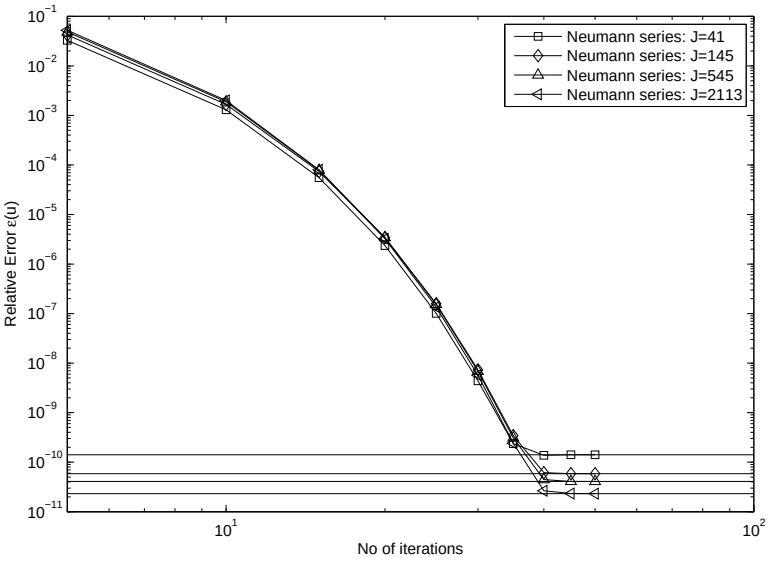

(a) Test 2.

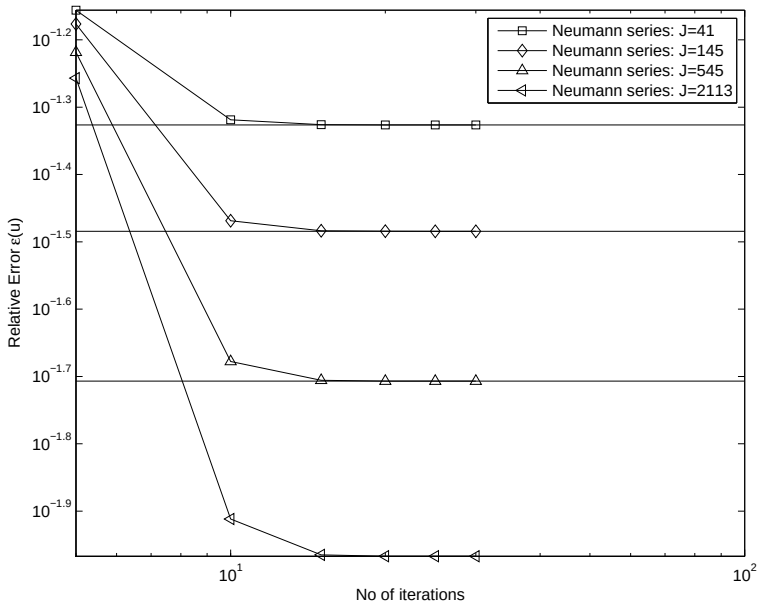

(b) Test 7.

Figure 4.8: Relative error of the solutions on circular domain vs. number of Neumann iterations, compared with the error of the LU decomposition solution (horizontal lines), for different number of mesh nodes J.

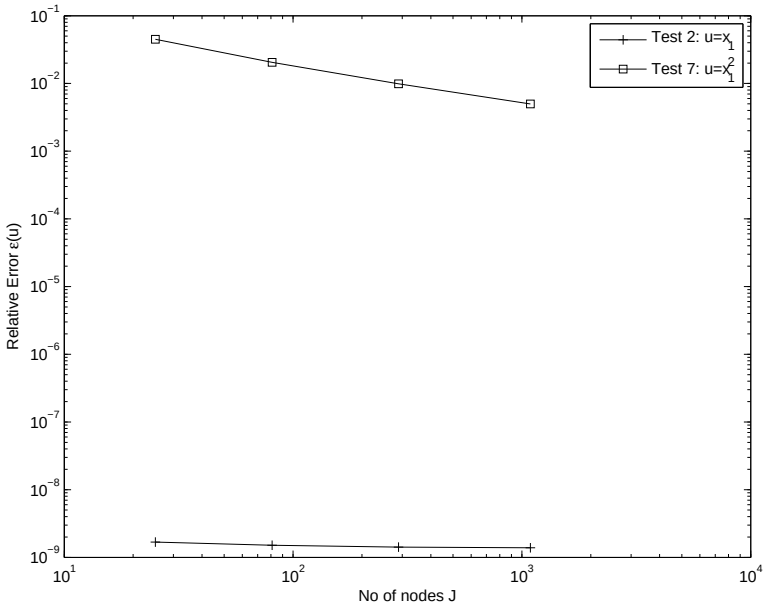

(a)

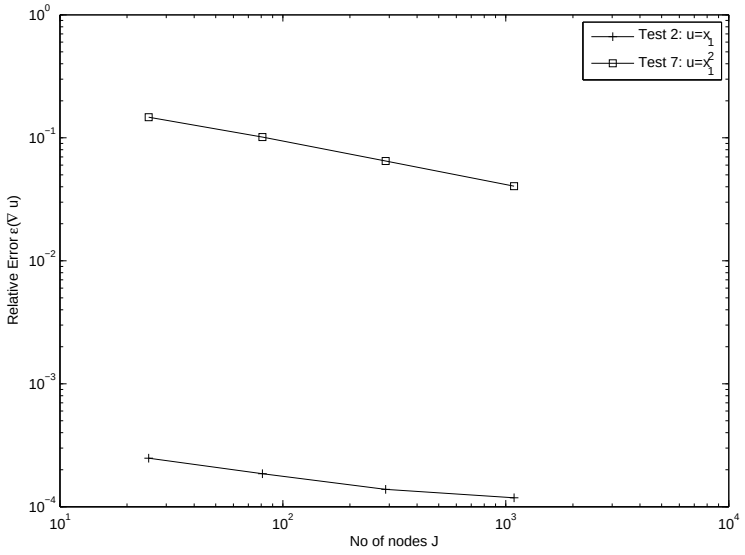

(b)

Figure 4.9: Relative errors of the approximate solutions (a) and their gradients (b), on the parallelogram vs. number of nodes J.

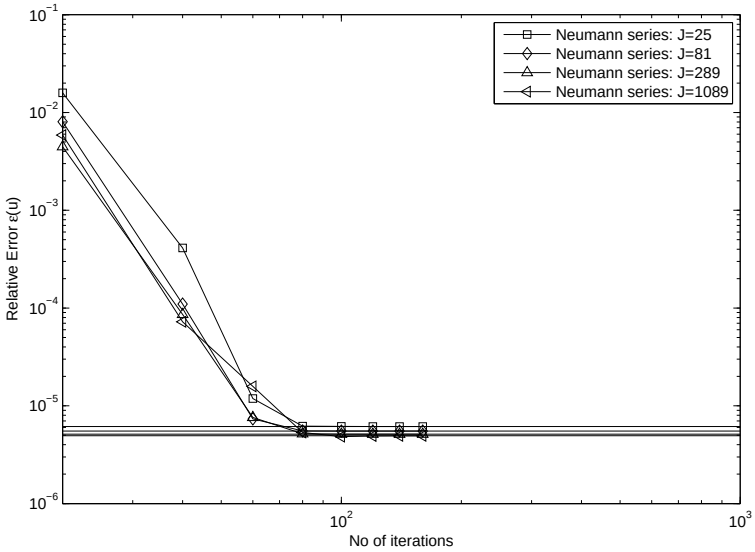

(a) Test 2.

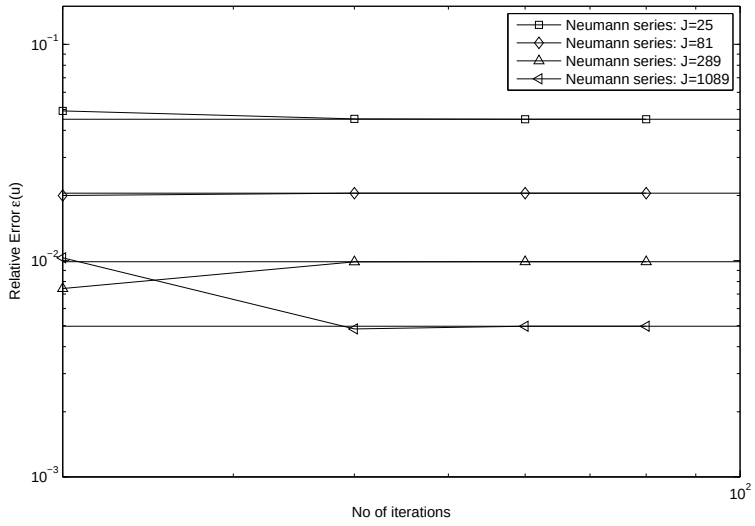

(b) Test 7.

Figure 4.10: Relative error of the solutions on parallelogram vs. number of Neumann iterations, compared with the error of the LU decomposition solution (horizontal lines), for different number of mesh nodes J.

From Figures 4.5, 4.7 and 4.9, we can see that the error of approximate solution $\epsilon(u)$ and the error of gradient $\epsilon(\nabla u)$ decrease.

Figures 4.6, 4.8 and 4.10 show the the solutions obtained by Neumann iterations converged to the solutions obtained by LU decomposition.

Similar to Section 3.3, we fitted the dependence of the error $\epsilon(u)$ on the number of nodes J with a power function (i.e. with straight line in the double logarithmic coordinates in the graphs), giving $\epsilon \sim J^{-q/2} \sim h^q$. We get $q \approx 1$ in Test 2 for square and parallelogram. For circular domain, the convergence rate is quite slow, i.e., $q \approx 0.6$. For Test 7, our numerical experiments shows $q \approx 1.5$ for square, $q \approx 1$ for circular domain and $q \approx 2$ for parallelogram.

For the gradient error we similarly have $\nabla\epsilon(u) \sim J^{-q'/2} \approx h^{q'}$, where $q' \approx 0.16$ for the square, $q' \approx 0.08$ for circular domains and $q' \approx 0.05$ for the parallelogram domain in Test 2, while $q' \approx 0.9$ for the square and parallelogram, and $q' \approx 0.4$ for the circular domain in Test 7.

As follows from Figures 4.6, 4.8 and 4.10 the Neumann series converges to solutions obtained from LU decomposition method, reaching the LU decomposition accuracy after $40 - 80$ iterations for the square, $40 - 50$ iterations for the circle and $90 - 100$ iterations for the parallelogram in Test 2 and after $20 - 40$ iterations for all domains in Test 7.

More Neumann iterations are needed to reach the accuracy of the LU decomposition numerical solution for Test 2 compared to Test 7 since the accuracy of the LU decomposition numerical solution taken for comparison for Test 2 is higher than Test 7.

This means that in addition to the dependence of the iteration number on the test (i.e. on the exact solution behaviour) and on the domain shape, it is also related with the different accuracy of the LU numerical solution taken for comparison.

4.2.6 Eigen-values for the System (4.17)

In the previous subsection, we have seen that the Neumann series expansion in (4.34) converges to the LU decomposition solutions for Test 2 and Test 7, i.e., when $a = x_2^2$. We will also investigate whether it holds for other variable coefficients $a(x)$ of the PDE for Dirichlet problem.

In this section, we want to investigate the eigen-values properties of the obtained algebraic systems (4.5) for a matrix operator K_4 that influences the convergence of the iterative method. It is well known that the Neumann series in the form of equation (4.34) for a matrix operator K_4 converges for any right hand side if and only if all eigen-values of the operator K_4 belong to the open unit disc. Moreover, if all eigen-values of the operator K_4 belongs to the open unit disc, maximum eigen-value modulus will reflects the number of iterations sufficient for Neumann series to converges to the LU decomposition solution.

Let $\widetilde{\lambda}_k,\ k = 1, 2, \cdots J$, denote the eigen-values of the matrix K_4 , i.e., the numbers $\widetilde{\lambda}_k$ for which the homogeneous equation

$$(\widetilde{\lambda}_k I - K_4)u = 0$$

has non-trivial solutions.

When the coefficient $a(x)$ is a constant, the remainder R vanishes but unlike to the BDIE system for the Neumann problem, the BDIDE (4.15) can not be split on the purely boundary integral equation for the boundary values (traces) of u on $\partial\Omega$, and on the representation formula for u in Ω because of the term with Tu. The same will also hold for its discrete counterpart (4.16).

In Section 3.3.3, we have made some conclusion about spectral properties for operator K_2 of the perturbed BDIE for PDE of Neumann problem. We have seen that, when the power k of the coefficient $a(x)$ increases, the imaginary values of the largest $\widetilde{\lambda}$ increase as well such that after some k, the eigen-values appear also outside the unit circle. This implies the divergence of the standard Neumann series expansion for coefficients $a(x)$ with big k even the direct methods such as LU decomposition and Gaussian elimination still reliable. However, the real values of the largest $\widetilde{\lambda}$ do not vary much and it is still belong to the interval

$(0, 1)$.

In the following discussions, we will see that similar conclusion can be made for BDIDE (4.15).

Figures 4.11-4.13 present the first eigen-values $\widetilde{\lambda}_k$ of the matrix K_4 with the largest moduli for the examples in Test 2 for square, circular and parallelogram domains, respectively.

Note that, in all examples in case 2, i.e., when coefficient $a(x) = x_2$, the maximal absolute values of eigen-values of the matrix K_4 are less than 1, that implies the convergence of the Neumann series. The Neumann series for the circular domain converges after 40 iterations and parallelogram needs 90 iterations to converge correlating well with max $|\lambda_k| = 0.5$ for the circular domain and $|\lambda_k| = 0.9$ for the parallelogram.

However, as we will see, this property does not hold generally as the order, k, of the coefficient $a(x)$ growth increases, the maximal eigen-values increase and above some value of k, some eigen-values appear also outside the unite circle, which can lead to divergence of the standard Neumann series. In investigating the influence of the coefficient $a(x)$ on the maximum eigen-values of the matrix K_4, we calculated them for $a(x) = x_2^k$ for $k = 0, 2, \cdots, 10$.

We show the maximum eigen-values of the operator K_4 for the finest meshes on each domains, i.e., when $J = 1089$ for the square and parallelogram and $J = 2113$ for circular domain. This result on each domain is shown in Figures 4.14- 4.16.

For the overlapping eigen-values seen on the figures our calculation shown that their eigen-functions are linearly independent, i.e., the eigen-values are geometrically multiple.

Note however that from these figures one can conclude that $0 < \mathrm{Re}\ \widetilde{\lambda}_k < 1$ for the all considered examples, similar to the constant coefficient case, while $|\mathrm{Im}\ \widetilde{\lambda}_k| < C$ with some constant $C < 2$.

Next, we will analyze of the eigen-values for discrete BDIDE. We consider equations (3.74)-(3.76) and by observing the spectral properties in Figures 4.14-4.16, we have

$$\max \left| \frac{L\nabla a}{a} \right| < 5, \tag{4.35}$$

for the spectral radius to be less than 1. Note that the condition obtained in (4.35) for

the BDIDE operator is the same as obtained in (3.77) for the perturbed Neumann BDIE operator.

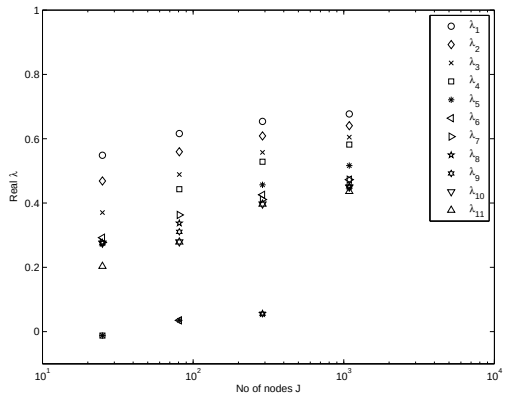

(a) Re λ.

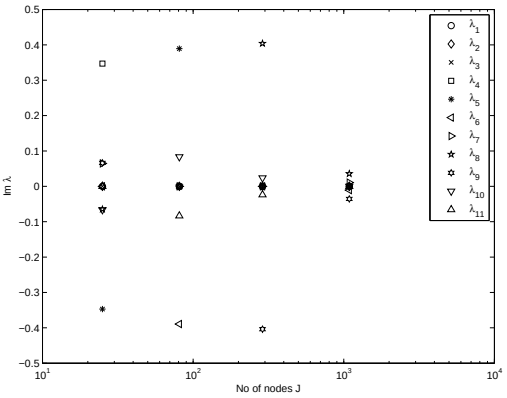

(b) Im λ.

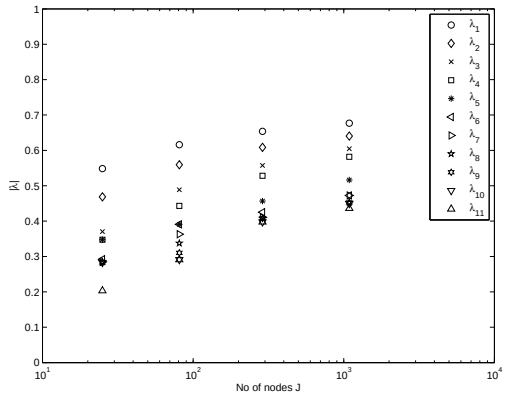

(c) $|\lambda|$.

Figure 4.11: Eigen -values of the matrix K_4 for the square domain vs. the number of nodes J.

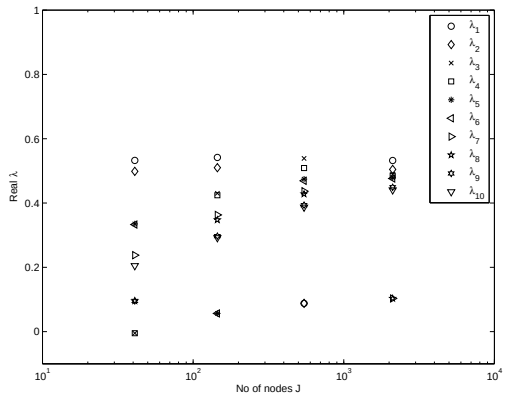

(a) Re λ.

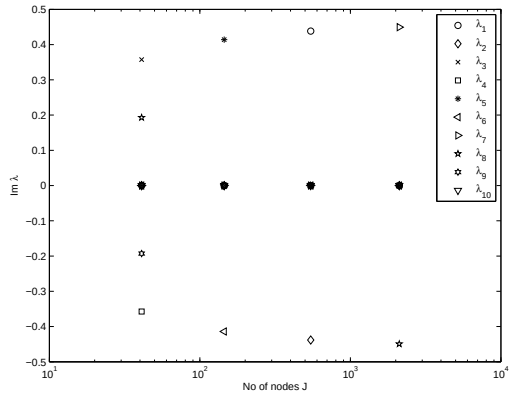

(b) Im λ.

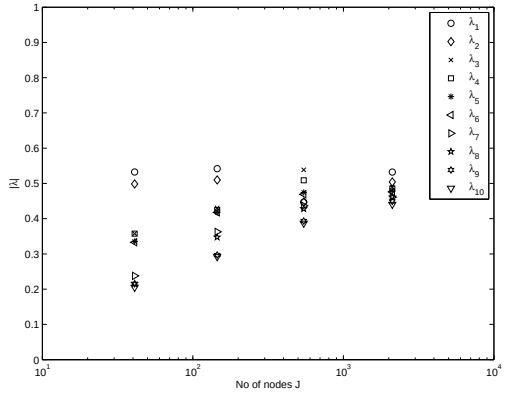

(c) $|\lambda|$.

Figure 4.12: Eigen -values of the matrix K_4 for the circular domain vs. the number of nodes J.

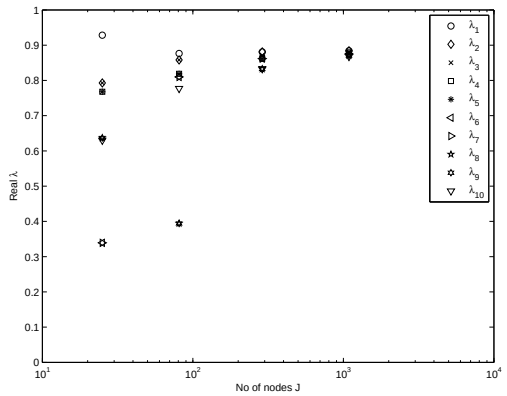

(a) Re λ.

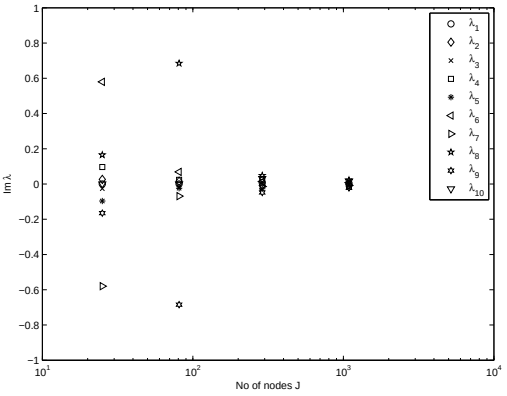

(b) Im λ.

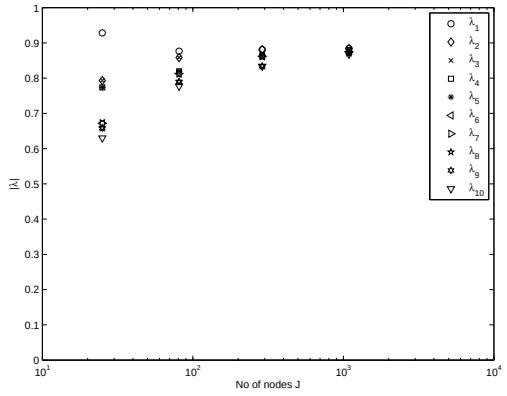

(c) $|\lambda|$.

Figure 4.13: Eigen -values of the matrix K_4 for the parallelogram vs. the number of nodes J.

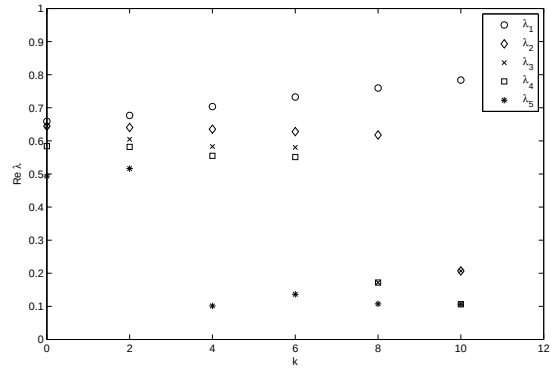

(a) Re λ.

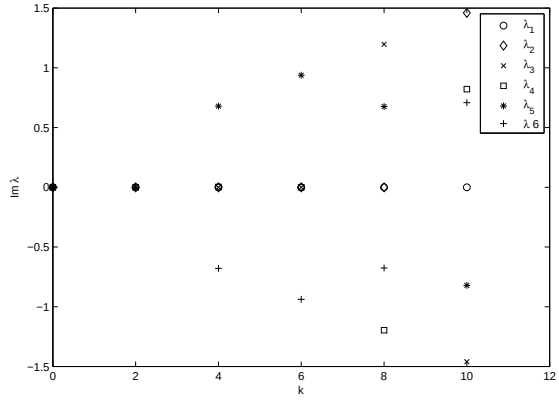

(b) Im λ.

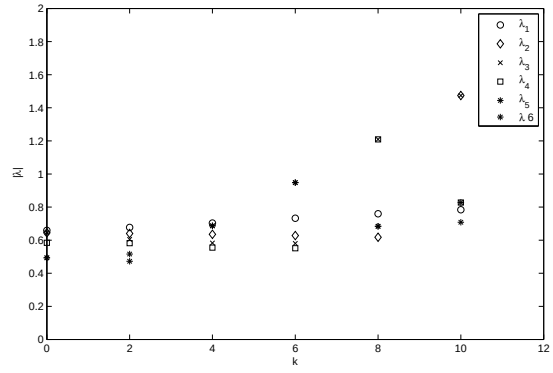

(c) $|\lambda|$.

Figure 4.14: The six largest eigen-values of the matrix K_4 on the square vs k for $a(x) = x_2^k$.

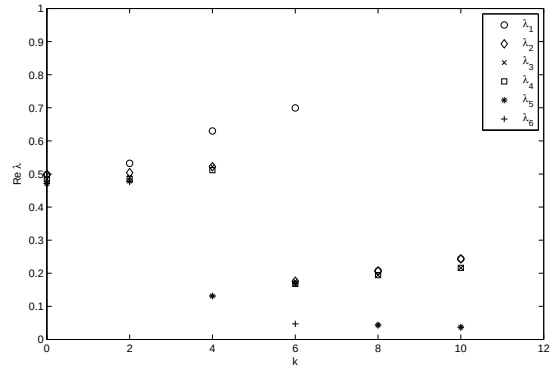

(a) Re λ.

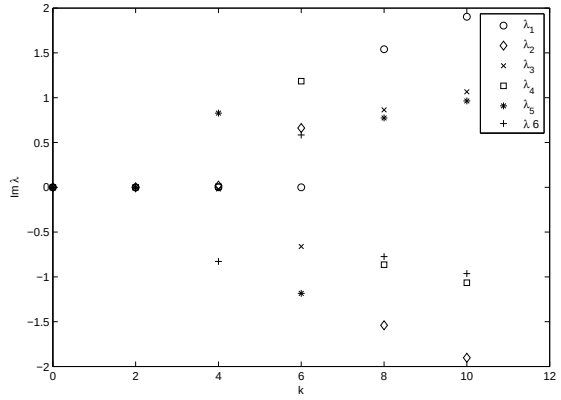

(b) Im λ.

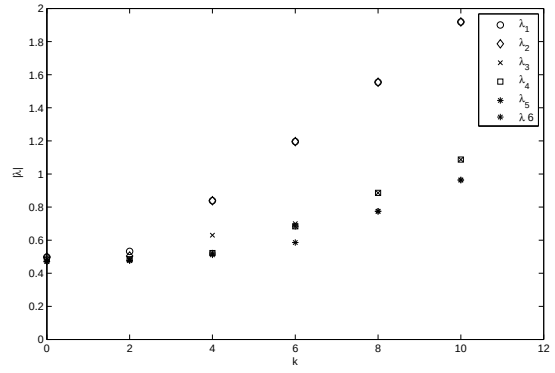

(c) $|\lambda|$.

Figure 4.15: The six largest eigen-values of the matrix K_4 on the circular domain vs k for $a(x) = x_2^k$.

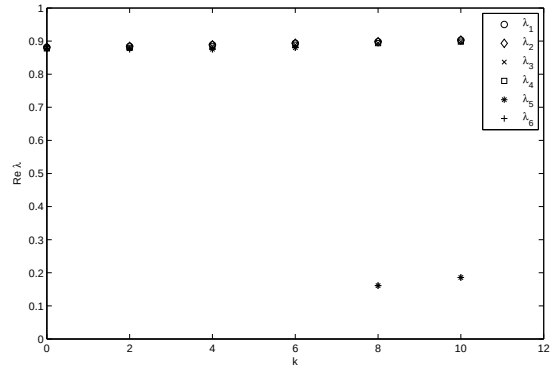

(a) Re λ.

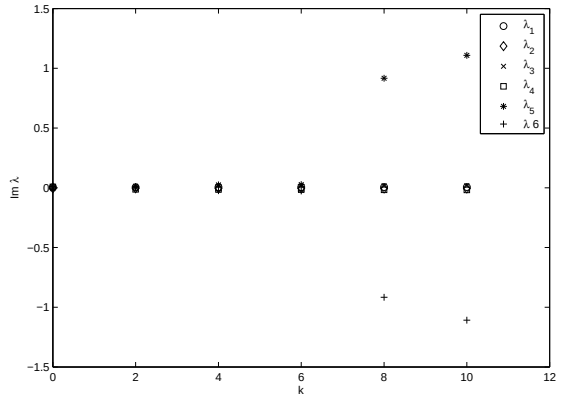

(b) Im λ.

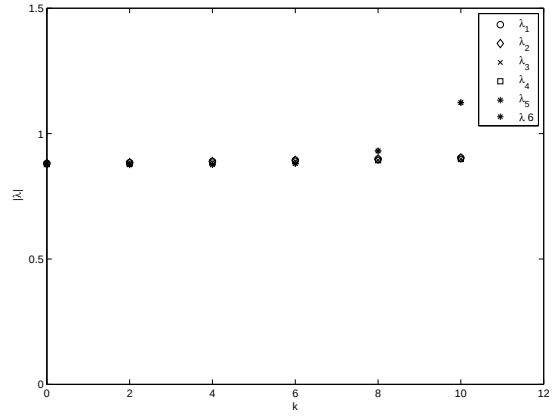

(c) $|\lambda|$.

Figure 4.16: The six largest eigen-values of the matrix K_4 on the parallelogram vs k for $a(x) = x_2^k$.

4.3 Conclusion

The numerical experiments and the analysis of the discrete BDIE's eigen-values related to Neumann problem is further extended to those of Dirichlet problem in this chapter. Unlike the BDIE related to Neumann problem, we don't have to add a perturbation operator in order to guarantee the BDIDEs to be an unconditionally and uniquely solvable integral equation. The numerical results presented in this chapter show that the mesh-based discretization of the BDIDE with a quadrilateral bilinear approximation leads to a system of linear algebraic equations that can be solved e.g. by LU-decomposition with linear convergence with respect to the linear element size. We showed that spectral properties of the BDIDE depend on the variable coefficients and shapes of the domains which also influence the convergence of the Neumann iterations. Similar to the BDIE related to Neumann problem, when the coefficient gradient is small or moderate (e.g. $\max\left|\frac{L\nabla a}{a}\right| < 5$ in the considered examples, where L is a characteristic size of the domain) the spectrum is contained in the unit circle, which implies the Neumann series convergence. Moreover, the number of terms in the Neumann series sufficient for the error to be lower than a prescribed value, can be estimated in terms of the maximum eigen-value modulus. For larger coefficient gradient, i.e., when $\max\left|\frac{L\nabla a}{a}\right| \geq 5$, some eigen-values appear also outside the unit circle, which can lead to divergence of the standard Neumann series. For the later case, the eigen-values are generally complex and can lay outside the unit circle. It is also interesting that real values of the eigen-values are always less than 1 for the all considered examples even for sufficiently sharp variation of the coefficient. This might leads to much easier work on mapping the exterior λ-domain to the exterior of the unit circle, which will lead to a converging modification of the Neumann series as suggested by (Kantorovich and Krylov (1964)) and (Kublanovskaya (1959)).

Unlike FEM, the system of linear algebraic obtained from boundary-domain integral equation is fully populated which prevent the use of well elaborated methods for sparsely populated systems. This fact may influence the computational time especially for higher number of nodes. Therefore, the standard Neumann iteration method is a good alternative to the direct methods when $\max\left|\frac{L\nabla a}{a}\right| < 5$.

Chapter 5

The Localized Boundary-Domain Integral Equation for Neumann and Dirichlet Problems

5.1 Introduction

In this chapter, we will discuss the Localized Boundary-Domain Integral Equations (LBDIEs) related to Neumann and Dirichlet problems. These LBDIEs are obtained by using localized parametrix $P_\chi(x, y)$. In our work, we chose a constant cut-off function χ. We explain the discretization of the LBDIEs which leads to systems of linear equations. The algebraic systems of linear equations are then solved by using LU decomposition method.

The advantage of LBDIE is in the possibility to reduce it to a linear algebraic sparsely populated system. Therefore, the time taken for calculation will be shorter than for fully populated system obtained from non-localised BDIE.

From our numerical experiments shown in this chapter, it will be seen that the maximal eigen-values for the LBDIEs' operators related to both Neumann and Dirichlet problems are not contained in a unit circle, therefore the Neumann problem diverges.

5.2 Localized Boundary-Domain Integral Equations

The idea to reduce the fully populated linear algebraic equations obtained from boundary-domain integral equation to a sparsely system of linear algebraic equations is discussed in (Mikhailov (2002)). Thus, we can consider the localized parametrix

$$P_\chi(x,y) = \chi(x,y)P(x,y), \tag{5.1}$$

where $\chi(x,y)$ is a cut-off function such that $\chi(y,y) = 1$ and $\chi(x,y) = 0$ at x not belonging to a localisation domain $\omega(y)$. The localized parametrix $P_\chi(x,y)$ has the same singularity as parametrix $P(x,y)$ at $x = y$ but it is non-zero only on the localisation domain $\omega(y)$.

Since $P_\chi(x,y)$ is a parametrix for the operator L in (3.1), it is a solution of the following equation:

$$L_x P_\chi(x,y) = \delta(x-y) + R_\chi(x,y), \tag{5.2}$$

where $\delta(x-y)$ is the Dirac delta function and the remainder $R_\chi(x,y)$ is defined as

$$R_\chi(x,y) = R(x,y) - L_x((1-\chi)P).$$

The third Green identity localized on the intersection $\omega(y) \cap \Omega$ and on its boundary $\partial[\omega(y) \cap \Omega]$ is as follows:

$$\begin{aligned} c(y)u(y) \quad &- \int_{\overline{w}(y)\cap\partial\Omega} u(x) T_x P_\chi(x,y)\, \mathrm{d}\Gamma(x) + \int_{\overline{w}(y)\cap\partial\Omega} P_\chi(x,y) Tu(x)\, \mathrm{d}\Gamma(x) \\ &- \int_{\Omega\cap\partial\omega(y)} u(x) T_x P_\chi(x,y)\, \mathrm{d}\Gamma(x) + \int_{\Omega\cap\partial\omega(y)} P_\chi(x,y) Tu(x)\, \mathrm{d}\Gamma(x) \\ &+ \int_{w(y)\cap\Omega} R_\chi(x,y) u(x)\, \mathrm{d}\Omega(x) = \int_{w(y)\cap\Omega} P_\chi(x,y) f(x)\, \mathrm{d}\Omega(x), \quad y \in \overline{\Omega}. \end{aligned} \tag{5.3}$$

We choose the cut-off function χ as

$$\chi(x,y) = \begin{cases} 1, & x \in \omega_y, \\ 0, & x \notin \omega_y. \end{cases} \tag{5.4}$$

Therefore, we have,

$$P_\chi(x,y) = \begin{cases} P(x,y), & x \in \omega_y, \\ 0, & x \notin \omega_y, \end{cases}$$

and

$$R_\chi(x,y) = \begin{cases} R(x,y), & x \in \omega_y, \\ 0, & x \notin \omega_{y^{\text{'}}}. \end{cases}$$

However, this cut-off function $\chi(x,y)$ is not smooth in $x \in \mathbb{R}^n$ which results in appearing the third and forth integrals in (5.3).

5.2.1 Localized Boundary-Domain Integral Equation Method for Neumann Problem

For Neumann problem, after imposing in (5.3)) the Neumann boundary condition, $Tu(x) = \bar{t}(x),\ x \in \partial\Omega$, the LBDIE can be written as

$$\begin{aligned} c(y)u(y) &- \int_{\partial\omega(y)} u(x) T_x P_\chi(x,y)\, \mathrm{d}\Gamma(x) + \int_{\Omega\cap\partial\omega(y)} P_\chi(x,y) Tu(x)\, \mathrm{d}\Gamma(x) \\ &+ \int_{\omega(y)\cap\Omega} R_\chi(x,y) u(x)\, \mathrm{d}\Omega(x) = -\int_{\overline{\omega}(y)\cap\partial\Omega} P_\chi(x,y)\bar{t}(x)\, \mathrm{d}\Gamma(x) \\ &+ \int_{\omega(y)\cap\Omega} P_\chi(x,y) f(x)\, \mathrm{d}\Omega(x), \quad y \in \overline{\Omega}. \end{aligned} \tag{5.5}$$

The Neumann problem is not unconditionally solvable, and when it is solvable, its solution can only be unique up to an additive constant. These properties are inherited by the BDIE, cf. (Chkadua et al. (2011a)).

As in Chapter 3, we add the perturbation operator in (3.9) but to the LBDIE for PDE of Neumann problem.

Therefore, we get the following perturbed LBDIE:

$$\begin{aligned} c(y)u(y) &+ \frac{1}{|\partial\Omega|}\int_{\partial\Omega} u(x)\, \mathrm{d}\Gamma(x) - \int_{\overline{\omega}(y)} u(x) T_x P_\chi(x,y)\, \mathrm{d}\Gamma(x) \\ &+ \int_{\Omega\cap\partial\omega(y)} P_\chi(x,y) Tu(x)\, \mathrm{d}\Gamma(x) + \int_{\omega(y)\cap\Omega} R_\chi(x,y) u(x)\, \mathrm{d}\Omega(x) \\ &= -\int_{\overline{\omega}(y)\cap\partial\Omega} P_\chi(x,y)\bar{t}(x)\, \mathrm{d}\Gamma(x) \\ &+ \int_{\omega(y)\cap\Omega} P_\chi(x,y) f(x)\, \mathrm{d}\Omega(x), \quad y \in \overline{\Omega}. \end{aligned} \tag{5.6}$$

By applying interpolation to equation (5.6) and placing the collocation point x^i for $x^i \in \overline{\Omega}$ at all J nodes of the mesh, we obtain the following system of J linear algebraic equations

for J unknowns $u(x^j)$, assuming that $\overline{\omega}(x^j) \subset \overline{\Omega}$ for any x^i and $\partial\omega(x^i)$ consists of only the element boundaries i.e. do not cut through the elements,

$$c(x^i)u(x^i) + \sum_{x^j \in \overline{\omega}(x^i)} K_{ij}u(x^j) + \sum_{x^j \in \partial\Omega} \overset{\circ}{K}_{ij}u(x^j) = Q_i + D_i,\ x^i \in \overline{\Omega}, \tag{5.7}$$

where K_{ij},$\overset{\circ}{K}_{ij}$, Q_i and D_i are defined as follows:

$$\begin{aligned}
K_{ij} &= -\int_{\partial\omega(x^i)} \phi_j(x) T_x P_\chi(x, x^i)\, \mathrm{d}\Gamma(x) + \int_{\Omega\cap\partial\omega(x^i)} P_\chi(x, x^i) \left[a(x)\frac{\partial\phi_j(x)}{\partial\nu(x)}\right] \mathrm{d}\Gamma(x) \\
&+ \int_{\omega(x^i)} \phi_j(x) R_\chi(x, x^i)\, \mathrm{d}\Omega(x), \qquad \text{if} \qquad x^j \in \overline{\omega}(x^i), \qquad (5.8)\\
K_{ij} &= 0, \qquad \text{if} \qquad x^j \notin \overline{\omega}(x^i), \qquad (5.9)\\
\overset{\circ}{K}_{ij} &= \frac{1}{|\partial\Omega|}\int_{\partial\Omega} \phi_j(x)\, \mathrm{d}\Gamma(x), \qquad (5.10)\\
Q_i &= -\int_{\overline{\omega}(x^i)\cap\partial\Omega} P_\chi(x, x^i)\bar{t}(x)\, \mathrm{d}\Gamma(x), \qquad (5.11)\\
D_i &= \int_{\omega(x^i)} P_\chi(x, x^i) f(x)\, \mathrm{d}\Omega(x). \qquad (5.12)
\end{aligned}$$

Since ϕ_j are nonzero only on $\overline{\omega}(x^j)$, we can write (5.8)- (5.12) as follows:

$$\begin{aligned}
K_{ij} &= -\sum_{\gamma_l \subset \partial\omega_l(x^i)\cap\overline{\omega}(x^j)} \int_{\gamma_l} \phi_j(x) T_x P_\chi(x, x^i)\, \mathrm{d}\Gamma(x) \\
&+ \sum_{\gamma_l \subset \partial\omega_l(x^i)\cap\overline{\omega}(x^j)\cap\Omega} \int_{\gamma_l} P_\chi(x, x^i) \left[a(x)\frac{\partial\phi_j(x)}{\partial\nu(x)}\right] \mathrm{d}\Gamma(x) \\
&+ \sum_{\Omega_m \subset \omega(x^i)\cap\omega(x^j)} \int_{\Omega_m} \phi_j(x) R_\chi(x, x^i)\, \mathrm{d}x, \qquad (5.13)\\
\overset{\circ}{K}_{ij} &= \frac{1}{|\partial\Omega|} \sum_{\partial\Omega_l \subset \overline{\omega}(x^j)} \int_{\partial\Omega_l} \phi_j(x)\, \mathrm{d}\Gamma(x), \qquad (5.14)\\
Q_i &= -\sum_{\partial\Omega_l \subset \overline{\omega}(x^i)} \int_{\partial\Omega_l} P_\chi(x, x^i)\bar{t}(x)\, \mathrm{d}\Gamma(x), \qquad (5.15)\\
D_i &= \sum_{\Omega_m \subset \omega(x^i)} \int_{\Omega_m} P_\chi(x, x^i) f(x)\, \mathrm{d}x. \qquad (5.16)
\end{aligned}$$

Here, γ_l is the discretized localisation boundaries.

Therefore, we can write equations (5.13)-(5.16) as follows:

$$K_{ij} = -\sum_{\gamma_l \subset \partial\omega_l(x^i)\cap\overline{\omega}(x^j)} A^l_{n(j,l),i}$$

$$
\begin{aligned}
&+ \sum_{\gamma_l \subset \partial\omega_l(x^i)\cap\overline{\omega}(x^j)\cap\Omega} C^l_{N(j,l),i} + \sum_{\Omega_m \subset \omega(x^i)\cap\omega(x^j)} G^m_{N(j,m),i},\\
\overset{\circ}{K}_{ij} &= \frac{1}{|\partial\Omega|} \sum_{\partial\Omega_l \subset \overline{\omega}(x^j)} B^l_{n(j,l)},\\
Q_i &= -\sum_{\partial\omega_l \subset \overline{\omega}(x^i)} F^l_i,\\
D_i &= \sum_{\Omega_m \subset \overline{\omega}(x^i)} H^m_i,
\end{aligned}
$$

where $n(j,l)$ is the local number of the node x^j on the boundary element $\partial\Omega_l$ and $N(j,m)$ is the local number of the node x^j on the domain element Ω_m.

Expressions $G^m_{N,i}$, $A^l_{n,i}$, $S^q_{n,i}$, $C^q_{N,i}$, F^l_i and H^m_i are given as

$$A^l_{n,i} = \int_{-1}^{1} \Psi_n(\eta) T_x P_\chi(x(\eta), x^i) J_{l1}(\eta)\, \mathrm{d}\eta, \tag{5.17}$$

$$C^l_{N,i} = \int_{-1}^{1} P_\chi(x(\eta), x^i) \left[a(x(\eta)) \left(\sum_{p=1}^{2} \sum_{k=1}^{2} \frac{\partial \Phi_N(\xi)}{\partial \xi_k} \frac{\partial \xi_k}{\partial x_p}\bigg|_{\xi=\xi(\eta)} \nu_p(x(\eta)) \right) \right] J_{l1}(\eta)\, \mathrm{d}\eta, \tag{5.18}$$

$$G^m_{N,i} = \int_{-1}^{1}\int_{-1}^{1} \Phi_N(\xi) R_\chi(x(\xi), x^i) J_{m2}(\xi)\, \mathrm{d}\xi_1 \mathrm{d}\xi_2, \tag{5.19}$$

$$F^l_i = \int_{-1}^{1} P_\chi(x(\eta), x^i) \bar{t}(x(\eta)) J_{l1}(\eta)\, \mathrm{d}\eta, \tag{5.20}$$

$$H^m_i = \int_{-1}^{1}\int_{-1}^{1} P_\chi(x(\xi), x^i) f(x(\xi)) J_{m1}(\xi)\, \mathrm{d}\xi_1 \mathrm{d}\xi_2. \tag{5.21}$$

In the following, we will present the numerical results of (5.7) solved by direct method (LU decomposition method).

We will use quadratic semi-analytic method to handle the influence of singularity $1/r$ when the collocation point x^i is near to the node that belongs to the integration element. This is due to improve convergence of the relative error for the approximate solutions as the number of nodes J increases.

$$
\begin{aligned}
A^l_{1i} &= \int_{-1}^{1} \Psi_1(\eta) T_x P(x^i, x(\eta)) J_{l1}(\eta)\, \mathrm{d}\eta\\
&= \int_{-1}^{1} \Psi_1(\eta) \left(a(x(\eta)) \left((x_1 - x^i_1)\nu_1(x) + (x_2 - x^i_2)\nu_2(x) \right) \frac{1}{2\pi r^2 a(x^i)} \right) J_{l1}(\eta)\, \mathrm{d}\eta,
\end{aligned}
$$

$$\begin{aligned} A^l_{2i} &= \int_{-1}^{1} \Psi_2(\eta) T_x P(x^i, x(\eta)) J_{l1}(\eta)\, \mathrm{d}\eta \\ &= \int_{-1}^{1} \Psi_2(\eta) \left(a(x(\eta)) \left((x_1 - x_1^i)\nu_1(x) + (x_2 - x_2^i)\nu_2(x) \right) \frac{1}{2\pi r^2 a(x^i)} \right) J_{l1}(\eta)\, \mathrm{d}\eta, \end{aligned}$$

where $\nu_k(x),\ k = 1, 2$, are constant on integration interval.

From (3.25) and (3.26), the linear interpolation of $a(x(\eta))$ can be written as

$$a(x(\eta)) \approx \Psi_1(\eta) a(x(-1)) + \Psi_2(\eta) a(x(1)),$$

which implies

$$\begin{aligned} \Psi_1(\eta) a(x(\eta)) &\approx \left(\Psi_1(\eta)\right)^2 a(x(-1)) + \Psi_1(\eta)\Phi_2(\eta) a(x(1)), \\ \Psi_2(\eta) a(x(\eta)) &\approx \Psi_1(\eta)\Phi_2(\eta) a(x(-1)) + \left(\Psi_2(\eta)\right)^2 a(x(1)). \end{aligned}$$

The quadratic semi-analytic formulas are arranged as follows:

$$\begin{aligned} A^l_{1i} &= G^l_{B1} - G^l_{A1}, \\ A^l_{2i} &= G^l_{B2} - G^l_{A2}, \end{aligned}$$

where

$$G^l_{B1} = \int_{-1}^{1} \left(\Psi_1(\eta) T_x P(x^i, x(\eta)) - g_{b1} \right) J_{l1}(\eta)\, \mathrm{d}\eta, \tag{5.22}$$

$$G^l_{B2} = \int_{-1}^{1} \left(\Psi_2(\eta) T_x P(x^i, x(\eta)) - g_{b2} \right) J_{l1}(\eta)\, \mathrm{d}\eta, \tag{5.23}$$

$$G_{A1} = \int_{-1}^{1} g_{b1} J_{l1}(\eta)\, \mathrm{d}\eta$$

$$\begin{aligned} &= \int_{-1}^{1} \left(\Psi_1(\eta)\right)^2 a(x(-1)) \left((x_1(-1) - x_1^i)\nu_1(x) + (x_2(-1) - x_2^i)\nu_2(x) \right) \frac{1}{2\pi r^2 a(x^i)} J_{l1}(\eta)\, \mathrm{d}\eta \\ &+ \int_{-1}^{1} \Psi_1(\eta)\Psi_2(\eta) a(x(1)) \left((x_1(1) - x_1^i)\nu_1(x) + (x_2(1) - x_2^i)\nu_2(x) \right) \frac{1}{2\pi r^2 a(x^i)} J_{l1}(\eta)\, \mathrm{d}\eta \end{aligned}$$

$$
\begin{aligned}
&= \frac{a(x(-1))\left((x_1(-1)-x_1^i)\nu_1(x)+(x_2(-1)-x_2^i)\nu_2(x)\right)}{8\pi a(x^i)}\int_{-1}^{1}(1-\eta)^2\left(\frac{1}{r^2}\right)J_{l1}(\eta)\,\mathrm{d}\eta\\
&+ \frac{a(x(1))\left((x_1(1)-x_1^i)\nu_1(x)+(x_2(1)-x_2^i)\nu_2(x)\right)}{8\pi a(x^i)}\int_{-1}^{1}(1-\eta)(1+\eta)\left(\frac{1}{r^2}\right)J_{l1}(\eta)\,\mathrm{d}\eta,
\end{aligned}
\tag{5.24}
$$

$$
\begin{aligned}
G_{A2} &= \int_{-1}^{1} g_{b2}J_{l1}(\eta)\,\mathrm{d}\eta\\
&= \int_{-1}^{1}\Psi_1(\eta)\Psi_2(\eta)a(x(-1))\left((x_1(-1)-x_1^i)\nu_1(x)+(x_2(-1)-x_2^i)\nu_2(x)\right)\frac{1}{2\pi r^2 a(x^i)}J_{l1}(\eta)\,\mathrm{d}\eta\\
&+ \int_{-1}^{1}\left(\Psi_2(\eta)\right)^2 a(x(1))\left((x_1(1)-x_1^i)\nu_1(x)+(x_2(1)-x_2^i)\nu_2(x)\right)\frac{1}{2\pi r^2 a(x^i)}J_{l1}(\eta)\,\mathrm{d}\eta\\
&= \frac{a(x(-1))\left((x_1(-1)-x_1^i)\nu_1(x)+(x_2(-1)-x_2^i)\nu_2(x)\right)}{8\pi a(x^i)}\int_{-1}^{1}(1-\eta)(1+\eta)\left(\frac{1}{r^2}\right)J_{l1}(\eta)\,\mathrm{d}\eta\\
&+ \frac{a(x(1))\left((x_1(1)-x_1^i)\nu_1(x)+(x_2(1)-x_2^i)\nu_2(x)\right)}{8\pi a(x^i)}\int_{-1}^{1}(1+\eta)^2\left(\frac{1}{r^2}\right)J_{l1}(\eta)\,\mathrm{d}\eta,
\end{aligned}
\tag{5.25}
$$

where

$$
\begin{aligned}
g_{b1} &= \left(\Psi_1(\eta)\right)^2\left(a(x(-1))\left((x_1(-1)-x_1^i)\nu_1(x)+(x_2(-1)-x_2^i)\nu_2(x)\right)\frac{1}{2\pi r^2 a(x^i)}\right)\\
&+ \Psi_1(\eta)\Psi_2(\eta)\left(a(x(1))\left((x_1(1)-x_1^i)\nu_1(x)+(x_2(1)-x_2^i)\nu_2(x)\right)\frac{1}{2\pi r^2 a(x^i)}\right),\\
g_{b2} &= \Psi_1(\eta)\Psi_2(\eta)\left(a(x(-1))\left((x_1(-1)-x_1^i)\nu_1(x)+(x_2(-1)-x_2^i)\nu_2(x)\right)\frac{1}{2\pi r^2 a(x^i)}\right)\\
&+ \left(\Psi_2(\eta)\right)^2\left(a(x(1))\left((x_1(1)-x_1^i)\nu_1(x)+(x_2(1)-x_2^i)\nu_2(x)\right)\frac{1}{2\pi r^2 a(x^i)}\right).
\end{aligned}
$$

The integrals G_{B1} and G_{B2} in (5.22) and (5.23), respectively, are calculated by using Gaussian quadrature and integrals G_{A1} and G_{A2} in equations (5.24) and (5.25), respectively, will be calculated analytically. The integrals G_{A1} and G_{A2} can be written as

$$
\begin{aligned}
G_{A1} &= \frac{a(x(-1))\left((x_1(-1)-x_1^i)\nu_1(x)+(x_2(-1)-x_2^i)\nu_2(x)\right)}{8\pi a(x^i)}g_{A1}\\
&+ \frac{a(x(1))\left((x_1(1)-x_1^i)\nu_1(x)+(x_2(1)-x_2^i)\nu_2(x)\right)}{8\pi a(x^i)}g_{A2},\\
G_{A2} &= \frac{a(x(-1))\left((x_1(-1)-x_1^i)\nu_1(x)+(x_2(-1)-x_2^i)\nu_2(x)\right)}{8\pi a(x^i)}g_{A2}
\end{aligned}
$$

$$+ \quad \frac{a(x(1))\left((x_1(1)-x_1^i)\nu_1(x)+(x_2(1)-x_2^i)\nu_2(x)\right)}{8\pi a(x^i)} g_{A3},$$

where

$$g_{A1} = \int_{-1}^{1} \frac{(1-\eta)^2}{r^2}\frac{ds}{d\eta}\,\mathrm{d}\eta, \tag{5.26}$$

$$g_{A2} = \int_{-1}^{1} \frac{(1+\eta)(1-\eta)}{r^2}\frac{ds}{d\eta}\,\mathrm{d}\eta, \tag{5.27}$$

$$g_{A3} = \int_{-1}^{1} \frac{(1+\eta)^2}{r^2}\frac{ds}{d\eta}\,\mathrm{d}\eta. \tag{5.28}$$

Next, we will show how we calculate integrals g_{A1}, g_{A2} and g_{A3} analytically.

Using (3.46), we can write (5.26)-(5.28) as

$$g_{A1} = \int_{-1}^{1} \left(\frac{(1-\eta)^2}{h^2+(d-s)^2}\right)\frac{ds}{d\eta}\,\mathrm{d}\eta, \tag{5.29}$$

$$g_{A2} = \int_{-1}^{1} \left(\frac{(1+\eta)(1-\eta)}{h^2+(d-s)^2}\right)\frac{ds}{d\eta}\,\mathrm{d}\eta, \tag{5.30}$$

$$g_{A3} = \int_{-1}^{1} \left(\frac{(1+\eta)^2}{h^2+(d-s)^2}\right)\frac{ds}{d\eta}\,\mathrm{d}\eta. \tag{5.31}$$

The analytic solutions for integrals g_{A1}, g_{A2} and g_{A3} in (5.29) -(5.31) are

$$g_{A1} = \frac{1}{W_2^4}\left(8J_{l1}(\eta)\left(W_2^2 - \frac{(W_1^2W_2^2 - W_2^4 + 2W_2^2W_3 - 2W_3^2)f_1}{\sqrt{W_1^2W_2^2 - W_3^2}} + (-W_2^2+W_3)f_2\right)\right),$$

$$g_{A2} = \frac{(4J_{l1}(\eta)\left(2(W_1^2W_2^2 + (W_2^2-2W_3)W_3)f_1 + \sqrt{W_1^2W_2^2-W_3^2}\left(-2W_2^2+(W_2^2-2W_3)f_2\right)\right)}{W_2^4\sqrt{W_1^2W_2^2-W_3^2}},$$

$$g_{A3} = \frac{(8J_{l1}(\eta)(((-W_1^2)W_2^2+2W_3^2)f_1 + \sqrt{W_1^2W_2^2-W_3^2}(W_2^2+W_3f_2)))}{(W_2^4\sqrt{W_1^2W_2^2-W_3^2})},$$

where

$$J_{l1}(\eta) = \frac{ds}{d\eta} = \frac{W_2}{2},$$

$$f_1 = ArcTan\left[\frac{\sqrt{W_1^2W_2^2-W_3^2}}{(W_1^2-W_3)}\right],$$

$$f_2 = \ln\left[\frac{(W_1^2+W_2^2-2W_3)}{W_1^2}\right],$$

and W_1, W_2 and W_3 are defined in (3.33)-(3.35).

5.2.2 Numerical Examples

In the following, we will presents the numerical results of the perturbed LBDIE related with Neumann problem (5.6) on several test domains. For easier comparison, we still use the same test regions as in previous test examples on BDIE related to Neumann and Dirichlet problems in Chapter 3 and Chapter 4 i.e. a square domain, a circular domain and a parallelogram. The geometry of the three test domains are shown in Figure 3.4.

For the numerical experiments, we also consider the interior Neumann problems that have been used in Chapter 3 i.e. Tests 2 and 7.

All the numerical computations in the implementations are done using Fortran package with the double precision. All the linear algebraic system (5.7) obtained from perturbed LBDIE for Neumann problem (5.6) will only be solved by using direct method. The Neumann iteration method's issues will be discussed later in the eigen-value section.

In the following, we present the figures of numerical results i.e. the relative error for the approximate solution $\epsilon(u)$ and and the relative errors for its gradient $\epsilon(\nabla u)$, as given in (3.67) and (3.68).

The comparative results for relative error of approximate solutions u_{approx} obtained by LU decomposition method and their gradient ∇u_{approx} versus number of nodes J for Test 2 and Test 7 on are shown in Figures 5.1-5.3.

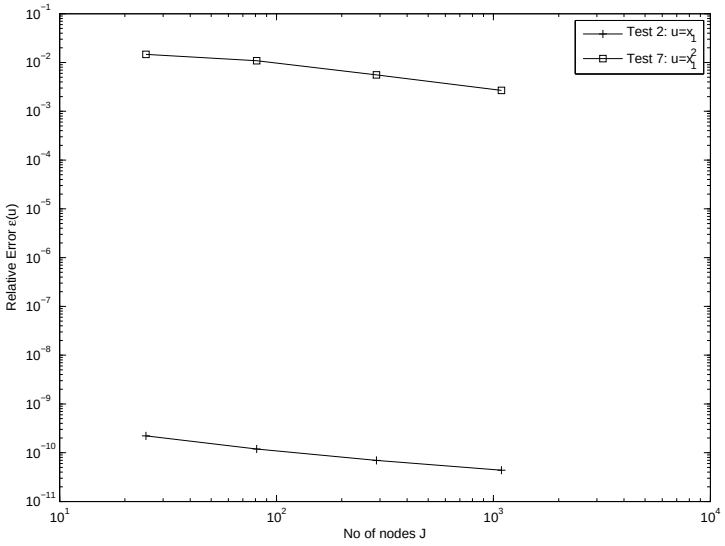

(a)

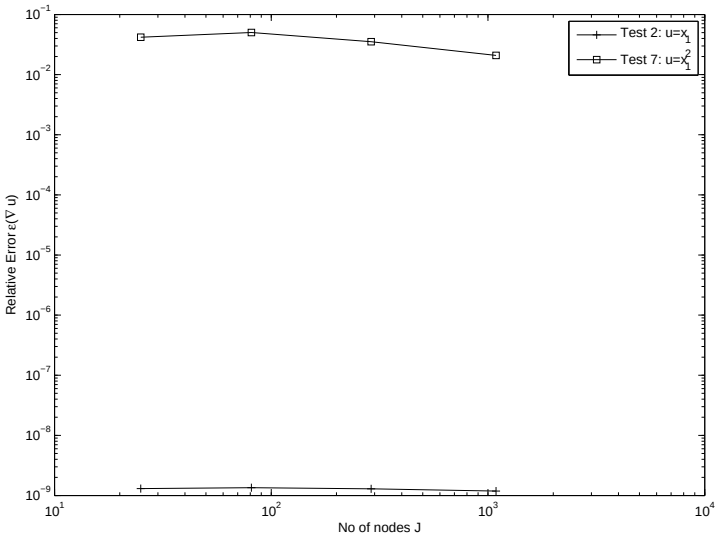

(b)

Figure 5.1: Relative errors of the approximate solutions (a) and their gradients (b), on the square vs. number of nodes J.

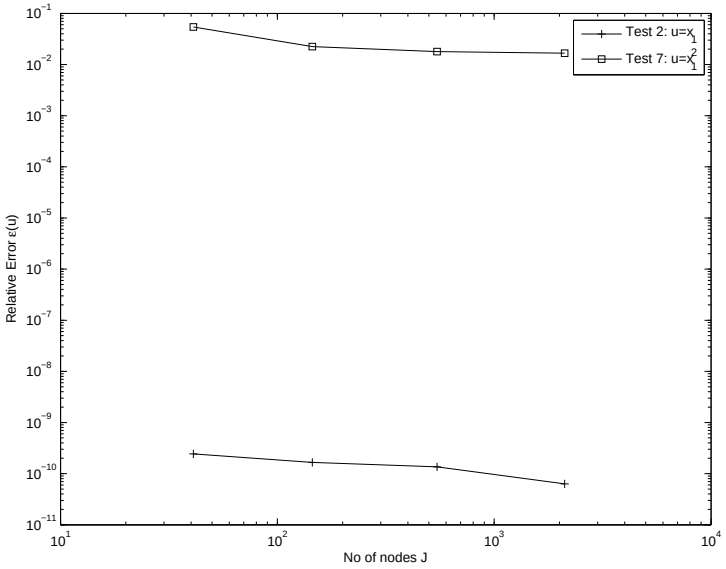

(a)

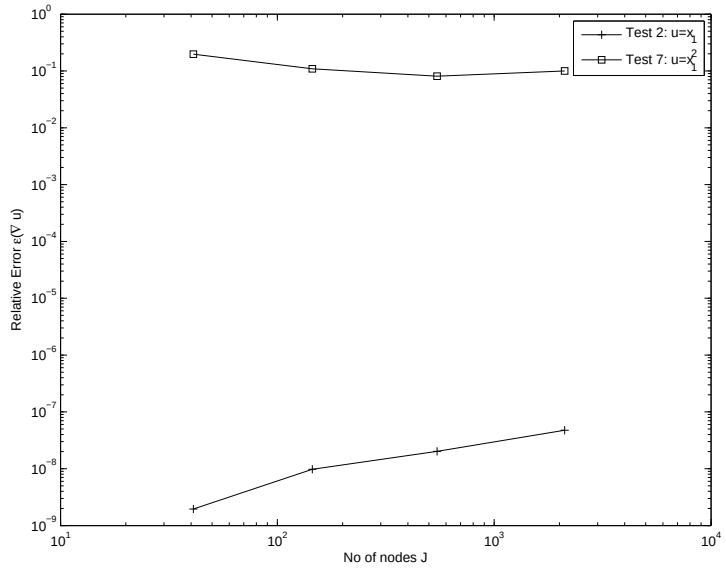

(b)

Figure 5.2: Relative errors of the approximate solutions (a) and their gradients (b), on circular test domain vs. number of nodes J.

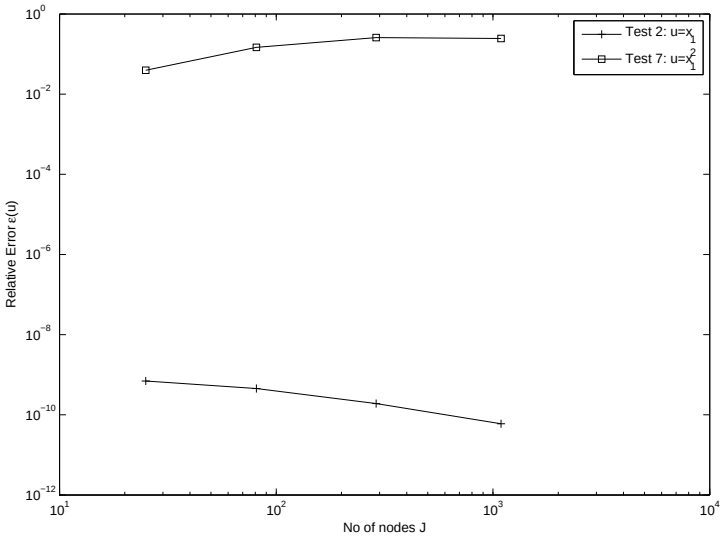

(a)

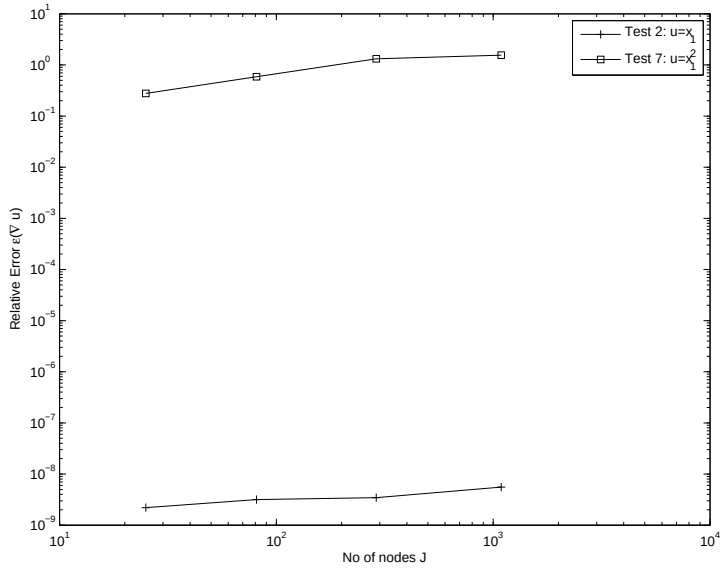

(b)

Figure 5.3: Relative errors of the approximate solutions (a) and their gradients (b), on parallelogram vs. number of nodes J.

We find the power function that fits the dependence of the error $\epsilon(u)$ on the number of nodes J such that $\epsilon \sim J^{-q/2} \sim h^q$. For Test 2 in our numerical experiments, we get $q \sim 1$ for square and parallelogram domains. This convergence rate is the same as for the non-localised BDIE related with Neumann problem in Chapter 3. For circular domain, we get slightly slower convergence i.e. $q \sim 0.7$. For Test 7, we obtained $q \sim 0.9$ for square domain, $q \sim 0.8$ for circle and $q \sim -0.9$ for parallelogram.

For the gradient error we similarly have $\epsilon(\nabla u) \sim J^{-q'/2} \sim h^{q'}$, where $q' \sim 0.05$ for the square and $q' \sim -1.4$ for circular domains and $q' = -0.4$ for the parallelogram domain in Test 2, while $q' = 0.4$ for the square and $q' = 0.3$ for circular domains and $q' = -0.9$ for the parallelogram domain in Test 7.

The accuracy in Test 2 is much higher than in Test 7 since the implemented piece-wise bi-linear interpolation is exact on the linear exact solution, and only the integral operator approximation error, related with the accuracy of the numerical integration, is involved. In the Test 7, on the contrary, the piece-wise bi-linear interpolation of the quadratic exact solution gives its contribution in the total error.

Eigen-values for Discrete Perturbed Neumann LBDIE Operator

In this subsection, we will investigate the spectral properties for the discrete LBDIE operators in Tests 1-6. When coefficient $a(x) = x_2^2$, we will see that the ten largest moduli of eigen-values for the operator K_5 for the discrete LBDIE operators in Test 2 are generally real and lay outside the unit circle. Then, we check whether this also holds for constant coefficient and other variable coefficients of the PDE as in Tests 1-6.

In order to apply Neumann iteration method in solving equation (5.7), we arrange (5.7) such that

$$(I - K_5)u = \mathcal{F}, \tag{5.32}$$

where

$$\begin{aligned} I &= \delta_{ij}, \\ u &= u(x^j), \end{aligned}$$

$$\begin{aligned} \mathcal{F} &= Q_i + D_i, \\ K_5 &= -c_{ij} + \delta_{ij} - K_{ij} - \overset{\circ}{K}_{ij}. \end{aligned} \tag{5.33}$$

This new version enable us to apply the Neumann series expansion

$$u = \sum_{n=0}^{N} K_5^n \mathcal{F}. \tag{5.34}$$

We denote

$$\begin{aligned} g_0 &= \mathcal{F}, \\ g_n &= K_5 g_{n-1}, \end{aligned}$$

such that the Neumann series expansion (5.34) can be written as

$$u = \sum_{n=0}^{N} K_5^n \mathcal{F} = \mathcal{F} + \sum_{n=1}^{N} g_n. \tag{5.35}$$

However, in our numerical results, the Neumann series expansion (5.35) failed to converge to the corresponding results obtained by LU decomposition method. To check why this happens, we will find the eigen-values of the matrix K_5.

Let $\widetilde{\lambda}_k,\ k = 1, 2, \cdots J$, denote the eigen-values of the matrix K_5 i.e. the numbers $\widetilde{\lambda}_k$ for which the perturbed homogeneous equation

$$(\widetilde{\lambda}_k I - K_5)u = 0$$

has non-trivial solutions.

Figure 5.4 shows the first ten eigen-values $\widetilde{\lambda}_k$ of the matrix K_5 in (5.33) for Test 2.

These ten eigen-values appear to be real for the square and circle and have an imaginary part less than 0.05 for the parallelogram.

The maximal modulus of the eigen-values of the matrix K_5 i.e. $\widetilde{\lambda}_1$ on Figures 5.4a-5.4c gives the spectral radius of the matrix K_5 influencing the behavior of the Neumann series on operator K_5. In all our exampless the radii are greater than one which explains why Neumann series diverges.

In order to investigate the influence of the coefficient $a(x)$ on the maximum eigen-values of the perturbed matrix K_5, we calculated them for $a(x) = x_2^k$ with different $0 \leq k \leq 10$ as in Tests 1- 6 in Chapter 3. (Note that our previous examples were calculated for $k = 2$ i.e. for Test 2.)

The results of influence of the coefficient $a(x)$ are presented in Figure 5.5 for the finest meshes, $J = 1089$ for the square and parallelogram, and $J = 2113$ for the circular domain.

For the overlapping eigen-values seen on the figures our calculation shown that their eigen-functions are linearly independent i.e. the eigen-values are geometrically multiple.

In our numerical experiments, the eigen-values of the discrete LBDIE operator related with Neumann problem are real and lay outside the unit circle. This means that the standard Neumann series for the LBDIE with such constant or variable coefficients will generally diverge.

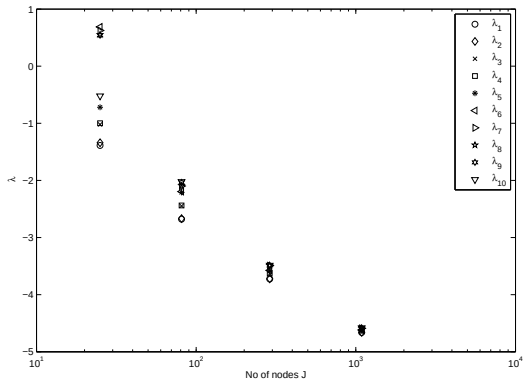

(a) Square domain.

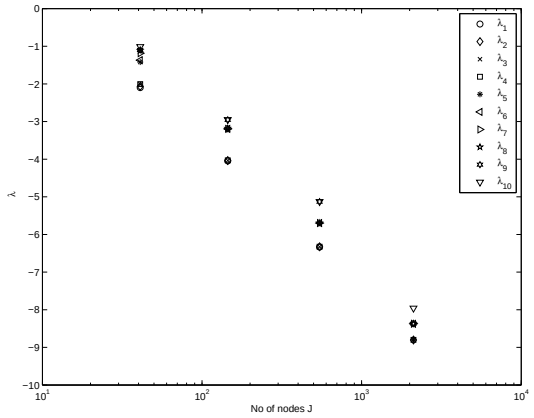

(b) Circular domain.

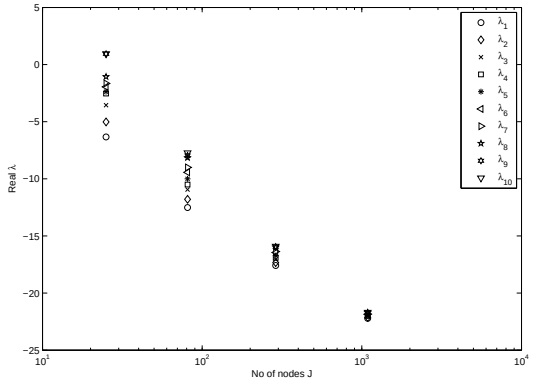

(c) Parallelogram domain.

Figure 5.4: Eigen-values of the matrix K_5 vs. the number of nodes J.

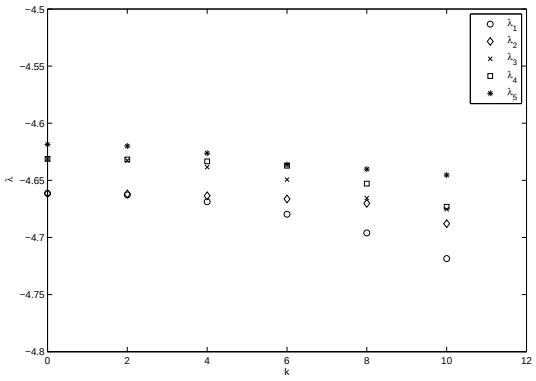

(a) Square domain.

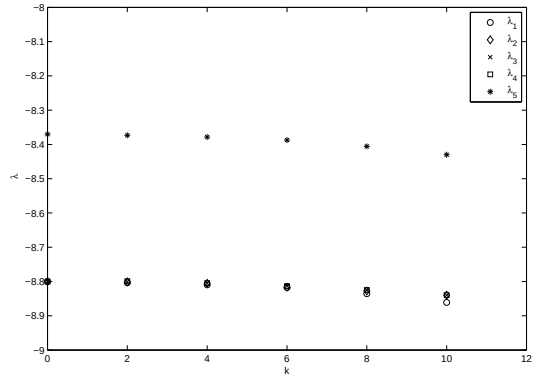

(b) Circular domain.

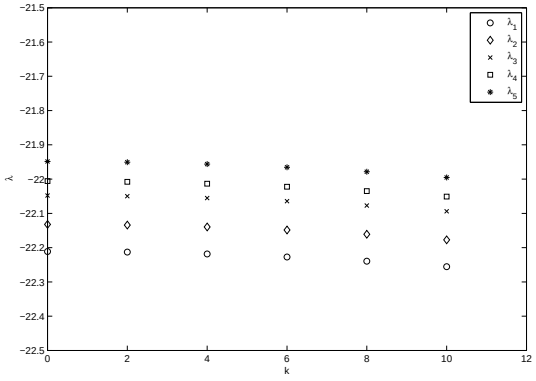

(c) Parallelogram domain.

Figure 5.5: The largest eigen-values of the matrix K_5 vs. k for $a(x) = x_2^k$.

5.2.3 Localized Boundary-Domain Integral Equation for Dirichlet Problem

For Dirichlet problem, we impose the Dirichlet boundary condition, $u(x) = \overline{u}(x),\ x \in \partial\Omega$, in the localised third Green identity (5.3) and obtain

$$\begin{aligned} c(y)u(y) \;-\; & \int_{\Omega\cap\partial\omega(y)} u(x)T_xP_\chi(x,y)\,\mathrm{d}\Gamma(x) + \int_{\partial\omega(y)} P_\chi(x,y)Tu(x)\,\mathrm{d}\Gamma(x) \\ +\; & \int_{\omega(y)\cap\Omega} R_\chi(x,y)u(x)\,\mathrm{d}\Omega(x) = \int_{\overline{\omega}(y)\cap\partial\Omega} \overline{u}(x)T_xP_\chi(x,y)\,\mathrm{d}\Gamma(x) \\ +\; & \int_{\omega(y)\cap\Omega} P_\chi(x,y)f(x)\,\mathrm{d}\Omega(x), \qquad y\in\overline{\Omega}. \end{aligned} \tag{5.36}$$

Partly using the Dirichlet in out-of-integral term, we obtain the modification of equation (5.36) given below.

$$\begin{aligned} u(y) \;-\; & \int_{\Omega\cap\partial\omega(y)} u(x)T_xP_\chi(x,y)\,\mathrm{d}\Gamma(x) + \int_{\partial\omega(y)} P_\chi(x,y)Tu(x)\,\mathrm{d}\Gamma(x) \\ +\; & \int_{\omega(y)\cap\Omega} R_\chi(x,y)u(x)\,\mathrm{d}\Omega(x) \\ =\; & (1-c(y))\overline{u}(y) + \int_{\overline{\omega}(y)\cap\partial\Omega} \overline{u}(x)T_xP_\chi(x,y)\,\mathrm{d}\Gamma(x) \\ +\; & \int_{\omega(y)\cap\Omega} P_\chi(x,y)f(x)\,\mathrm{d}\Omega(x), \qquad y\in\overline{\Omega}. \end{aligned} \tag{5.37}$$

By applying interpolation to u in equation (5.37) and satisfying the equation at the collocation points $x^i \in \overline{\Omega}$ at all J nodes of the interpolation mesh, we obtain the system of J linear algebraic equations for J unknowns $u(x^j)$,

$$u(x^i) + \sum_{x^j\in\overline{\omega}(x^i)} K^D_{ij}u(x^j) = (1-c(x^i))\overline{u}(x^i) + Q^D_i + D^D_i,\ x^i\in\overline{\Omega}, \tag{5.38}$$

where K^D_{ij}, Q^D_i and D_i are defined as follows:

$$\begin{aligned} K^D_{ij} \;=\; & -\int_{\Omega\cap\partial\omega(x^i)} \phi_j(x)T_xP_\chi(x,x^i)\,\mathrm{d}\Gamma(x) + \int_{\partial\omega(x^i)} P_\chi(x,x^i)\left[a(x)\frac{\partial\phi_j}{\partial\nu(x)}\right]\,\mathrm{d}\Gamma(x) \\ +\; & \int_{\omega(x^i)\cap\Omega} \phi_j(x)R_\chi(x^i,x)\,\mathrm{d}\Omega(x), \end{aligned} \tag{5.39}$$

$$Q^D_i \;=\; \int_{\overline{\omega}(x^i)\cap\partial\Omega} \overline{u}(x)T_xP_\chi(x,x^i)\,\mathrm{d}\Gamma(x), \tag{5.40}$$

$$D_i^D = \int_{\omega(x^i)\cap\Omega} P_\chi(x,x^i) f(x)\, \mathrm{d}\Omega(x). \tag{5.41}$$

We then can write (5.39)- (5.41) as follows:

$$\begin{aligned} K_{ij}^D &= -\sum_{\gamma_l\subset\partial\omega_l(x^i)\cap\overline{\omega}(x^j)} \int_{\gamma_l} \phi_j(x) T_x P_\chi(x,x^i)\, \mathrm{d}\Gamma(x) \\ &+ \sum_{\gamma_l\subset\partial\omega_l(x^i)\cap\overline{\omega}(x^j)\cap\Omega} \int_{\gamma_l} P_\chi(x,x^i) \left[a(x)\frac{\partial\phi_j(x)}{\partial\nu(x)}\right] \mathrm{d}\Gamma(x) \\ &+ \sum_{\Omega_m\subset\omega(x^i)\cap\omega(x^j)} \int_{\Omega_m} \phi_j(x) R_\chi(x,x^i)\, \mathrm{d}\Omega(x), \end{aligned} \tag{5.42}$$

$$Q_i^D = \sum_{\partial\Omega_l\subset\overline{\omega}(x^i)} \int_{\partial\Omega_l} \overline{u}(x) T_x P_\chi(x,x^i)\, \mathrm{d}\Gamma(x), \tag{5.43}$$

$$D_i^D = \sum_{\Omega_m\subset\omega(x^i)} \int_{\Omega_m} P_\chi(x,x^i) f(x)\, \mathrm{d}\Omega(x). \tag{5.44}$$

Therefore, we can write equations (5.42)-(5.44) as follows:

$$\begin{aligned} K_{ij}^D &= -\sum_{\gamma_l\subset\partial\omega_l(x^i)\cap\overline{\omega}(x^j)} A^l_{n(j,l),i} + \sum_{\gamma_l\subset\partial\omega_l(x^i)\cap\overline{\omega}(x^j)\cap\Omega} C^l_{N(j,l),i} \\ &+ \sum_{\Omega_m\subset\omega(x^i)\cap\omega(x^j)} G^m_{N(j,m),i}, \\ Q_i^D &= \sum_{\partial\Omega_l\subset\overline{\omega}(x^i)} \widetilde{F}_i^l, \\ D_i^D &= \sum_{\Omega_m\subset\omega(x^i)} H_i^m, \end{aligned}$$

where $A^l_{N,i}$, $C^q_{N,i}, G^m_{N,i}$, and H_i^m are given in (5.17)- (5.20), while $\widetilde{F}_i^l$,

$$\widetilde{F}_i^l = \int_{-1}^{1} \overline{u}(x(\eta)) T_x P(x(\eta),x^i) J_{l1}(\eta)\, \mathrm{d}\eta.$$

Defining

$$F(x^i) = (1-c(x^i))\overline{u}(x^i) + Q_i^D + D_i^D,$$

we can then write (5.38) as

$$u(x^i) + \sum_{x^j\in\overline{\omega}(x^i)} K_{ij}^D u(x^j) = F(x^i) \tag{5.45}$$

Similar to the case of non-localised BDIDE, instead of taking the collocation point x^i for $x^i \in \overline{\Omega}$ at all J nodes of the mesh, we can take the collocation point x^i only for $x^i \in \Omega$ at $J - J_D$ nodes of the mesh during the interpolation process. Here J_D is the number of boundary nodes of the mesh.

For the rest of the collocation points i.e. $x^i \in \partial\Omega$, the solution $u(x^i)$ is known from the boundary condition, $u(x^i) = \overline{u}(x)$ on $\partial\Omega$.

Therefore $\sum_{x^j \in \overline{\omega}(x^i)} K_{ij}^D u(x^j)$ in (5.38) can be splited to two parts i.e.

$$\sum_{x^j \in \overline{\omega}(x^i)} K_{ij}^D u(x^j) = \sum_{x^j \in \overline{\omega}(x^i) \cap \Omega} K_{ij}^D u(x^j) + \sum_{x^j \in \overline{\omega}(x^i) \cap \partial\Omega} K_{ij}^D \overline{u}(x^j).$$

The second part $\sum_{x^j \in \overline{\omega}(x^i) \cap \partial\Omega} K_{ij}^D \overline{u}(x^j)$ can be transferred to the right-hand side.

Thus, from (5.38) we obtain the system of $J - J_D$ linear algebraic equations for $J - J_D$ unknowns $u(x^j)$, as in the following:

$$u(x^i) + \sum_{x^j \in \overline{\omega}(x^i) \cap \Omega} K_{ij}^D u(x^j) = (1 - c(x^i))\overline{u}(x^i) - \sum_{x^j \in \overline{\omega}(x^i) \cap \partial\Omega} K_{ij}^D \overline{u}(x^j) + Q_i^D + D_i^D, \; x^i \in \Omega, \tag{5.46}$$

where K_{ij}, Q_i^D and D_i^D are defined as in (5.39) - (5.41).

5.2.4 Numerical Examples

Numerical Solution for System (5.46)

In the following discussion, we show the numerical results of the LBDIE discretisation (5.46) i.e. by taking the collocation points x^i only for $x^i \in \Omega$ at $J - J_D$ nodes of the mesh. All the numerical computations are done using Fortran with the double precision. The linear algebraic system (5.46) is solved by using direct method only.

In the following figures, we present the relative errors for the approximate solution $\epsilon(u)$ and and for its gradient $\epsilon(\nabla u)$, as defined in (3.67) and (3.68).

The comparative results for relative errors of approximate solutions u_{approx} obtained by LU decomposition method and their gradient ∇u_{approx} versus number of nodes J for Test 2 and Test 7 are shown in Figures 5.6- 5.8.

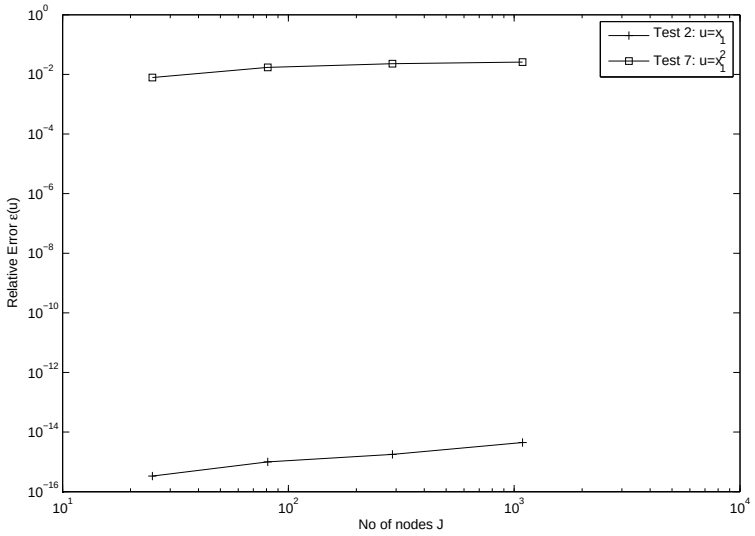

(a)

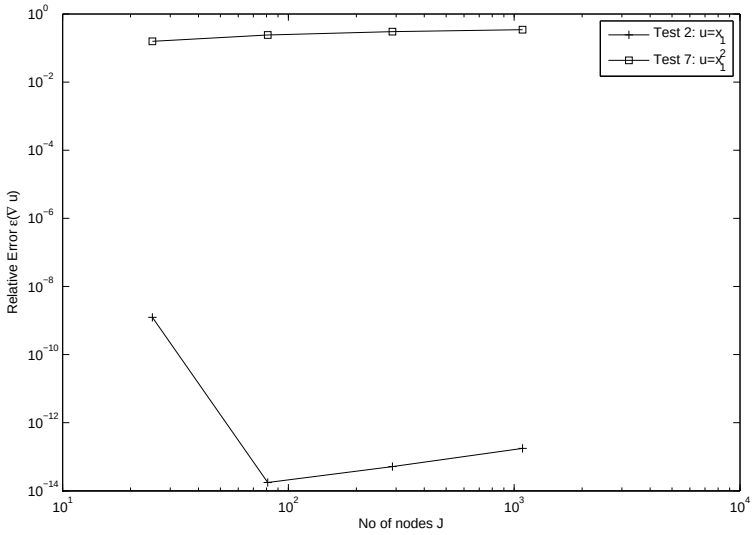

(b)

Figure 5.6: Relative errors of the approximate solutions (a) and their gradients (b), on the square vs. number of nodes J.

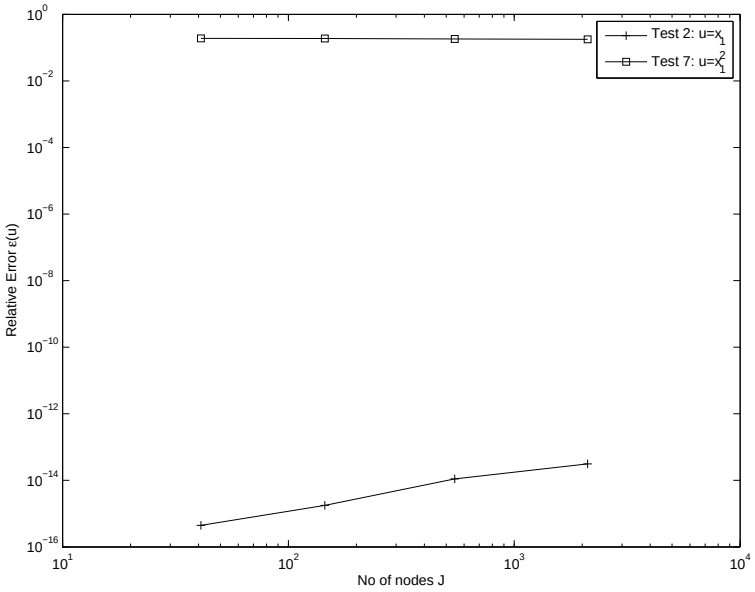

(a)

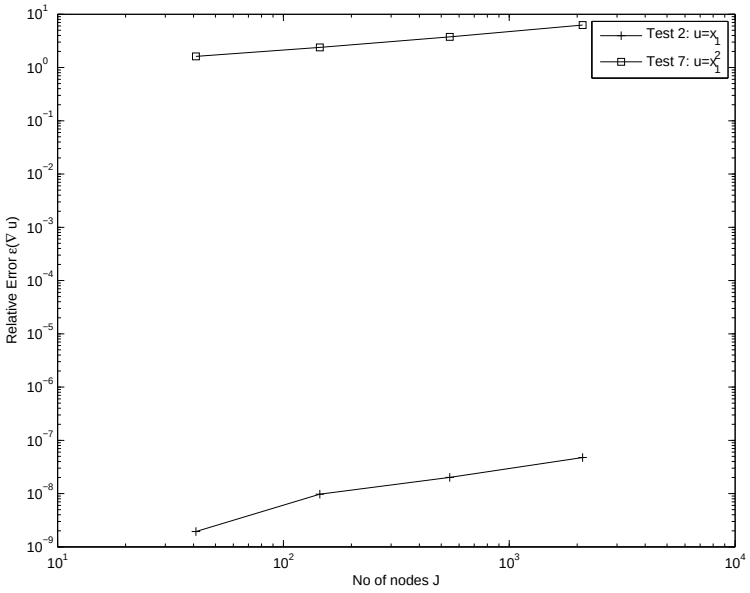

(b)

Figure 5.7: Relative errors of the approximate solutions (a) and their gradients (b), on circular test domain vs. number of nodes J.

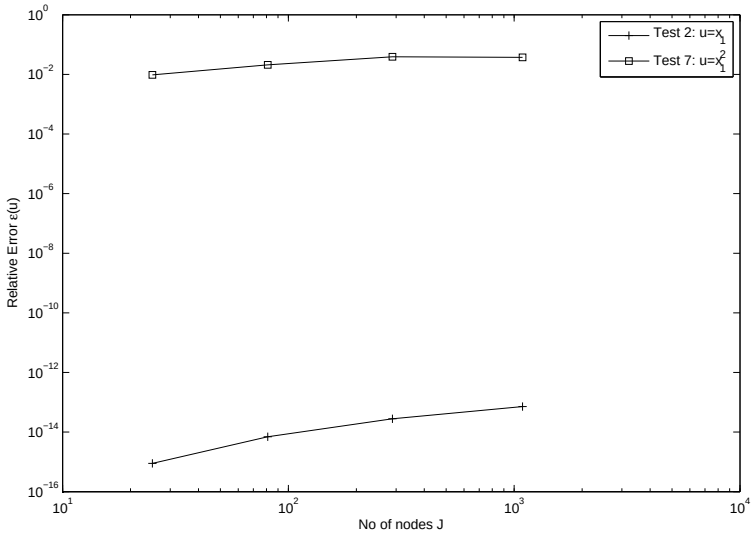

(a)

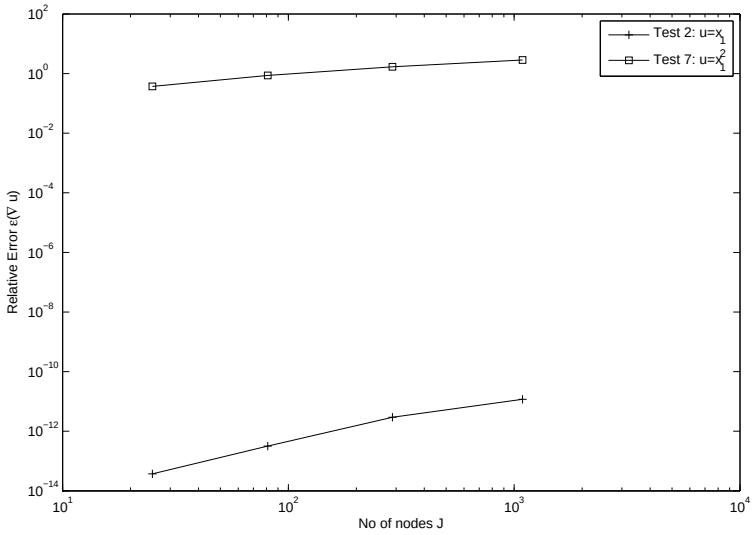

(b)

Figure 5.8: Relative errors of the approximate solutions (a) and their gradients (b), on parallelogram vs. number of nodes J.

The numerical experiments for LBDIE related with Dirichlet problem of equation (5.46) shows that no convergence is achieved as the number of nodes J increases. For Test 2, given that $\epsilon(u) \sim J^{-q/2} \sim h^q$, we obtain $q \sim -1.3$ for square, $q \sim -2$ for circular domain and $q \sim -2.3$ for parallelogram. For Test 7, we get $q \sim -0.6$ for square, $q \sim -0.02$ for circular domain and $q \sim -0.7$ for parallelogram.

These results might be due to the round-off error during the implementing of Test 2. For Test 7, we believe that the diverges of the error $\epsilon(u)$ is because of not sufficient approximation since we only used linear interpolation for boundary integrals.

This seems to be important even for square domain since interpolation functions are not only to describe the geometry of the elements but also approximate functions over the elements.

Since the gradient error $\epsilon(\nabla u)$ corresponds to the error $\epsilon(u)$, we might expect the divergence of the gradient error $\epsilon(\nabla u)$ with the increase of J.

Indeed, given $\epsilon(\nabla u) \sim J^{-q'/2} \sim h^{q'}$, we have $q' \sim -1.6$ for the square, $q' = -1.5$ for circle and $q' = -3$ for parallelogram in Test 2.

In Test 7, we have $q' \sim -0.4$ for the square, $q' = -0.6$ for circle and $q' = -1$ parallelogram

The eigen-values of the operator in equation (5.46) can tend to infinity by the same reason as for the non-localised equation (4.5). More interesting would be to analyse the eigen-values of the operator in equation (5.45).

Numerical Solution for System (5.45)

In this subsection, we will present the numerical results of the discrete LBDIE (5.45) obtained by taking the collocation points x^i for $x^i \in \overline{\Omega}$ i.e. at all J nodes. Similar to Section 5.2.4, the system of algebraic equations is solved by using direct method only. However, we have now J algebraic equations instead of only $J - J_D$ for system (5.46).

In the following, we present the graphs for the relative errors for the approximate solution $\epsilon(u)$ and and for its gradient $\epsilon(\nabla u)$. The comparative results for relative error of approximate solutions u_{approx} obtained by LU decomposition method and their gradient ∇u_{approx} versus number of nodes J for Test 2 and Test 7 are shown in Figures 5.9-5.11.

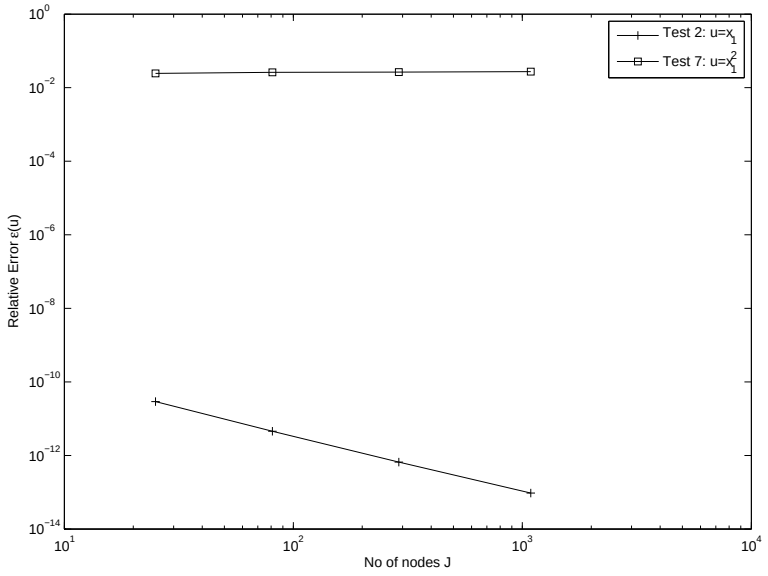

(a)

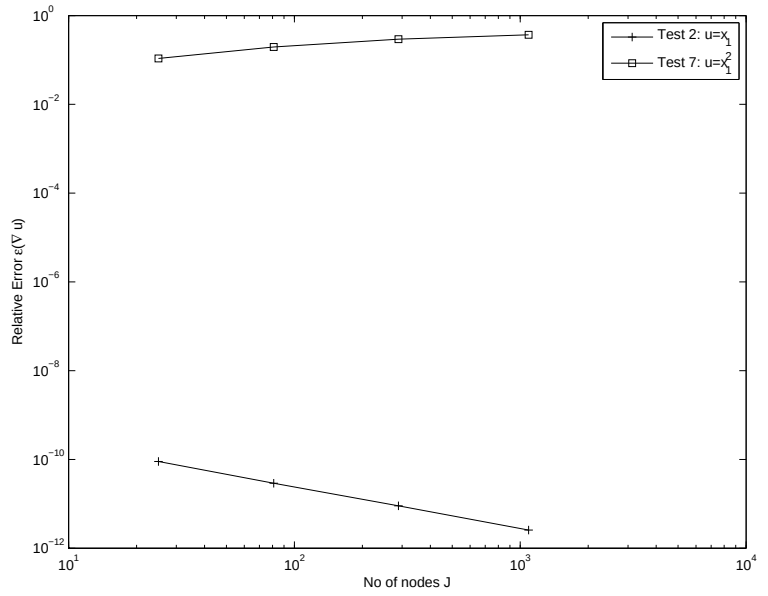

(b)

Figure 5.9: Relative errors of the approximate solutions (a) and their gradients (b), on the square vs. number of nodes J.

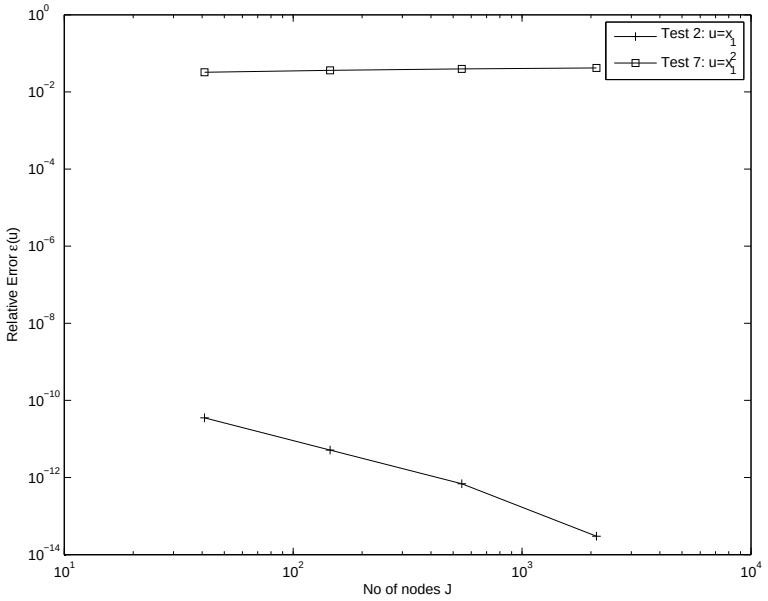

(a)

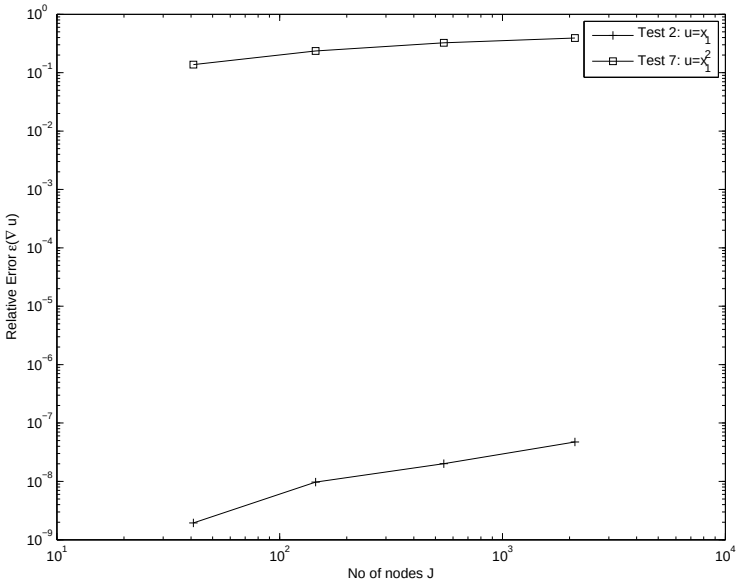

(b)

Figure 5.10: Relative errors of the approximate solutions (a) and their gradients (b), on circular test domain vs. number of nodes J.

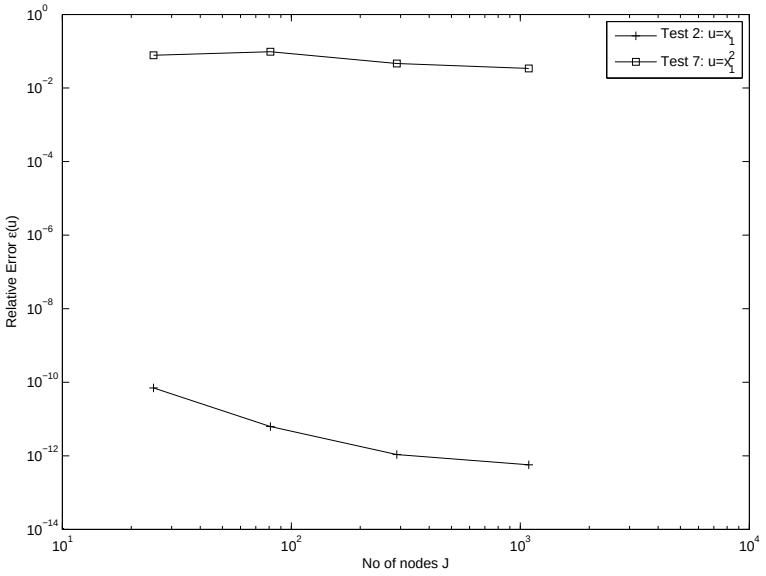

(a)

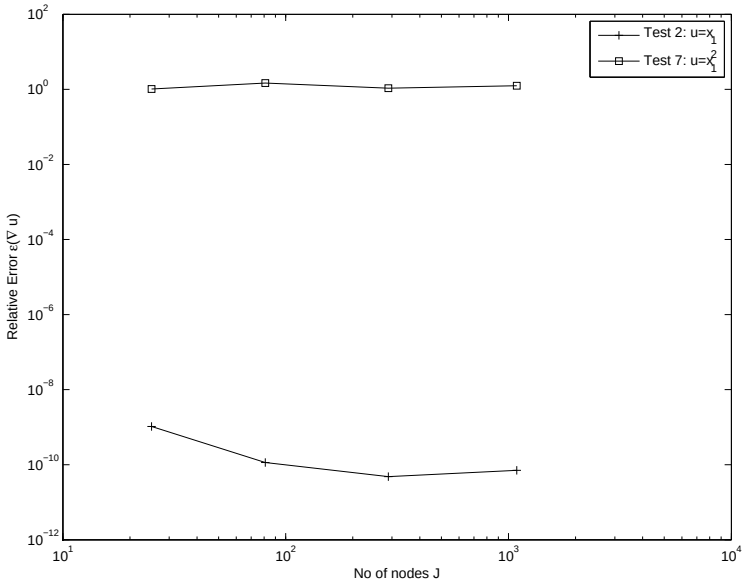

(b)

Figure 5.11: Relative errors of the approximate solutions (a) and their gradients (b), on parallelogram vs. number of nodes J.

As in Neumann LBDIE, the numerical experiments for Dirichlet LBDIE (5.45) shows that we achieved convergence as the number of nodes J increases for square domain and parallelogram for Test 2. For Test 2, given that $\epsilon(u) \sim J^{-q/2} \sim h^q$, we obtain $q \sim 3$ for square, $q \sim 3.4$ for circular domain and $q \sim 2.4$ for parallelogram. For Test 7, we get $q \sim -0.04$ for square, $q \sim -0.12$ for circular domain and $q \sim -0.2$ for parallelogram.

Since the gradient error $\epsilon(\nabla u)$ is related to the error $\epsilon(u)$, we might expect the divergence of the gradient error $\epsilon(\nabla u)$ with the increasing J for all regions in Test 7. Similarly, given $\epsilon(\nabla u) \sim J^{-q'/2} \sim h^{q'}$, we have $q' \sim 2$ for the square, $q' = -1.5$ for circle and $q' = 1.4$ for the parallelogram in Test 2. For Test 7, we have $q' \sim -0.6$ for the square and circle while $q' = -0.04$ parallelogram.

Eigen-values for the System (5.45)

In solving equation (5.45) by using Neumann series expansion, we write (5.45) as

$$(I - K_6)u = \mathcal{F},$$

where

$$\begin{aligned} I &= \delta_{ij}, \\ u &= u(x^j), \\ K_6 &= -K_{ij}^D, \\ \mathcal{F} &= F(x^i). \end{aligned}$$

This arrangement enables us to apply the Neumann series expansion as in the following:

$$u = \sum_{n=0}^{N} K_6^n \mathcal{F}. \tag{5.47}$$

We construct g_n such that

$$\begin{aligned} g_0 &= \mathcal{F}, \\ g_n &= K_6 g_{n-1}. \end{aligned}$$

Therefore (5.47) can be written as

$$u = \sum_{n=0}^{N} K_6^n \mathcal{F} = \mathcal{F} + \sum_{n=1}^{N} g_n. \tag{5.48}$$

Our numerical experiments shown that the Neumann series (5.48) diverges for Test 2 and Test 7 i.e. when $a = x_2^2$. We will also investigate whether it holds for constant coefficient and other variable coefficients $a(x)$ of the PDE for Dirichlet problem.

If all eigen-values of the operator K_6 belong to the open unit disc, then the Neumann series in the form of equation (5.48) for a matrix operator K_6 converges for any right hand side.

Let $\widetilde{\lambda}_k,\ k = 1, 2, \cdots J$, denotes the eigen-values of the matrix K_6 i.e. the numbers $\widetilde{\lambda}_k$ for which the homogeneous equation

$$(\widetilde{\lambda}_k I - K_6)u = 0,$$

has non-trivial solutions.

In the following experiments, we will see that the conclusion similar to the one that have been made for perturbed LBDIE of Neumann problem (5.6) in Section 5.2.2 holds also for LBDIE of Dirichlet problem (5.37).

Figures 5.12-5.14 present the first eigen-values $\widetilde{\lambda}_k$ of the matrix K_6 with the largest moduli in Test 2 for square, circular and parallelogram domains, respectively.

From the numerical experiments, we can presented the spectral radii of discretize LBDIE operator related to Dirichlet problem K_6 for all the test regions lay outside the unit circle.

Investigating the influence of the coefficient $a(x)$ on the maximum eigen-values of the matrix operator K_6, we calculated them for $a(x) = x_2^k$ for $k = 0, 2, \cdots, 10$. The results are shown in Figure 5.15.

Like in previous chapters, we presented the maximum eigen-values of the operator K_6 for the finest meshes on each domains i.e. when $J = 1089$ for the square and parallelogram and $J = 2113$ for circular domain.

For the overlapping eigen-values seen on the figures our calculation shown that their eigen-functions are linearly independent i.e. the eigen-values are geometrically multiple.

Note that in all the experiments even for constant coefficient, five/six largest eigen-values of the operator K_6 are all real and the spectral radii $\lambda_1 > 1$ for all the domains which implies the diverges of the Neumann iterations.

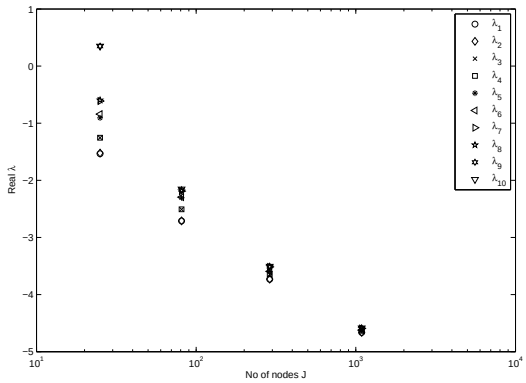

(a) Re λ.

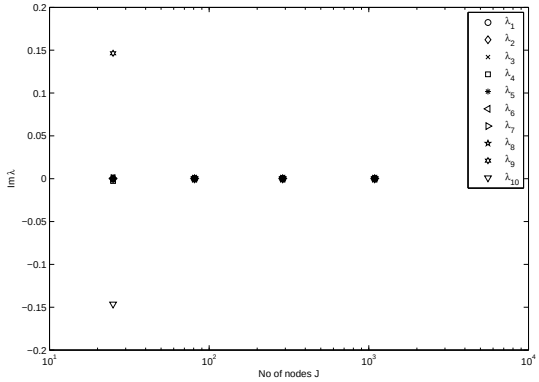

(b) Im λ.

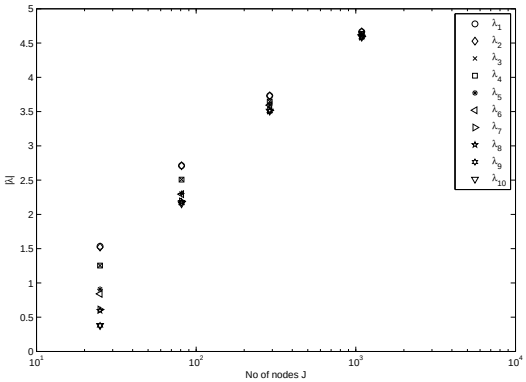

(c) $|\lambda|$.

Figure 5.12: Eigen-values of the matrix K_6 for the square domain vs. the number of nodes J.

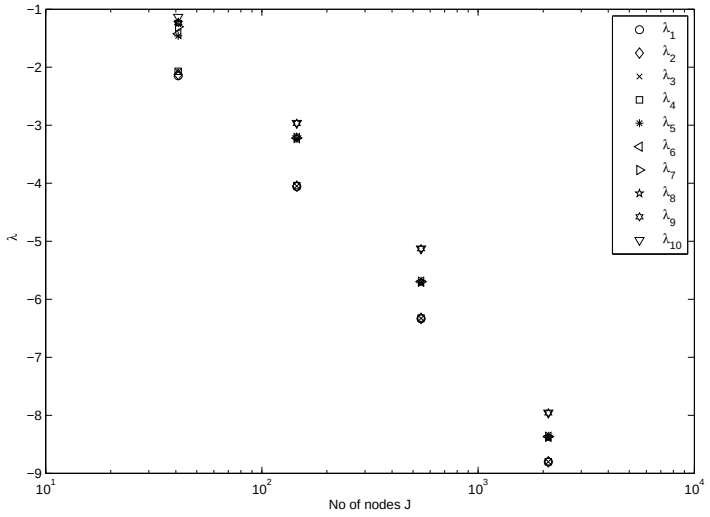

Figure 5.13: Eigen-values of the matrix K_6 for the circular domain vs. the number of nodes J.

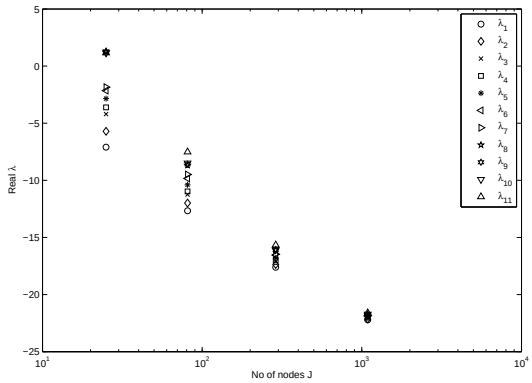

(a) Re λ.

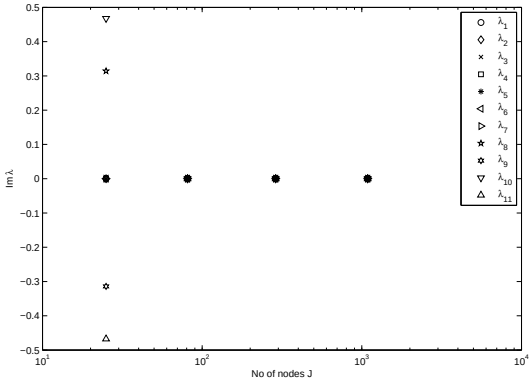

(b) Im λ.

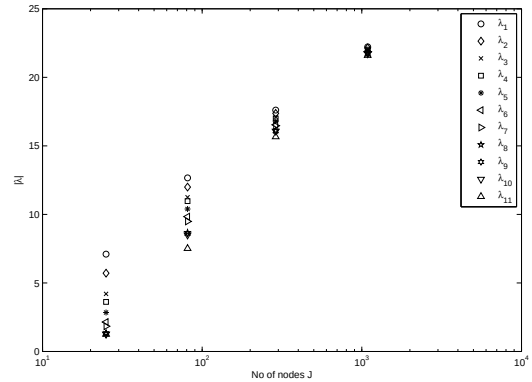

(c) $|\lambda|$.

Figure 5.14: Eigen -values of the matrix K_6 for the parallelogram vs. the number of nodes J.

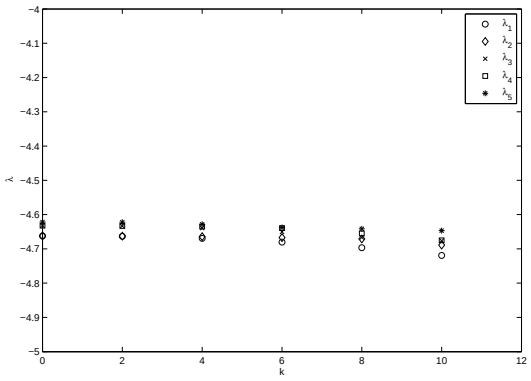

(a) Square domain.

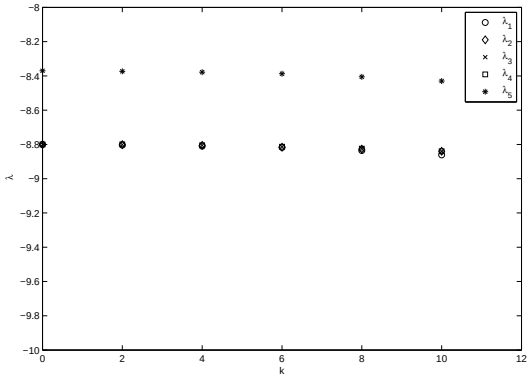

(b) Circular domain.

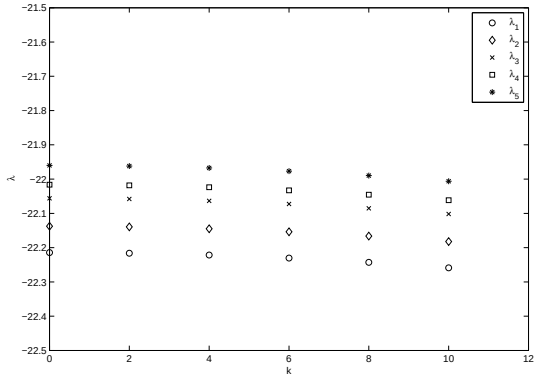

(c) Parallelogram domain.

Figure 5.15: The largest eigen-values of the matrix K_6 vs k for $a(x) = x_2^k$.

5.3 Conclusion

In this Chapter, we have seen that the BVPs for PDE with variable coefficient can be reduced to the Localized Boundary-Domain Integral Equations (LBDIEs) related with Neumann and Dirichlet problems by using localized parametrix $P_\chi(x, y)$. The parametrix $P(x, y)$ is not unique based on the fact that all parametrixes $P(x, y)$ for a differential operator L have the same singularity at $x = y$ but can differ at other points. We chose the localized parametrix $P_\chi(x, y)$ to be constant when $x \in \omega_y$ and we present the discretization process in solving the LBDIEs numerically. The discretization of the LBDIEs led to systems of linear equations which is then solved by using direct method (LU decomposition method).

No theoretical analysis about the spectral properties of the LBDIEs operators related to the Neumann and Dirichlet problems is available, but we can conclude from the numerical experiments that spectral radii of discretize LBDIEs' operators exceed 1 and mainly real numbers. This is not only occurs when we deal with BVP for PDE with variable coefficient but also for BVP for PDE with constant coefficient. Therefore, for LBDIEs' operators, the Neumann iteration generally does not converge regardless of the coefficient. Hence, the direct methods seem to be more appropriate in solving the system of algebraic equations obtained from LBDIEs.

Chapter 6

Conclusions and Future Research

The research that have been carried out in this thesis includes: (i) solving numerically the discretized BDIEs and LBDIEs related to the Neumann and Dirichlet boundary value problem for a scalar elliptic PDE with variable coefficient by using direct method and iteration method when it converges; (ii) analyzing the behavior of eigen-values of the corresponding discrete BDIEs and LBDIEs operators for a scalar elliptic PDE with several different variable coefficients by taking the effect of the maximal eigen-values of the discrete BDIEs and LBDIEs.

First, we considered Boundary-Domain Integral Equations of the Neumann and Dirichlet value problems for PDE with variable coefficient. The reduction of the BVPs to BDIEs is possible by using a parametrix which is more widely available than a fundamental solution. We made an overview on how we discretized the boundary $\partial\Omega$ and the domain Ω with linear boundary element and quadrilateral domain elements, respectively. Assembling proses of the element contributions obtained from the integration of each element to a global matrix based on the relation between local nodes and global nodes were explained. Three test domains, square, circular, and parallelogram that were used in all the numerical experiments in all chapters were introduced.

The BDIE related to Neumann problem was reduced to a uniquely solvable one by adding an appropriate perturbation operator. The numerical experiments on the perturbed BDIE related to the Neumann problem for PDE with variable coefficient was presented in Chapter

3 and the numerical experiments on BDIE related to the Dirichlet problem for PDE with variable coefficient was reported in Chapter 4. The linear algebraic system obtained from BDIE (discretised BDIE) related to Neumann problem was solved by the Neumann iterations and LU decomposition method. The numerical examples illustrated that high accuracy can be achieved.

The spectral properties obtained numerically from the discrete BDIE operator were also presented. We also discovered that the eigen-values essentially depend on the coefficient function $a(x)$. Detailed analysis of the discrete Neumann BDIE eigen-values demonstrated that when the PDE coefficient moderately varies with coordinates i.e. when the coefficient gradient is small or moderate (e.g. $\max\left|\frac{L\nabla a}{a}\right| < 5$ in the considered examples, where L is a characteristic size of the domain) the spectrum is contained in the unit circle, which implies the Neumann series convergence. For $\max\left|\frac{L\nabla a}{a}\right| \geq 5$, the imaginary part of the maximal eigen-values exceeded 1 and led to divergence of the Neumann iteration method. An interesting feature is that the real value of the maximal eigen-values remained less than 1. Following (Kantorovich and Krylov (1964)) and (Kublanovskaya (1959)) one can map the exterior of this λ-domain to the exterior of the unite circle, which will lead to a converging modification of the Neumann series. This method looks interesting to be done in the future studies. Therefore, we can say that the standard Neumann iteration method is a good alternative to the direct methods, especially when the computer storage and CPU time needs for the latter become prohibitive.

However, this spectrum property does not hold generally, and when the order of the coefficient varies such that $\max\left|\frac{L\nabla a}{a}\right| \geq 5$, some eigen-values appear also outside the unit circle, which can lead to divergence of the standard Neumann series; in these cases the modified Neumann series, other iterative (e.g. GMRES) or direct methods will be more appropriate.

In Chapter 4, we showed the results of numerical implementations on the BDIDE related to the Dirichlet problem for PDE with variable coefficient. Unlike the BDIE related with Neumann problem implemented, we had not one but two ways of discretisation. The first way is by employing the BDIDEs at the collocation points x^i for $x^i \in \overline{\Omega}$ at all J nodes.

Similar to the BDIE (discretised BDIE) related to Neumann problem in Chapter 3, the system obtained from BDIDE (discretised BDIE) related to Dirichlet problem is solved by the Neumann iterations and LU decomposition method. We reported on the maximal eigen-values of the corresponding discrete BDIE operator obtained numerically as in Chapter 3 for BDIE related with Neumann problem. From the numerical experiments, we obtained very similar behavior of the eigen-values for discretized Dirichlet BDIDE operator to the discretized Neumann BDIE operator. The analysis of the discrete Dirichlet BDIDE eigen-values also demonstrated that when the PDE coefficient moderately varies with coordinates i.e. when the coefficient gradient is small or moderate (e.g. $\max\left|\frac{L\nabla a}{a}\right| < 5$ in the considered examples, where L is a characteristic size of the domain) the spectrum is contained in the unit circle, which implies the Neumann series convergence. For $\max\left|\frac{L\nabla a}{a}\right| \geq 5$, the imaginary part of the maximal eigen-values also exceeded 1 and led to divergence of the Neumann iteration method. The real part of the maximal eigen-values remained less than 1. The second way in the interpolation process is by employing the BDIDE only at the collocation points $x^i \in \Omega$ at $J - J_D$ nodes of the mesh during the interpolation process where J_D is the number of nodes on the boundary $\partial\Omega$. In this second setting, we only solved the system by LU decomposition method since the Neumann iterations diverge.

In Chapter 5, we discussed on the Localized Boundary-Domain Integral Equation (LBDIE) for PDE of Neumann and Dirichlet problems. The advantage of LBDIE is that after discretisation its system of linear algebraic equations is sparsely populated. Therefore, the time taken for calculation of elements of the matrix as well as solving system of equations is shorter than for fully populated system obtained from non-localised BDIE. The reduction from the BVPs to the LBDIEs are possible by using a localized parametrix $P_\chi(x, y)$. We chose the cut-off function χ such that $\chi(x, y) = 1$ when $x \in \omega_y$ and $\chi(x, y) = 0$ when $x \notin \omega_y$. The discretization process of the LBDIEs was explained. We then solved the system of equations by using direct method (LU decomposition method). In the experiments regarding linear exact solution with the collocation points $x^i \in \overline{\Omega}$ at J nodes of the mesh, we have achieved convergence of the relative error as J increases. These linear solution problems were used to check the spectral radii of discrete LBDIEs' operator. The experimental results for

Dirichlet problems regarding linear exact solution by taking the collocation points x^i only for $x^i \in \Omega$ at $J - J_D$ nodes of the mesh do not attain converges as $J - J_D$ increases due to the round-off error. In order to achieve the convergence as $J - J_D$ increases, one should set higher precision in the the numerical codes. For the quadratic exact solution for Neumann and Dirichlet problems, we generally failed to achieve the converges as J increases. This is due to not enough approximation order as we use only linear and bilinear approximations. In handling the problem, one should use higher order of approximations.

We can conclude from the numerical experiments that spectral radii of discrete LBDIEs' operators tested for linear exact solutions are all exceed 1 and relatively real numbers. This is not only occurs for the LBDIE associated with BVP for PDE with variable coefficient but also for the LBDIE in case of the constant coefficient. Therefore, for LBDIE operators, we conclude that the Neumann iterations generally do not converge regardless of the coefficient. Thus, the direct methods seem to be more appropriate in solving the system of algebraic equations obtained from the LBDIEs. For the future research, it is beneficial to use specialized algorithms and data structures that take advantage of the sparse structure of the matrix. The operations using standard dense matrix structures and algorithms are slow and may consume large data storage. The sparse data can be compressed, and this compression can result in significantly less amounts of memory. There are several, iterative and direct methods available for solving sparse matrix systems. The commonly known iterative methods for sparse matrix are conjugate gradient method and GMRES. Further improvement on the numerical implementations can be done by using higher order approximations. The use of semi-analytic method can also be applied for the domain integrations to replace the duffy transformations in handling singularity.

Bibliography

M.H. Aliabadi. *The Boundary Element Method, Vol. 2, Applications in Solids and Structures*. Wiley, Chichester, 2002.

M. Ameen. *Computational Elasticity: Theory of Elasticity, Finite and Boundary Element Methods*. Alpha Science International Ltd, Harrow, UK, 2005.

R.A. Archer and R.N. Horne. Flow simulation in heterogeneous reservoirs using the dual reciprocity boundary element method and the Green element method. In *ECMOR VI Conference*, Peebles, Scotland, 1998.

R.A. Archer and R.N. Horne. The Green element method for numerical well test analysis. In *SPE Annual Technical Conference and Exhibition*, Dallas, Texas, 1–4 October 2000. Society of Petroleum Engineers.

R.A. Archer and R.N. Horne. Green element method and singularity programming for numerical well test analysis. *Engineering Analysis with Boundary Elements*, 26(6):537–546, 2002.

R.A. Archer, R.N. Horne, and O. Onyejekwe. Petroleum reservoir engineering applications of the dual reciprocity boundary element method and the Green element method. In *21st World Conference on the Boundary Element Method*, Oxford University, 25–27 August 1999.

K. E. Atkinson. *The Numerical Solution of Integral Equations of the Second Kind*. Cambridge University Press, 1997.

S.N. Atluri and T. Zhu. New concepts in meshless methods. *International Journal for Numerical Methods in Engineering*, 47(1–3):537556, 2000.

S.N. Atluri, J. Sladek, V. Sladek, and T. Zhu. The local boundary integral equation (LBIE) and its meshless implementation for linear elasticity. *Comp. Mech.*, 25:180–198, 2000.

G. Beer. *Programming the Boundary Element Method.* John Wiley & Wiley, west Sussex, 2001.

C.A. Brebbia, J.C.F. Telles, and L.C. Wrobel. *Boundary Element Techniques.* Springer, Berlin, 1984.

M.D. Buhmann. Radial basis functions. *Acta Numerica 2000*, 9:1–38, 2000.

M.D. Buhmann. *Radial Basis Functions : Theory and Implementations.* Cambridge University Press, Cambridge, 2003.

Alexander H.-D. Cheng and Daisy T. Cheng. Heritage and early history of the boundary element method. *Engineering Analysis with Boundary Elements*, 29:268–302, 2005.

O. Chkadua, S.E. Mikhailov, and D. Natroshvili. Analysis of some boundary-domain integral equations for variable-coefficient problems with cracks. In *Advances in Boundary Integral Methods. Proceedings of the 7th UK Conference on Boundary Integral Methods*, pages 37–51, Nottingham University Publ., UK, 2009a.

O. Chkadua, S.E. Mikhailov, and D. Natroshvili. Analysis of direct boundary-domain integral equations for a mixed BVP with variable coefficient. Part I. Equivalence and invertibility. *J. Integral Equations Appl.*, 21(4):499–542, 2009b.

O. Chkadua, S.E. Mikhailov, and D. Natroshvili. Localized boundary-domain integral equation formulation for mixed type problems. *Georgian Math. J.*, 17:469–494, 2010a.

O. Chkadua, S.E. Mikhailov, and D. Natroshvili. Analysis of direct boundary-domain integral equations for a mixed BVP with variable coefficient. Part II. Solution regularity and asymptotics. *J. Integral Equations Appl.*, 22(1):19–37, 2010b.

O. Chkadua, S.E. Mikhailov, and D. Natroshvili. Analysis of segregated boundary-domain integral equations for variable-coefficient problems with cracks. *Numer. Meth. for PDEs*, 27(1):121–140, 2011a.

O. Chkadua, S.E. Mikhailov, and D. Natroshvili. Analysis of segregated boundary-domain integral equations for mixed variable-coefficient bvps in exterior domains. In C. Constanda and P. Harris, editors, *Integral Methods in Science and Engineering: Computational and Analytic Aspects*, pages 109–128, Springer (Birkhuser): Boston, 2011b.

O. Chkadua, S.E. Mikhailov, and D. Natroshvili. Localized boundary-domain integral equations method for an interface crack problem. In D. Lesnic, editor, *Proceedings of the 8th UK Conference on Boundary Integral Methods*, pages 49–56, Leeds, UK, 2011c.

O. Chkadua, S.E. Mikhailov, and D. Natroshvili. Localized boundary-domain integral equations for dirichlet problem for second order elliptic equations with matrix variable coefficients. In D. Lesnic, editor, *Proceedings of the 8th UK Conference on Boundary Integral Methods*, pages 119–126, Leeds, UK, 2011d.

O. Chkadua, S.E. Mikhailov, and D. Natroshvili. Analysis of direct segregated boundary-domain integral equations for variable-coefficient mixed BVPs in exterior domains. *Analysis and Applications*, 2013 (to appear).

J.B. Conway. *A course in functional analysis*. Springer-Verlag, London, 1990.

M. Costabel. Boundary integral operators on Lipschitz domains: Elementary results. *SIAM J. Math. Anal.*, 19:613–626, 1988a.

M. Costabel. Principles of Boundary Element Methods. *SIAM J. Math. Anal.*, 19(3):613–626, 1988b.

Baodong Dai and Yumin Cheng. An improved local boundary integral equation method for two-dimensional potential problems. *Int. J. Appl. Mechanics*, 2(2):421–436, 2010.

Xiao-Wei Gao. The radial integration method for evaluation of domain integrals with boundary-only discretization. *Engineering Analysis with Boundary Elements*, 26(10):905–916, 2002.

C.F. Gauss. *Allgemeine Lehrsätze in Beziehung auf die im verkehrten Verhăltnisse des Quadrats der Entfernung wirkenden Anziehungs-und Abstoβungskrăfte, Gauss' Werke.* Göttingen, 1877.

E. Goursat. *A Course in Mathematical Analysis, Vol. 3, Part 2: Integral equations, Calculus of variations.* Ginn & Co., Boston, Mass, 1964.

G. Green. *An essay on the application of mathematical analysis to the theories of electricity and magnetism.* [Eng.: Printed for the author, by T. Wheelhouse], Nottingham, 1828.

J. Hadamard. *Sur les problèmes aux dérivées partielles et leur signification physique.* Princeton University Bulletin, 1902.

J. Hadamard. *Le problme de Cauchy et les quations aux drives partielles linaires hyperboliques.* Herman, Paris, 1932.

H. Helmholtz. Theorie der Luftschwingungen in Röhren mit offenen Enden. *Journal für die reine und angewandte Mathematik*, 57:1–72, 1860.

D. Hilbert. *Grundzüge einer allgemeinen Theorie der linearen Integral- gleichungen.* Teubner, Leipzig, 1912.

L. Hörmander. Pseudo-differential operators. *Commun. Pure Appl. Math.*, 18(3):501–517, 1965.

L. Hörmander. *The Analysis of Linear Partial Differential Operators III.* Springer, New York, 1985.

G.C. Hsiao and W.L. Wendland. *Boundary Integral Equation.* Springer & Wiley, Berlin, 2008.

J.K. Hunter and B. Nachtergaele. *Applied analysis.* World Scientific, London, 2001.

L.V. Kantorovich and V. I. Krylov. *Approximate methods of higher analysis.* Interscience Publishers, New York, 1964.

T. Kato. *Perturbation Theory for Linear Operators.* Springer-Verlag, New York, 1980.

J.T. Katsikadelis. *Boundary Elements Theory and Applications.* Elsevier, Oxford, 2002.

E. Kreyszig. *Introductory functional analysis with applications.* John Wiley & Sons. Inc, Canada, 1978.

V.N. Kublanovskaya. Application of analytic continuation by change of variables in numerical analysis. *Proc. Mathem. Inst. Acad. Sci. USSR*, 53:145–185, 1959.

V.D. Kupradze. *Boundary value problems for second order elliptic equations.* North-Holland Publishing Company, Amsterdam, 1968.

V.D. Kupradze and M. A. Aleksidze. The method of functional equations for the approximate solution of certain boundary value problems. *USSR Comput Math Math Phys.*, 4:82–126, 1964.

E.E. Levi. I problemi dei valori al contorno per le equazioni lineari totalmente ellittiche alle derivate parziali. *Mem. Soc. Ital. dei Sc. XL*, 16:1–112, 1909.

D. Levin. The approximation power of moving least-squares. *Math. Comp.*, 67:1517–1531, 1998.

Ying Lung-An. *Numerical Methods for Exterior Problems.* World Scientific, Singapore, 2006.

M. Costabel. Some historical remarks on the positivity of boundary integral operators. In *In Boundary element analysis, Lect. Notes Appl. Comput. Mech.*, volume 29, pages 1–27, Berlin, 2007.

R. Mathon and R. L. Johnston. The approximate solution of elliptic boundary value problems by fundamental solutions. *SIAM J. Numer. Anal.*, 14(4):638–650, 1977.

W. McLean. *Strongly Elliptic Systems and Boundary Integral Equations.* Cambridge University Press, 2000.

D. Medková. The Neumann problem for the Laplace equation on general domains. *Czechoslov. Math. J.*, 57:11071139, 2007.

D. Medková. BEM and the Neumann problem for the Poisson equation on Lipschitz domains. *Preprint, Institute of Mathematics, AS CR, Prague*, pages 1–21, 2009.

S.E. Mikhailov. Finite-dimensional perturbations of linear operators and some applications to boundary integral equations. *Engineering Analysis with Boundary Elements*, 23:805–813, 1999.

S.E. Mikhailov. Localized boundary-domain integral formulations for problems with variable coefficients. *Engineering Analysis with Boundary Elements*, 26:681–690, 2002.

S.E. Mikhailov. Some localized boundary-domain integro-differential formulations for quasi-linear problems with variable coefficients. In R. Gallego and M.H. Aliabadi, editors, *Advances in Boundary Element Techniques IV*, pages 289–294, Queen Mary, Univ. of London, 2003.

S.E. Mikhailov. About localized boundary-domain integro-differential formulations for a quasi-linear problem with variable coefficients. In C. Constanda, M. Ahues, and A. Largillier, editors, *Integral Methods in Science and Engineering: Analytic and Numerical Techniques*, pages 139–144, Birkhäuser, 2004.

S.E. Mikhailov. Localized direct boundary-domain integro-differential formulations for some non-linear problems with variable coefficients. *J. Engineering Math.*, 51:283–302, 2005a.

S.E. Mikhailov. Will the boundary (-domain) integral equation method survive? preface to the special issue on non-traditional boundary (-domain) integral equation methods. *J. Engineering Math.*, 51:197–198, 2005b.

S.E. Mikhailov. Direct localized boundary-domain integro-dierential formulations for physically nonlinear elasticity of inhomogeneous body. *Engineering Analysis with Boundary Elements*, 29:1008–1015, 2005c.

S.E. Mikhailov and N.A. Mohamed. Iterative solution of boundary-domain integral equation for BVP with variable coefficient. In D. Lesnic, editor, *Proceedings of the 8th UK Conference on Boundary Integral Methods*, pages 127–134, Leeds, UK, 2011.

S.E. Mikhailov and N.A. Mohamed. Numerical solution and spectrum of boundary-domain integral equation for the Neumann BVP with variable coefficient. *International J. Computer Math.*, 89:1488–1503, 2012.

S.E. Mikhailov and I.S. Nakhova. Mesh-based numerical implementation of the Localized Boundary-Domain Integral-Equation Method to a variable-coefficient Neumann problem. *Journal of Engineering mathematics*, 51:251–259, 2005.

S.G. Mikhlin. *Integral Equations and Application to Certain Problems in Mechanics.* Pergamon Press, New York, 1957.

C. Miranda. *Partial differential equations of elliptic type, Second revised edition.* Springer-Verlag, Berlin, 1970.

S. Mukherjee and Y.X. Mukherjee. *Boundary Methods: Elements, Contours, and Nodes.* CRC Press, Taylor & Francis, Boca Raton, 2005.

C. Neumann. *Untersuchungen uber das logarithmische und Newtonsche Potential.* B. G. Teubner, Leipzig, 1877.

C. Neumann. *Über die Methode des arithmetischen Mittels.* Hirzel, Leipzig, 1887.

O.O. Onyejekwe. An efficient green element algorithm for radial flow. *Applied Mathematics and Computation*, 165(3):635–645, 2005.

O.O. Onyejekwe. A note on green element method discretization for poisson's equation in polar coordinates. *Appl. Math. Lett.*, 19(8):785–788, 2006.

F. Paris and J. Cañas. *Boundary element method fundamentals and applications.* Oxford University Press, Oxford, 1997.

P.W. Partridge, C.A. Brebbia, and L.C. Wrobel. *The Dual Reciprocity Boundary Element Method*. Jouthampton Boston, Computational Mechanics Publications, 1992.

J. Plemelj. *Potentialtheoretische Untersuchungen*. Teubner-Verlag, Leipzig, 1911.

A. Pomp. *The Boundary-domain Integral Method for Elliptic Systems with Applications in Shells*. Lect. Notes in Math. 1683, Springer-Verlag, Berlin-Heidelberg, 1998.

D. Porter and D. S.G. Stirling. *Integral Equation: a Practical Treatment, From Spectral Theory to Applications*. Cambridge University Press, Cambridge, 2004.

S.E. Mikhailov. Analysis of united boundary-domain integro-differential and integral equations for a mixed BVP with variable coefficient. *Math. Methods Appl. Sci.*, 29(6):715–739, 2006.

J. Sladek, V. Sladek, and S.N. Atluri. Local boundary integral equation (LBIE) method for solving problems of elasticity with nonhomogeneous material properties. *Comp. Mech.*, 24:456–462, 2000a.

J. Sladek, V. Sladek, J. Krivacek, and Ch. Zhang. Local BIEM for transient heat conduction analysis in 3-D axisymmetric functionally graded solids. *Comput Mech*, 32:169–176, 2003.

J. Sladek, V. Sladek, and Ch. Zhang. A local BIEM for analysis of transient heat conduction with nonlinear source terms in FGMs. *Engng Anal Bound Elem*, 28:1–11, 2004a.

J. Sladek, V. Sladek, and Ch. Zhang. A meshless local boundary integral equation method for heat conduction analysis in nonhomogeneous solids. *Journal of the Chinese Institute of Engineers*, 27(4):517–539, 2004b.

V. Sladek, J. Sladek, S.N. Atluri, and R. Van Keer. Numerical integration of singularities in meshless implementation of local boundary integral equations. *Comp. Mech.*, 25:394–403, 2000b.

V. Sladek, J. Sladek, and Ch. Zhang. Domain element local integral equation method for potential problems in anisotropic and functionally graded materials. *In Computational Mechanics*, 37:78–85, 2005.

C. Somigliana. Sopra lequilibrio di un corpo elastico isotropo. *Nuovo Cimento, ser*, 3:17–20, 1885.

O. Steinbach and W.L. Wendland. On C. Neumann's method for second-order elliptic systems in domains with non-smooth boundaries. *J. Math. Anal. Appl.*, 262:733–748, 2001.

A.E. Taigbenu. The Green element method. *International Journal for Numerical Methods in Engineering*, 38:2241–2263, 1995.

A.E. Taigbenu. *The Green Element Method*. Kluwer Academic Press, Boston, USA, 1999.

A.E. Taigbenu. 2D internal flux compatibility equation of the flux green element method for transient nonlinear potential problems. *Numerical Methods for Partial Differential Equations*, 26(6):13001315, 2010.

A.E. Taigbenu and A. Elvin. The Green element method applied to plate bending. In *Proc. of Boundary Element Techniques VII*, pages 203–209, Naples-Italy, 2006.

H. Wendland. Local polynomial reproduction and moving least squares approximation. *IMA J. Numer. Anal.*, 21:285–300, 2001.

L.C. Wrobel. *The Boundary Element Method, Vol. 1, Applications in Thermo-Fluids and Acoustics*. Wiley, Chichester, 2002.

T. Zhu, J-D. Zhang, and S.N. Atluri. A local boundary integral equation (LBIE) method in computational mechanics, and a meshless discretization approach. *Computational Mechanics*, 21:223–235, 1998.

T. Zhu, J-D. Zhang, and S.N. Atluri. A meshless numerical method based on the local boundary integral equation LBIE to solve linear and non-linear boundary value problems. *Engineering Analysis with Boundary Elements*, 23:375–389, 1999.